STABILITY OF COUPLING ALGORITHMS

A Thesis

by

ABHINEETH AKKASALE

Submitted to the Office of Graduate Studies of
Texas A&M University
in partial fulfillment of the requirements for the degree of

MASTER OF SCIENCE

May 2011

Major Subject: Mechanical Engineering

STABILITY OF COUPLING ALGORITHMS

A Thesis

by

ABHINEETH AKKASALE

Submitted to the Office of Graduate Studies of
Texas A&M University
in partial fulfillment of the requirements for the degree of

MASTER OF SCIENCE

Approved by:

Chair of Committee,	K. B. Nakshatrala
Committee Members,	Steve Suh
	J. N. Reddy
Head of Department,	Dennis O'Neal

May 2011

Major Subject: Mechanical Engineering

ABSTRACT

Stability of Coupling Algorithms. (May 2011)
Abhineeth Akkasale, B.E., Bangalore University
Chair of Advisory Committee: Dr. Kalyana Nakshatrala

Many technologically important problems are coupled in nature. For example, blood flow in deformable arteries, flow past (flexible) tall buildings, coupled deformation-diffusion, degradation, etc. It is, in general, not possible to solve these problems analytically, and one needs to resort to numerical solutions. An important ingredient of a numerical framework for solving these problems is the *coupling algorithm*, which couples individual solvers of the subsystems that form the coupled system, to obtain the coupled response.

A popular coupling algorithm widely employed in numerical simulations of such coupled problems is the *conventional staggered scheme* (CSS). However, there is no systematic study on the stability characteristics of the CSS. The stability of coupling algorithms is of utmost importance, and assessment of the stability on real problems is not feasible given the computational costs involved. The main aim of this thesis, is to address this issue - assess the accuracy and stability characteristics of CSS using various canonical problems. In this thesis we show that the stability of CSS depends on the relative sizes of the domain, disparity in material properties, and the time step.

To *Amma* and *Anna*

ACKNOWLEDGMENTS

First and foremost, I thank Dr. Kalyana B. Nakshatrala for being an incredible advisor and for his time and patience in constantly guiding me through my research. I am indebted to him for his guidance and encouragement through tough times. I would also like to thank the members of my examination committee, Dr. J. N. Reddy and Dr. Steve Suh for their time and effort in going through my work and for their valuable suggestions. I thank my friends and colleagues at TAMU, especially Arun Ravishankar and Maruti Kumar Mudunuru for being generous with their time and advice.

I cannot thank my family enough for all they have done for me. I am forever indebted to my parents, Basavaraj and Vaijayanthi, for the love and support, for their endless patience and faith in me when most needed. And the least I can do, is thank my beloved uncles, Babaloo and Chickoo; this work could not have come through without their encouragement.

TABLE OF CONTENTS

Page

LIST OF TABLES

LIST OF FIGURES

FIGURE Page

FIGURE Page

FIGURE Page

FIGURE Page

FIGURE Page

CHAPTER I

INTRODUCTION AND MOTIVATION

Numerous scientific and engineering applications of importance involve interactions between two or more (or a group) of components that are functionally related and together, form what can be called a *system*. Systems, in general, are analyzed by breaking down as necessitated by the specific analysis. Restricting ourselves to engineering applications and in particular, mechanical, it is quite normal to breakdown a system into partitions that are suitable for computer simulation. The aim of such simulations is to describe or predict the state of the system under specific conditions that are viewed as external to the system. Of eventual importance is the *response* or the behaviour of the said system under these external conditions which is nothing but a set of states ordered to a parameter such as time (as in dynamic response of a system) or load levels, etc.

By breakdown of a system into partitions, it is meant that the system in consideration, whose response is sought, is spatially/functionally separated into what can be called *subsystems*. And since we are driven by requirements of computations and simulations that are necessary to understanding the response, we relegate this breaking down or partitioning into subsystems that are computationally disparate. By 'computationally disparate subsystem', it is meant that each of the subsystem can be mathematically modeled and described by their field equations. Some examples for such subsystems are solids, fluids, heat, electromagnetics, etc., that are treated by individual field equations as described by continuum theories. These subsystems are, as is common practice, separated based on physics of these subsystems and hence are

---

The journal model is *IEEE Transactions on Automatic Control*.

also commonly termed as multi-physics problems.

A *coupled system*, as described by Felippa, Park and Farhat [1], is a system in which there is dynamic interaction between physically or computationally disparate subsystems. The response of the overall system is obtained by solving simultaneously the coupled equations that model the system. In other words, a dynamic coupled system is one where the state of a subsystem is linked to that of the other subsystems through two-way interacting equations [2].

Many complex systems in various fields of engineering are examples of such coupled interactions, and can broadly be classified as follows:

- fluid - structure interaction;
- thermal - structure interaction;
- control - structure interaction;
- fluid - thermal interaction, etc.

These are but a few of the categories into which a vast number of coupled problems fall under. There can be numerous others that are different combinations of the above mentioned fields, or might also include fields such as electromagnetics, controls, etc. A few specific examples, and especially for fluid structure interactions include problems on blood circulation - blood flow in deformable arteries; off shore submerged structures; wind engineering; aircraft applications [3] - airfoil fluttering [4]; loads due to winds on tall buildings; flow through deformable porous solids, etc. Fluid - Structure Interaction (FSI) is one such phenomenon where a fluid flow exerts pressure to deform a solid structure which in turn affects the flow field of the fluid.

Coupled field or multi-physics problems such as the ones described above form a vast majority of problems of current interest in the fields of engineering technol-

ogy. Solution techniques to obtain complete dynamic responses is still in its nascent state, and poses enormous technological challenge to the scientific world. Computer simulations and computations of these problems forms a subject of vast interest, and has led to the development of a very few successful techniques to obtain complete dynamic responses of such systems.

A. Approaches to solving a coupled system

Analysis of problems involving a single field is fairly simple owing to the ready availability of numerous commercial software [2]. Whereas when faced with a coupled system governed by different field equations, three courses of action are usually followed to obtain the overall response of the system:

1. *Field elimination.* Elimination of one or more fields by integral transform, or model reduction techniques and the subsequent treatment of the remaining field by a time stepping scheme. Although, this method is restricted to special linear problems, where efficient decoupling is permitted; the method also often leads to higher order differential systems in time, which could lead to numerical difficulties [1].

2. *Simultaneous solution.* Also known by the more popular name - *monolithic* scheme/solution, involves treating the full system as one computational entity, simultaneously advancing all field state variables in time.

$$\begin{bmatrix} \boldsymbol{K}_{AA} & \boldsymbol{K}_{AB} \\ \boldsymbol{K}_{BA} & \boldsymbol{K}_{BB} \end{bmatrix} \begin{Bmatrix} \boldsymbol{u}_A^{(n+1)} \\ \boldsymbol{u}_B^{(n+1)} \end{Bmatrix} = \begin{Bmatrix} \boldsymbol{R}_A^{(n)} \\ \boldsymbol{R}_B^{(n)} \end{Bmatrix} \tag{1.1}$$

3. *Partitioned solution.* The individual components of the system are treated as isolated entities, and the time integration process is carried out over each, follow-

ing a sequential or a parallel execution of the single-field analyzers. Interactions are accounted for by making use of techniques such as prediction, substitution, etc.

$$\begin{bmatrix} \boldsymbol{K}_{AA} & \mathbf{0} \\ \mathbf{0} & \boldsymbol{K}_{BB} \end{bmatrix} \begin{Bmatrix} \boldsymbol{u}_A^{(n+1)} \\ \boldsymbol{u}_B^{(n+1)} \end{Bmatrix} \approx \begin{Bmatrix} \boldsymbol{R}_A^{(n)} - \boldsymbol{K}_{AB}\boldsymbol{u}_B^{(n)} \\ \boldsymbol{R}_B^{(n)} - \boldsymbol{K}_{BA}\boldsymbol{u}_A^{(n+1)} \end{Bmatrix} \tag{1.2}$$

The complete transient analysis of the already described coupled problems involves simultaneous solutions of the coupled-field equations; direct time integration of which presents numerous computational difficulties, that are not normally encountered in problems involving just a single field. The vastly different response characteristics of the isolated subsystems means that the discretization and solution techniques exclusive to these fields are necessary for them to perform well. For instance, in a fluid-structure interaction problem, the time scale of the fluid subsystem is much slower than that of the solid subsystem [5].

Additionally, numerous engineering analysis software and solution techniques have been developed over the years to solve individual subsystems, or single-field problems. The partitioned approach facilitates reuse of these existing software to solve the coupled field equations involving those fields either by sequential, or parallel execution of these solvers.

The *finite element methods* are one of the most powerful techniques in the numerical solutions of many complex problems in engineering and are widely used to develop numerical formulations for solving the partial differential equations that arise in solid and fluid mechanics. The methods' features for handling complex geometries, its treatment of boundary conditions and flexibility of programming in a general format make it a very popular technique to handle such problems.

A common finite element formulation, the *(Bubnov-) Galerkin finite element method* is based on the *Galerkin* principle - use of the same function space for trial and test functions [6]. The Galerkin principle provides stable weak formulations to problems in heat conduction and structural mechanics, hence rendering the Galerkin finite element formulation a very successful method in applications to these problems. For a detailed explanation, see Reddy [7], Hughes [6], Brenner and Scott [8] and Braess [9].

A *coupling algorithm*, thus is aimed at such a solution procedure where individual field solvers are utilized to effectively and efficiently obtain complete transient response of a coupled system. In their seminal paper discussing the partitioned analysis of coupled systems, Felippa et al. [1], mention the following keywords that favor the partitioned approach of solution of a coupled system: customization, independent modeling, software reuse and modularity. Functionally, it enforces kinematic and dynamic continuity along the interface that divides the subsystems (fluid and structure sub-domains, for instance - in an FSI problem). Despite the availability of a vast amount of literature on such partitioned techniques and coupling algorithms, development of stable and accurate techniques for transient, coupled problems is still in an early stage and forms a very active area of research.

B. Common terminology

The dynamic interaction between two or more heterogeneous mechanical components constitutes a *coupled system*. The response of the system is obtained by solving simultaneously the coupled equations that model the system. For simulation, coupled systems can be decomposed into physical fields or *sub-domains*, often governed by different field equations. A coupled system is characterized according to the number

of different fields that appear in such a physical decomposition as two-field, three-field, etc. Fig. 1 is a general illustration of a coupling algorithm between two sub-systems A and B.

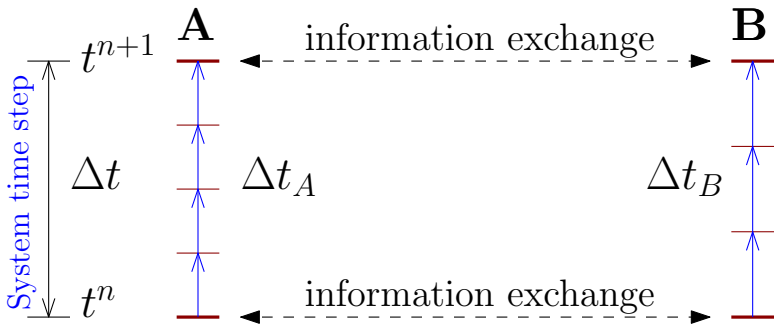

Fig. 1. Illustration of a coupling algorithm

Field partitioning is the field-wise decomposition of the spatial discretization and *splitting* is a decomposition of the temporal (time) discretization of a field within its time step.

Numerically, transient responses of systems are often obtained by dividing the time into discrete time intervals and solving the equations at each time step. The governing equations of the materials that constitute the sub-domains might necessitate using different time steps for each. A *sub-domain time step*, Δt_A and Δt_B in Fig. 1, is the time step used to numerically integrate the equation governing the particular sub-domain. *System time step*, Δt is the time step at which all the sub-domains are synchronized, that is, where information (kinematic/dynamic variables) is exchanged between the sub-domains. The sub-domain time steps can either be less than or equal to the system time step. *Mixed time integration methods* are procedures used to integrate semi-discretizations of partial differential equations where individual sub-domains of the mesh are assigned different time integrators. Time integration procedures in which different sub-domain time steps are used in the mesh

are called *sub-cycling*. A method that allows sub-cycling is also sometimes referred to as a *multi-time-step method*. For a detailed explanation of the terminologies and methods, see [10, 11, 12, 13, 14].

C. Classification of coupling algorithms

Coupling algorithms are generally classified based on the partitioning of the computational grid (element or node), the nature of the mesh at the interface (conforming or non-conforming), the nature of the solution procedure used (monolithic or staggered) or the decomposition into sub-domains (overlapping or non-overlapping).

1. Element partitioning vs. node partitioning

Belytschko and Mullen [15, 16] reported and studied the stability of nodal partitions. Central to these methods were the introduction of a layer of interface elements between the sub-domains, since the sub-domains were each assigned different sets of nodes. Nodal partitioning methods generally lead to complex coupling algorithms, that are expensive and also computationally, have a drawback since these methods do not create symmetric amplification matrices leading to complicated stability analysis [5]. Fig. 2 shows an illustration of element vs. node partitioning.

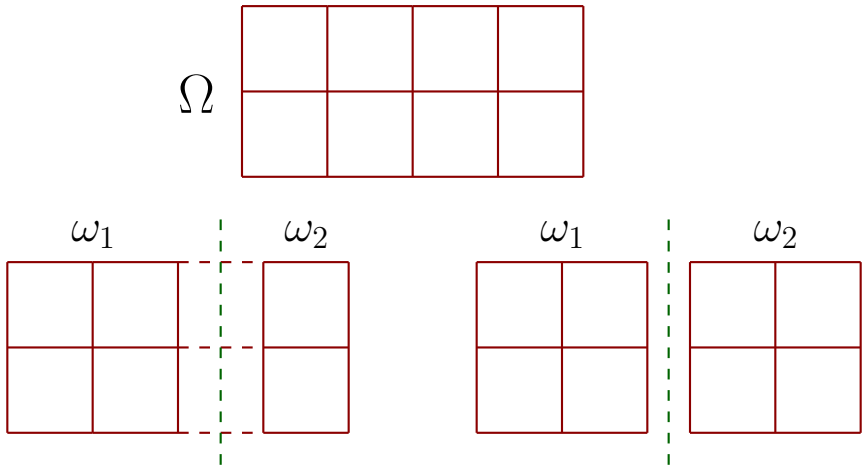

Fig. 2. Element vs. node partitioning. Left: Element partitioned domains; Right: Node partitioning

Hughes and Liu [10] first developed the elemental partitions. In these methods, the interface is made of shared nodes between the sub-domains, which are assigned different sets of elements and hence are completely independent of each other. The sub-domains are solved independently and are coupled together by imposing continuity conditions at the shared nodes. These methods are relegated to applications in finite element methods only. Fig. 3 shows different types of meshes at the interface.

2. Conforming vs. non-conforming methods

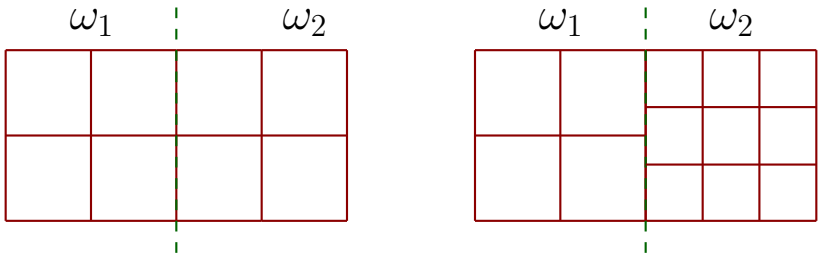

Fig. 3. Conforming vs. non-conforming mesh at interface

In the conforming type of methods for domain-decomposition, the meshes of the sub-domains are aligned to match at the interface; whereas in the non-conforming methods, the meshes of the sub-domains do not match at the interface.

3. Monolithic vs. staggered schemes

The monolithic architecture/scheme is such that the equations of all the sub-domains are solved in a single numerical framework built by integrating the solution procedures of individual sub-domains [17, 18]. On the one hand, such methods improve stability by simultaneously updating all the variables at the interface in the computational domain through global iterations. Yet, on the other, these methods suffer from the inability to use current solvers for individual components.

Staggered schemes for transient solutions of coupled problems, and particularly in Fluid-Structure Interactions are widely used in simulations [19, 4]. Each of the sub-domains are alternately integrated in time by their individual solvers. The interaction between the sub-domains are taken care of by applying boundary conditions at their interface. The lag in time in integrating the individual domains may result in instability, and predictor-corrector methods are often employed for improved stability and accuracy. For a detailed analysis of these algorithms and their stability, see Giles [20, 21] and Prananta et al. [22].

D. Main contributions of the thesis

Scientific literature on partitioned analysis is replete with numerous coupling algorithms, each with different analysis and time integration techniques. The task of selecting the *best* algorithm, thus, remains quite a formidable proposition and one that requires a thorough understanding of the stability and accuracy performance

of the coupling algorithms. The analysis of stability and accuracy of these coupling algorithms is significantly difficult than those of single field analyzers as there is no single method/approach as such. Full fledged analysis of the stability of these algorithms on real problems is not feasible owing to the computational costs involved, and the degree of uniqueness of each of these problems, hence necessitating simpler model problems which help evaluate the performance of the algorithms.

The current investigation is one such attempt at a systematic study of the stability of one of the more popular coupling algorithms, the *conventional staggered scheme* algorithm. Simple canonical problems are identified, and the coupling algorithm implemented on them to evaluate the performance - stability and accuracy. The algorithm is applied to simple single-degree-of-freedom problems to arrive at the conditions for stability of the algorithm, by varying the parameters of the lumped system. We then test the algorithm on realistic model problems - one and two dimensional linear heat conduction problems to further analyze the performance of the CSS algorithm; the factors influencing its stability and rates of convergence.

To this end, a finite element framework has been developed to address transient problems in linear heat conduction, based on the standard Galerkin formulation. The model problems are discretized using this framework, and the conventional staggered scheme algorithm applied to them, thus analyzing the performance - stability and convergence rates of the algorithm with respect to material disparity and differences in the sizes of the domains coupled.

E. Organization of the thesis

The remainder of the thesis is organized as follows. In Chapter II we present the coupling algorithm whose stability we investigate, the conventional staggered scheme

algorithm. We discuss briefly the various aspects of the algorithm, and factors considered and assumptions made in the present work. We then describe the stability criterion utilized to test the coupling algorithm, and its intricacies. In Chapter III we present the stability analysis of the conventional staggered scheme algorithm as applied to simple single-degree-of-freedom problems. We test the stability by testing it on first order and second order systems coupled using this algorithm and evaluate its stability utilizing the amplification factor technique. In Chapter IV, we present realistic model problems and analyze the performance of the CSS algorithm - stability and convergence. We present four model problems, two in one - dimensional heat conduction and two in two - dimensional heat conduction. Convergence rates are checked for against analytical solutions that are available. Conclusions, result assessments, discussions and future perspectives are provided in Chapter 5.

CHAPTER II

CONVENTIONAL STAGGERED SCHEME AND THE STABILITY CRITERION

A staggered coupling algorithm can be conceptualized as follows: a procedure to couple partitioned subsystems through sequential execution of the single field analyzers of the respective subsystems. The term *staggered* arising from the zigzag appearance as the solution state progresses as is evident from Fig. 4 below. Through the rest of the work, we focus interest on the 'conventional staggered scheme', a staggered coupling algorithm as the basis of our study.

A. Conventional staggered scheme

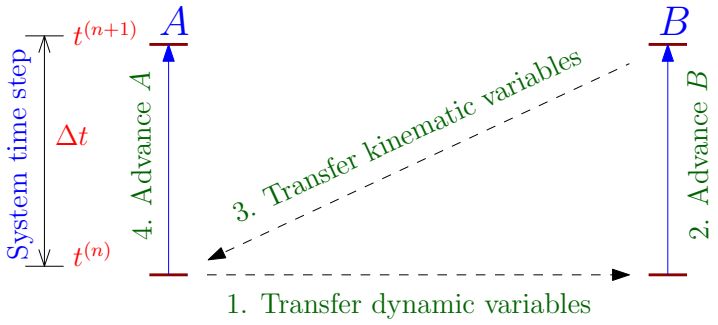

Fig. 4. Conventional staggered scheme

Fig. 4 shows an illustration of the Conventional Staggered Scheme coupling algorithm as could be applied to a Fluid-structure interaction problem. The solution state of this coupled system is advanced in time by executing sequentially, the fluid and structure subsystem analyzers. Assuming knowledge of the complete solution vector at some time t^n, we utilize linear multi-step time integration methods to arrive at the solution vector at time t^{n+1}. The steps involved in the working of the CSS coupling algorithm is as follows:

1. The known dynamic quantities are supplied from the fluid to the structure at t^n, i.e. pressures, stresses, etc.

2. The structure subsystem is then solved using these updated quantities from the fluid subsystem to obtain the structural quantities at t^{n+1}.

3. At this point, the known structural quantities at t^{n+1} are supplied to the fluid subsystem which is still at t^n.

4. The fluid subsystem is now solved using these updated quantities from the structure, to obtain the complete solution set at state t^{n+1}.

5. Steps 1 - 4 are repeated (iterated) until we arrive at the time where the solution is required.

The solution of each of the subsystems is independent of the other, hence allowing for mixed methods of time integration, i.e. one of the subsystems may be solved using an implicit time integration scheme, and the other using explicit, and so on.

In the present study, we assume the following:

- No sub-cycling is assumed.

- No mixed mode time integration is assumed, i.e. consistent time integration schemes for both the subsystems.

- The subsystem that supplies the first set of variables to the other subsystem is called the *predicting* subsystem or domain. (We hereby make no distinction between the words domain and subsystem and are used interchangeably to imply the meaning - the subsystem that is governed by its exclusive field equation.)

- The subsystem that is solved first is called the *iterated* subsystem or domain.

B. Stability criterion

We consider the behaviour of the first order, homogeneous model equation:

$$\dot{d} + \lambda\, d = 0 \tag{2.1}$$

This first order differential equation is easily solved, and the solution for d at time t_{n+1} for the initial value $d(t_n)$, $t_{n+1} > t_n$, is

$$d^{(n+1)} = \exp\left(-\lambda(t_{n+1} - t_n)\right) d^{(n)} \tag{2.2}$$

and from which it follows that

$$\begin{aligned} |d^{(n+1)}| < |d^{(n)}|, \quad \lambda > 0 \\ d^{(n+1)} = d^{(n)}, \quad \lambda = 0 \end{aligned} \tag{2.3}$$

The temporally discrete model equation can be written as

$$d^{(n+1)} = A\, d^{(n)} \tag{2.4}$$

where A is called the amplification factor. From this definition of A, the second condition of (2.3) is automatically established, and the first condition is equivalent to

$$|A| < 1 \tag{2.5}$$

The above is the case for a scalar first order equation. Similarly, any linear multi-step formula can be represented as: $\mathbf{d}^{(n+1)} = \mathbf{A}\, \mathbf{d}^{(n)}$, where $\mathbf{d}$ is known as the state vector, and $\mathbf{A}$ is the amplification matrix (or transfer matrix) and (n) and $(n+1)$ are the time levels. Let $\rho(x)$ be the characteristic polynomial of the transfer matrix $\mathbf{A}$, then, the *root condition for stability* is stated as [23]:

A linear multi-step formula is stable if and only if the all the roots of the characteristic polynomial, $\rho(x)$ satisfy $|x| \leq 1$, and any root with $|x| = 1$ is simple.

It is to be noted that a simple root does not mean that the root has to be non-repetitive. As an example, consider matrices $\mathbf{A_1}$ and $\mathbf{A_2}$:

$$\mathbf{A_1} = \begin{bmatrix} 1 & 0 \\ 0 & 1 \end{bmatrix}, \qquad \mathbf{A_2} = \begin{bmatrix} 1 & 1 \\ 0 & 1 \end{bmatrix} \tag{2.6}$$

$\mathbf{A_1}$ and $\mathbf{A_2}$ have both their eigenvalues equal to 1. In $\mathbf{A_1}$, the repetitive eigenvalue is simple as there are two distinct eigenvectors corresponding to this, that span $\mathbb{R}^2$. In $\mathbf{A_2}$, however, the eigenvalues are not simple, as no two such eigenvectors exist.

Violations of the first condition, $|x| \leq 1$ produce *explosive instabilities*, which grow as $[\gamma(\mathbf{A})]^n$; where $\gamma(\mathbf{A}) = max\{x_i(\mathbf{A})\}$, (where x_i are the eigenvalues of $\mathbf{A}$) is the spectral radius of the amplification matrix $\mathbf{A}$, and n is the number of time steps. If the second condition, the requirement that modulus one eigenvalue be simple, is violated, produce *weak instabilities* where the growth is considerably smaller. It is easy to see that in the n^{th} powers of the matrices:

$$\mathbf{A_1^n} = \begin{bmatrix} 1^n & 0 \\ 0 & 1^n \end{bmatrix}, \qquad \mathbf{A_2^n} = \begin{bmatrix} 1^n & (n)1^{n-1} \\ 0 & 1^n \end{bmatrix} \tag{2.7}$$

which implies that the solution grows linearly with respect to the number of time steps n and hence the condition for a root $|x| = 1$ be simple enforces stability. See Hughes [6] for further details.

The above stability criterion is now tested on model problems, referred to as *split - degree of freedom*, which are obtained by splitting a simple single - degree freedom lumped parameter system into two single - degree of freedom systems, subjected to a constraint.

CHAPTER III

REPRESENTATIVE NUMERICAL EXAMPLES

In this section, we describe simple linear model problems and study the stability of the conventional staggered scheme algorithm as applied to these problems. We evaluate the performance of the conventional staggered scheme as applied to a simple split single-degree-of-freedom (SDOF) problems, a 1-D linear heat conduction problem and a 2-D linear heat conduction problem. The results for stability are presented at the end. We assume *no* subcycling, and hence the term 'time step' is used in the general sense. It is also assumed that the time steps are uniform.

A. Split SDOF: first order system

A simple coupling problem is that of the SDOF system. For the case of the first order linear system, we consider a single point mass connected to two dash-pots in series. A simple first order system is shown in Fig. 5.

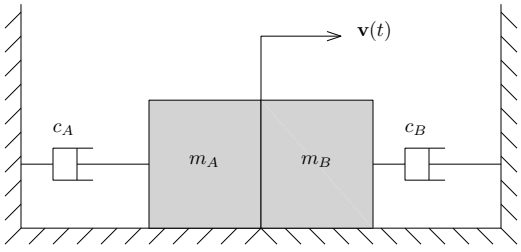

Fig. 5. A first order system

The governing equations of motion for this SDOF system can be written as:

$$(m_A + m_B)\,\dot{v}(t) + (c_A + c_B)\,v(t) = 0 \tag{3.1}$$

where $a(t) = \dot{v}(t)$ is the acceleration and $v(t)$ is the velocity.

Now, the same system can equivalently be split by subjecting it to the constraint $v_A(t) - v_B(t) = 0$ as the following coupled system:

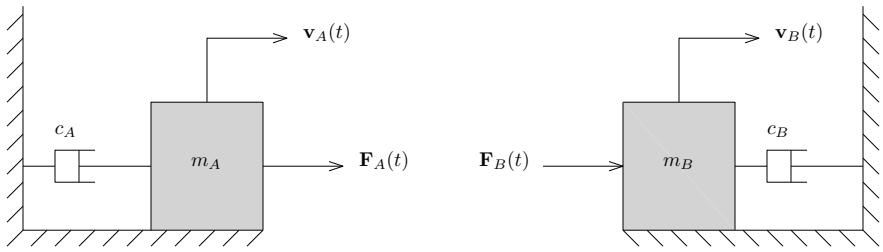

Fig. 6. A first order system with split degrees of freedom

The governing equations for such a system, as shown in Fig. 6, with split degrees of freedom can be written as:

$$\begin{aligned} m_A\,\dot{v}_A(t) + c_A\,v_A(t) &= F_A(t) \\ m_B\,\dot{v}_B(t) + c_B\,v_B(t) &= F_B(t) \\ v_A(t) - v_B(t) &= 0 \\ F_A(t) + F_B(t) &= 0 \end{aligned} \tag{3.2}$$

The above split SDOF equations are discretized into N time intervals denoted by $t_n (n = 0, ..., N)$. The time steps are assumed to be uniform, and are denoted by $\Delta t := t_n - t_{n-1}$. Any discretized quantity $z(t)$ at the instant of time t_n is represented as:

$$z^{(n)} \approx z(t = t_n) \quad n = 0, \cdot, N$$

We use the generalized trapezoidal family of time integrators for both the sub-systems A and B. The governing equations (3.2) for the split 1^{st} order system are discretized

in accordance to the following set rules:

- First order equation/heat conduction equation

$$m_i\, a_i^{(n+1)} + c_i\, v_i^{(n+1)} = F_i^{(n+1)} \quad i = A, B \tag{3.3}$$

- Trapezoidal rule:

$$v_i^{(n+1)} = v_i^{(n)} + \Delta t \left[(1-\gamma_i) a_i^{(n)} + (\gamma_i) a_i^{(n+1)} \right] \tag{3.4}$$

- Dynamic continuity (for the conventional staggered scheme as in Fig. 4):

$$F_B^{(n+1)} = -F_A^{(n)} \tag{3.5}$$

- Kinematic continuity:

$$v_A^{(n+1)} = (1-\alpha) v_B^{(n)} + (\alpha) v_B^{(n+1)} \tag{3.6}$$

where $v^{(n)} = v(t = t_n)$, $a^{(n)} = \dot{v}(t = t_n)$ and α is the relaxation parameter.

1. CSS implementation and stability of a first order system

The governing equations of the first order system, the equations for dynamic and kinematic continuities, and the trapezoidal equations for the two constituents together form a system of linear equations solvable for the variables v_A, a_A, F_A, v_B, a_B and F_B. The steps involved in coupling the subsystems A and B using the conventional staggered scheme is shown below:

1. Enforce dynamic continuity through predictors from subsystem A to B through:

$$F_B^{(n+1)} = -F_A^{(n)} \tag{3.7}$$

2. Solve subsystem B using the following equations:

$$m_B\, a_B^{(n+1)} + c_B\, v_B^{(n+1)} = F_B^{(n+1)} \tag{3.8}$$

$$v_B^{(n+1)} = v_B^{(n)} + \Delta t \left[(1-\gamma_B)a_B^{(n)} + (\gamma_B)a_B^{(n+1)}\right] \tag{3.9}$$

3. Enforce kinematic continuity between the subsystems through:

$$v_A^{(n+1)} = (1-\alpha)v_B^{(n)} + (\alpha)v_B^{(n+1)} \tag{3.10}$$

4. Solve subsystem A using the following equations:

$$v_A^{(n+1)} = v_A^{(n)} + \Delta t \left[(1-\gamma_A)a_A^{(n)} + (\gamma_A)a_A^{(n+1)}\right] \tag{3.11}$$

$$m_A\, a_A^{(n+1)} + c_A\, v_A^{(n+1)} = F_A^{(n+1)} \tag{3.12}$$

From these equations, we arrive at the following relation at every time step t_n

$$\mathbf{L}\mathbf{x}^{(n+1)} = \mathbf{R}\mathbf{x}^{(n)} \tag{3.13}$$

The amplification/transfer matrix is constructed using the above relation and can be written as:

$$\mathbf{A} = \mathbf{L}^{-1}\mathbf{R} \tag{3.14}$$

where $\mathbf{L}$, $\mathbf{R}$, $\mathbf{x}^{(n+1)}$ and $\mathbf{x}^{(n)}$ are defined as below:

$$\mathbf{L} := \begin{bmatrix} 0 & 0 & 0 & 0 & 0 & 1 \\ 0 & 0 & c_B & m_B & 0 & -1 \\ 0 & 0 & 1 & -(\Delta t)\gamma_B & 0 & 0 \\ 1 & 0 & -\alpha & 0 & 0 & 0 \\ 1 & -(\Delta t)\gamma_A & 0 & 0 & 0 & 0 \\ c_A & m_A & 0 & 0 & -1 & 0 \end{bmatrix} \tag{3.15}$$

$$\mathbf{R} := \begin{bmatrix} 0 & 0 & 0 & 0 & -1 & 0 \\ 0 & 0 & 0 & 0 & 0 & 0 \\ 0 & 0 & 1 & (\Delta t)(1-\gamma_B) & 0 & 0 \\ 0 & 0 & 1-\alpha & 0 & 0 & 0 \\ 1 & (\Delta t)(1-\gamma_A) & 0 & 0 & 0 & 0 \\ 0 & 0 & 0 & 0 & 0 & 0 \end{bmatrix} \tag{3.16}$$

$$\mathbf{x}^{(n+1)} = \begin{Bmatrix} v_A^{(n+1)} \\ a_A^{(n+1)} \\ v_B^{(n+1)} \\ a_B^{(n+1)} \\ F_A^{(n+1)} \\ F_B^{(n+1)} \end{Bmatrix}, \qquad \mathbf{x}^{(n)} = \begin{Bmatrix} v_A^{(n)} \\ a_A^{(n)} \\ v_B^{(n)} \\ a_B^{(n)} \\ F_A^{(n)} \\ F_B^{(n)} \end{Bmatrix} \tag{3.17}$$

B. Split SDOF: second order system

For a simple second order SDOF system, we consider a single point mass connected to two linear springs in series. A simple second order system is shown in Fig. 7.

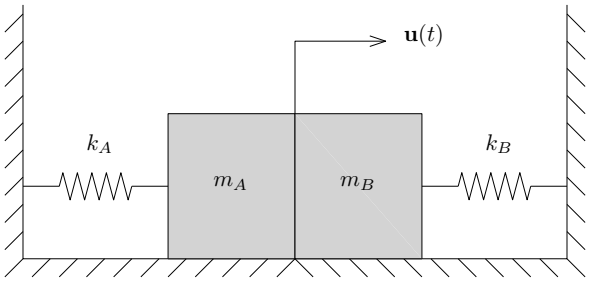

Fig. 7. A second order system

The governing equations of motion for the second order SDOF system can be

written as:

$$(m_A + m_B)\,\ddot{u}(t) + (k_A + k_B)\,u(t) = 0 \tag{3.18}$$

where $a(t) = \ddot{u}(t)$ is the acceleration and $u(t)$ is the displacement.

The equivalent split SDOF system of the above second order system is:

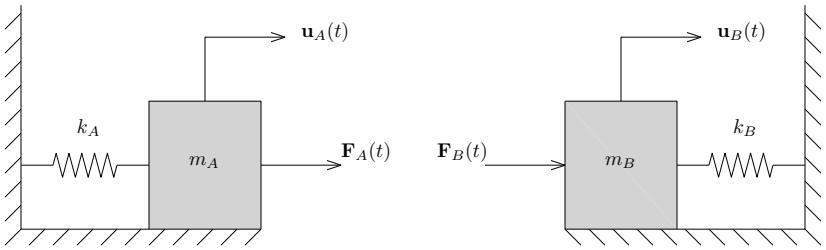

Fig. 8. A second order system with split degrees of freedom

The governing equations for such a system, shown in Fig. 8, with split degrees of freedom can be written as:

$$\begin{aligned} m_A\,\ddot{u}_A(t) + k_A\,u_A(t) &= F_A(t) \\ m_B\,\ddot{u}_B(t) + k_B\,u_B(t) &= F_B(t) \\ u_A(t) - u_B(t) &= 0 \\ F_A(t) + F_B(t) &= 0 \end{aligned} \tag{3.19}$$

The governing equations (3.19) for the split 2^{nd} order system are discretized in accordance to the following set rules:

- Equilibrium equation for the second order system

$$m_i\,a_i^{(n+1)} + k_i\,d_i^{(n+1)} = F_i^{(n+1)} \quad i = A, B \tag{3.20}$$

- Newmark equations:

$$\begin{aligned} d_i^{(n+1)} &= d_i^{(n)} + \Delta t v_i^{(n)} + \left[(1-2\beta_i)a_i^{(n)} + (2\beta_i)a_i^{(n+1)}\right] \\ v_i^{(n+1)} &= v_i^{(n)} + \Delta t \left[(1-\gamma_i)a_i^{(n)} + (\gamma_i)a_i^{(n+1)}\right] \end{aligned} \tag{3.21}$$

- Dynamic continuity (for the conventional staggered scheme as in Fig. 4):

$$F_B^{(n+1)} = -F_A^{(n)} \tag{3.22}$$

- Kinematic continuity:

$$v_A^{(n+1)} = (1-\alpha)v_B^{(n)} + (\alpha)v_B^{(n+1)} \tag{3.23}$$

where $a^{(n)} = \ddot{u}(t_n)$, $v^{(n)} = \dot{u}(t_n)$ and $d^{(n)} = u(t_n)$

1. CSS implementation and stability of a second order system

The governing equations of the second order system, the equations for dynamic and kinematic continuities, and the Newmark equations for the two constituents together form a system of linear equations solvable for the variables $d_A, v_A, a_A, F_A d_B, v_B, a_B$ and F_B. The steps involved in coupling the subsystems A and B using the conventional staggered scheme is shown below:

1. Enforce dynamic continuity through predictors from subsystem A to B through:

$$F_B^{(n+1)} = -F_A^{(n)} \tag{3.24}$$

2. Solve subsystem B using the following equations:

$$m_B\, a_B^{(n+1)} + k_B\, d_B^{(n+1)} = F_B^{(n+1)} \tag{3.25}$$

$$d_B^{(n+1)} = d_B^{(n)} + (\Delta t) v_B^{(n)} \left(\frac{\Delta t^2}{2}\right) \left[(1-2\beta_B) a_B^{(n)} + (2\beta_B) a_B^{(n+1)}\right] \tag{3.26}$$

$$v_B^{(n+1)} = v_B^{(n)} + \Delta t + \left[(1-\gamma_B) a_B^{(n)} + (\gamma_B) a_B^{(n+1)}\right] \tag{3.27}$$

3. Enforce dynamic continuity through predictors from subsystem A to B through:

$$v_A^{(n+1)} = (1-\alpha) v_B^{(n)} + (\alpha) v_B^{(n+1)} \tag{3.28}$$

4. Solve subsystem A using the following equations:

$$v_A^{(n+1)} = v_A^{(n)} + \Delta t \left[(1-\gamma_A) a_A^{(n)} + (\gamma_A) a_A^{(n+1)}\right] \tag{3.29}$$

$$d_A^{(n+1)} = d_A^{(n)} + (\Delta t) v_A^{(n)} + \left(\frac{\Delta t^2}{2}\right) \left[(1-2\beta_A) a_A^{(n)} + (2\beta_A) a_A^{(n+1)}\right] \tag{3.30}$$

$$m_A\, a_A^{(n+1)} + k_A\, v_A^{(n+1)} = F_A^{(n+1)} \tag{3.31}$$

The matrices $\mathbf{L}$, $\mathbf{R}$, $\mathbf{x}^{(n+1)}$ and $\mathbf{x}^{(n)}$ are defined as below:

$$\mathbf{L} := \begin{bmatrix} 0 & 0 & 0 & 0 & 0 & 0 & 0 & 1 \\ 0 & 0 & 0 & k_B & 0 & m_B & 0 & -1 \\ 0 & 0 & 0 & 1 & 0 & -(\Delta t^2)\beta_B & 0 & 0 \\ 0 & 0 & 0 & 0 & 1 & -(\Delta t)\gamma_B & 0 & 0 \\ 0 & 1 & 0 & 0 & -\alpha & 0 & 0 & 0 \\ 0 & 1 & -(\Delta t)\gamma_A & 0 & 0 & 0 & 0 & 0 \\ 1 & 0 & -(\Delta t^2)\beta_A & 0 & 0 & 0 & 0 & 0 \\ k_A & 0 & m_A & 0 & 0 & 0 & -1 & 0 \end{bmatrix} \tag{3.32}$$

$$\mathbf{R} := \begin{bmatrix} 0 & 0 & 0 & 0 & 0 & 0 & -1 & 0 \\ 0 & 0 & 0 & 0 & 0 & 0 & 0 & 0 \\ 0 & 0 & 0 & 1 & \Delta t & \left(\frac{\Delta t^2}{2}\right)(1-2\beta_B) & 0 & 0 \\ 0 & 0 & 0 & 0 & 1 & (\Delta t)(1-\gamma_B) & 0 & 0 \\ 0 & 0 & 0 & 0 & 1-\alpha & 0 & 0 & 0 \\ 0 & 1 & (\Delta t)(1-\gamma_A) & 0 & 0 & 0 & 0 & 0 \\ 1 & \Delta t & \left(\frac{\Delta t^2}{2}\right)(1-2\beta_A) & 0 & 0 & 0 & 0 & 0 \\ 0 & 0 & 0 & 0 & 0 & 0 & 0 & 0 \end{bmatrix} \tag{3.33}$$

$$\mathbf{x}^{(n+1)} = \begin{Bmatrix} d_A^{(n+1)} \\ v_A^{(n+1)} \\ a_A^{(n+1)} \\ d_B^{(n+1)} \\ v_B^{(n+1)} \\ a_B^{(n+1)} \\ F_A^{(n+1)} \\ F_B^{(n+1)} \end{Bmatrix}, \qquad \mathbf{x}^{(n)} = \begin{Bmatrix} d_A^{(n)} \\ v_A^{(n)} \\ a_A^{(n)} \\ d_B^{(n)} \\ v_B^{(n)} \\ a_B^{(n)} \\ F_A^{(n)} \\ F_B^{(n)} \end{Bmatrix} \tag{3.34}$$

C. Results and discussions

The conventional staggered scheme was tested for stability of the first order and the second order systems as shown in Sec. A and B. Amplification matrices are obtained as discussed earlier through the modal amplification system. As defined in Chapter II, stability is observed when the magnitude of the eigenvalues of the amplification matrix, $|x_i| \leqslant 1$. We use the in-built MATLAB functionality to obtain the eigenvalues of the amplification matrices to determine the stability of the split SDOF systems.

It is evident here, that the factors affecting the magnitude of the eigenvalues, (and hence the stability) are the values of material properties of the two fields (c_A and c_B or k_A and k_B), the masses of the fields (m_A and m_B), the relaxation parameter α, the trapezoidal or Newmark time integration parameters, γ and β and the time step used(Δt). For a complete and systematic study of the stability of CSS, it is necessary to vary each of the parameters against the others to determine its effect on the stability.

Numerous test cases were run to this effect by varying each of the parameters, keeping the rest constant. The magnitude of the eigenvalues are plotted in each case, by varying the time steps from 10^{-5} to 1. The following cases were studied in this current study.

1. Results: first order

For the first order system, the time integration scheme utilized on the two subsystems was mid-point Euler ($\gamma = 0.5$), an unconditionally stable, second order accurate scheme, since our focus is to observe the stability as a result of material properties of the subsystems and the performance of the CSS, and hence no instabilities due to the time integration scheme was to be allowed. Various test cases were considered by varying c_A, c_B, m_A, m_B and α. Table I summarizes the stability of the CSS as applied to the split first order SDOF. The reference figures are available in the appendix.

Fig. 9 shows the general trend observed when the material properties are all equal, we observe stability since the eigenvalues of the amplification matrix at all time step sizes are $\leqslant 1$.

Table I. Summary of the stability of CSS for the first order split SDOF

Predicting domain: A			
Parameters varied	Other parameters	Stability	Reference figures
$c_A > c_B$	$m_A = m_B = 1$; $\alpha = 1$	Conditional	Fig. 36-39
$c_B \geqslant c_A$	$m_A = m_B = 1$; $\alpha = 1$	Stable	
$c_A > c_B$	$m_A = m_B = 1$; $\alpha = 0.5$	Conditional	Fig. 44-47
$c_B \geqslant c_A$	$m_A = m_B = 1$; $\alpha = 0.5$	Stable	
$m_A > m_B$	$c_A = c_B = 1$; $\alpha = 1$	Unstable	Fig. 40-43
$m_B \geqslant m_A$	$c_A = c_B = 1$; $\alpha = 1$	Stable	
$m_A > m_B$	$c_A = c_B = 1$; $\alpha = 0.5$	Unstable	Fig. 48-51
$m_B \geqslant m_A$	$c_A = c_B = 1$; $\alpha = 0.5$	Stable	

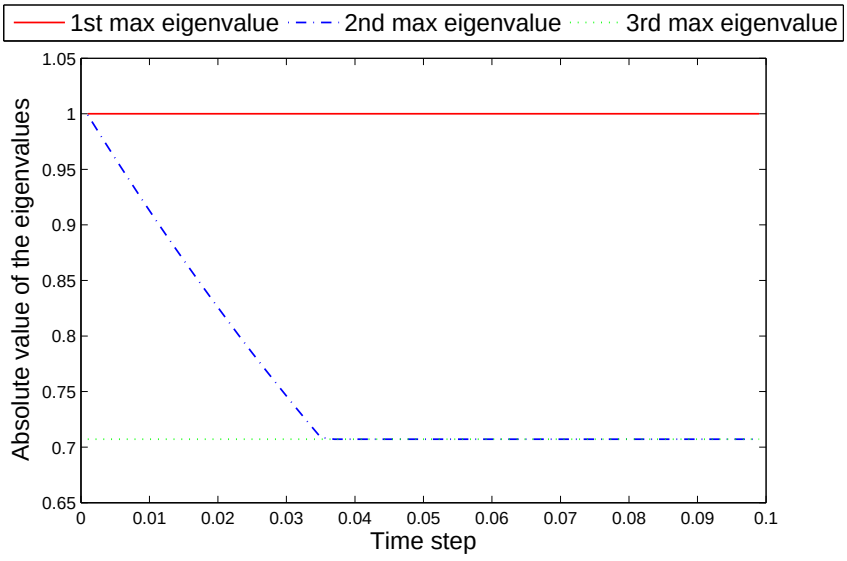

Fig. 9. A stable case considering all properties equal, $c_A = c_B = m_A = m_B = 1$ and with α dissipation, $\alpha = 0.5$

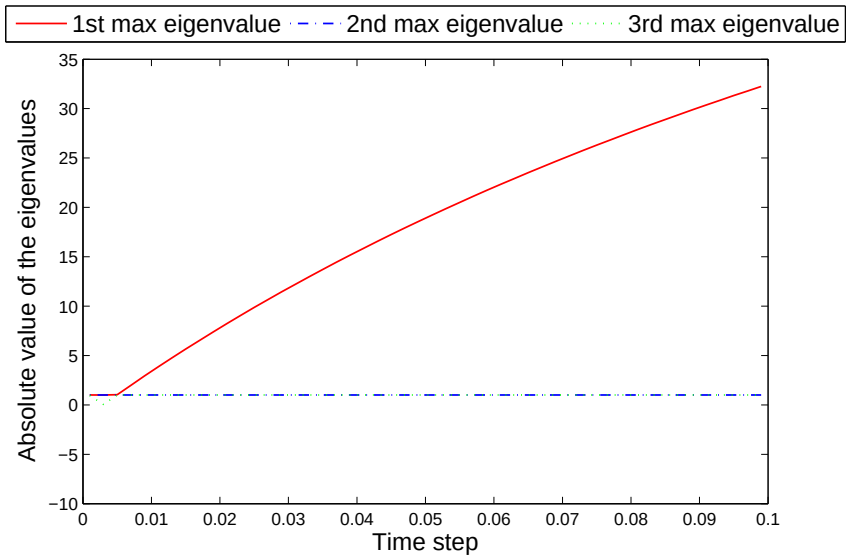

Fig. 10. Conditional stability observed with $c_A > c_B$. The material properties: $c_A = 100$; $c_B = 1$; $m_A = m_B = 1$; $\alpha = 1$

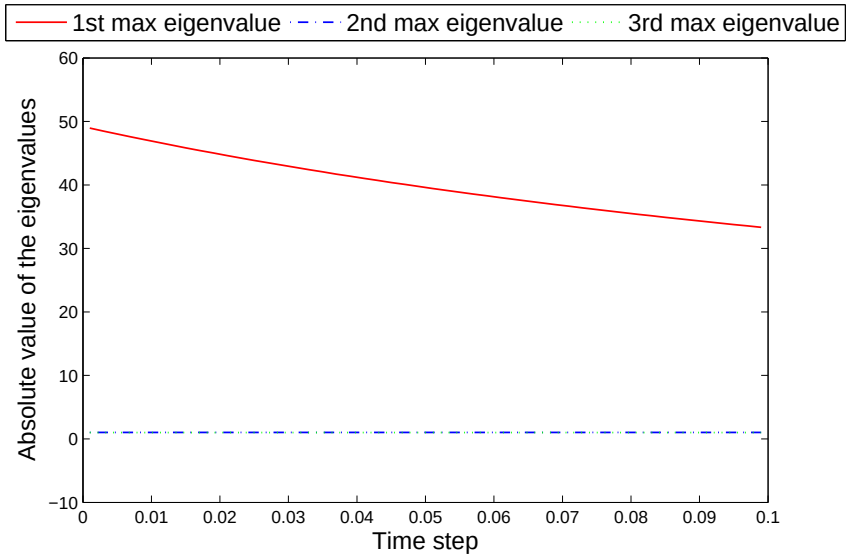

Fig. 11. An unstable case with $m_A > m_B$. The material properties are: $c_A = c_B = 1$; $m_A = 100$; $m_B = 1$; $\alpha = 0.5$

Fig. 10 and Fig. 11 show the general trends seen for conditional stability and instability as observed when $c_A > c_B$ and $m_A > m_B$ respectively.

From the above list, it can be inferred that for the case of a first order system where the two fields are coupled using the conventional staggered scheme, the scheme turns out to be conditionally stable when the properties of A are greater than the properties of B. More precisely,

1. The scheme is unstable for all cases when $m_A > m_B$, given $c_A = c_B$.
2. The scheme is conditionally stable when $c_A > c_B$, given $m_A = m_B$.

2. Results: second order

For the second order system, two time integration schemes were tested along with varying the material properties and the relaxation parameter α. Newmark average acceleration method, ($\gamma = 0.5$, $\beta = 0.25$) and the damped Newmark scheme, ($\gamma = 0.6$, $\beta = 0.3025$) were the two time integration schemes tested. Various test cases were considered by varying c_A, c_B, m_A, m_B and α. Table II summarizes the stability of the CSS as applied to the split second order SDOF. The reference figures are available in the appendix.

Table II. Summary of the stability of CSS for the second order split SDOF

Predicting domain: A			
Parameters varied	Other parameters	Stability	Reference figures
$k_A > k_B$	$m_A = m_B = 1$, $\alpha = 1$, avg. accn.	Conditional	Fig. 52-55
$k_B \geqslant k_A$	$m_A = m_B = 1$, $\alpha = 1$, avg. accn.	Stable	
$k_A > k_B$	$m_A = m_B = 1$, $\alpha = 0.5$, damped	Conditional	Fig. 60-63
$k_B \geqslant k_A$	$m_A = m_B = 1$, $\alpha = 0.5$, damped	Stable	
$k_A > k_B$	$m_A = m_B = 1$, $\alpha = 0.5$, damped	Conditional	Fig. 68-71
$k_B \geqslant k_A$	$m_A = m_B = 1$, $\alpha = 0.5$, damped	Stable	
$m_A > m_B$	$k_A = k_B = 1$, $\alpha = 1$, avg. accn.	Unstable	Fig. 56-59
$m_B > m_A$	$k_A = k_B = 1$, $\alpha = 1$, avg. accn.	Conditional	
$m_B = m_A$	$k_A = k_B = 1$, $\alpha = 1$, avg. accn.	Stable	
$m_A > m_B$	$k_A = k_B = 1$, $\alpha = 0.5$, damped	Unstable	Fig. 64-67
$m_B > m_A$	$k_A = k_B = 1$, $\alpha = 0.5$, damped	Conditional	
$m_B = m_A$	$k_A = k_B = 1$, $\alpha = 0.5$, damped	Stable	
$m_A > m_B$	$k_A = k_B = 1$, $\alpha = 0.5$, damped	Unstable	Fig. 72-75
$m_B > m_A$	$k_A = k_B = 1$, $\alpha = 0.5$, damped	Conditional	
$m_B = m_A$	$k_A = k_B = 1$, $\alpha = 0.5$, damped	Stable	

Figs. 12 - 13 show the stable cases of the CSS algorithm, where the material properties were all equal, and where the spring constant was varied such that $k_B > k_A$ respectively. Similar trends were observed for all the test cases where $k_B > k_A$ as in Fig. 13.

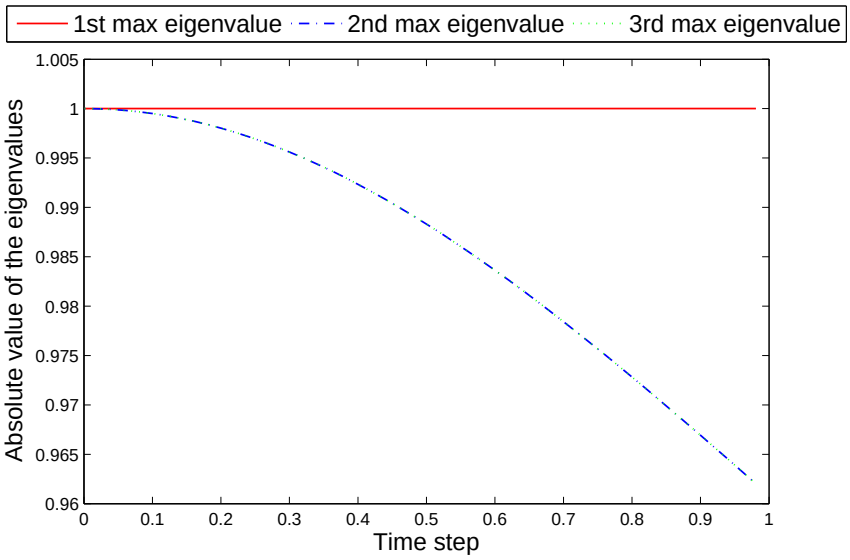

Fig. 12. A stable case considering all properties equal, $k_A = k_B = m_A = m_B = 1$; $\alpha = 0.5$, and damped Newmark scheme, $\gamma = 0.6$; $\beta = 0.3025$

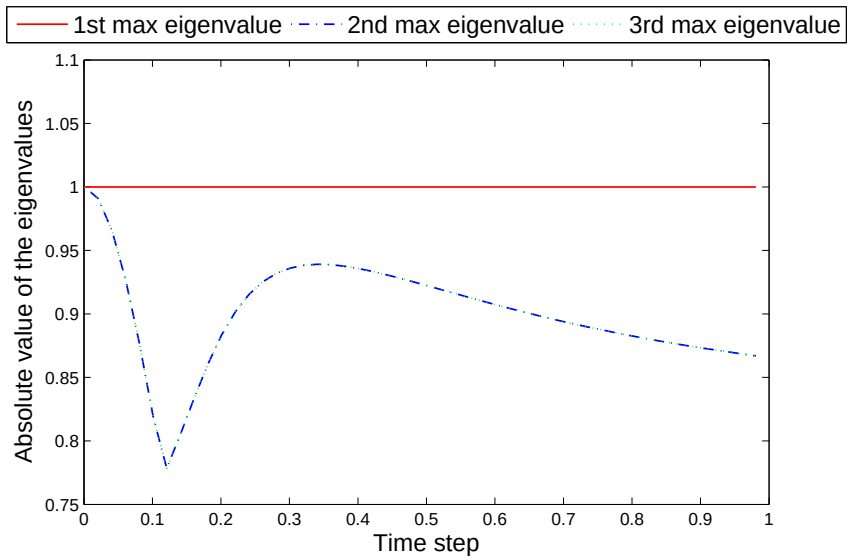

Fig. 13. Stability observed with $k_B > k_A$. The material properties: $k_B = 100$; $k_A = 1$; $m_A = m_B = 1$; $\alpha = 1$; $\gamma = 0.5$; $\beta = 0.25$

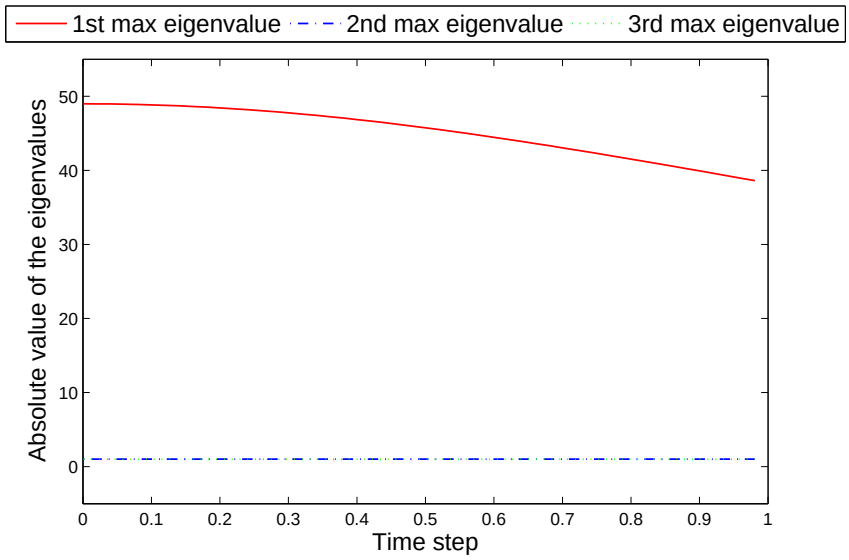

Fig. 14. Instability, as observed with $m_A > m_B$. The other properties: $m_A = 100$; $m_B = 1$; $k_A = k_B = 1$; $\alpha = 1$; $\gamma = 0.5$; $\beta = 0.25$

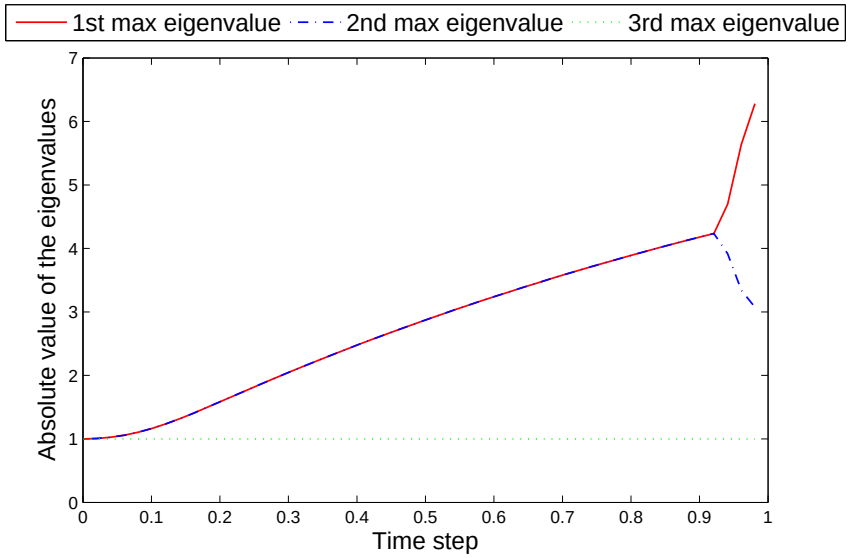

Fig. 15. Conditional stability observed with $k_A > k_B$. The material properties: $k_A = 100$; $k_B = 1$; $m_A = m_B = 1$; $\alpha = 1$; $\gamma = 0.6$; $\beta = 0.3025$

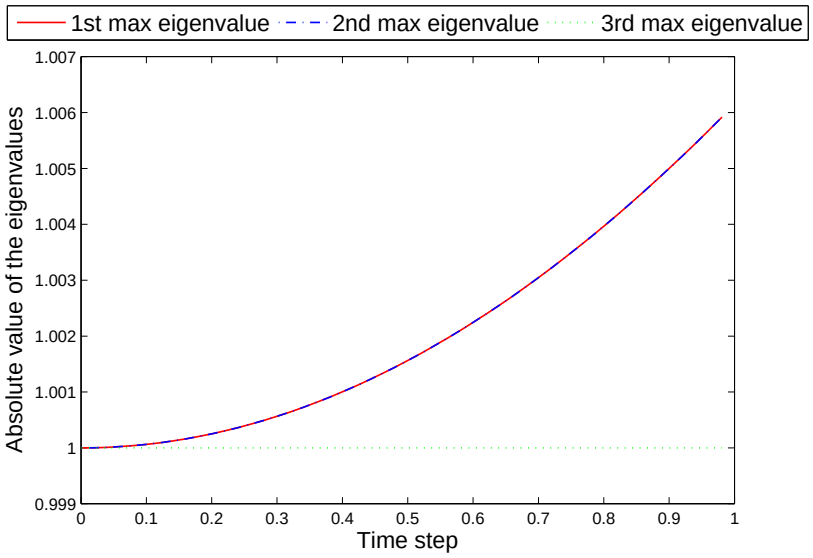

Fig. 16. Conditional stability observed with $m_B > m_A$. The material properties: $m_B = 100$; $m_A = 1$; $k_A = k_B = 1$; $\alpha = 1$; $\gamma = 0.6$; $\beta = 0.3025$

Fig. 14 shows the unconditional instability as observed when $m_A = 100$; $m_B = 1$. Similar trend was observed for all cases where $m_A > m_B$. Fig. 15 and Fig. 16 represent the trends shown when $k_A > k_B$ and $m_B > m_A$ respectively. It is quite evident from these figures that CSS is only conditionally stable despite using stable time integration schemes.

D. Remarks

This study on the performance of the conventional staggered scheme algorithm on simple SDOF problems (with domain A as the predicting domain) has shown that:

1. for a first order system
    - Unconditional instability is seen when $m_A > m_B$.
    - Conditional stability observed when $c_A > c_B$.
    - Unconditional stability in all other cases.
2. for a second order system
    - CSS is unconditionally unstable for $m_A > m_B$.
    - Conditional stability when $m_B > m_A$.
    - Conditional stability when $k_A > k_B$.
    - Unconditional stability in rest of the cases.

CHAPTER IV

MODEL PROBLEMS IN LINEAR HEAT CONDUCTION

In this chapter, we provide example problems in linear heat conduction, and investigate the performance of the conventional staggered scheme algorithm as applied to these. We discuss the effects of subsystem sizes, and subsystem material properties on the stability and convergence of the CSS algorithm.

The governing equations, notations and definitions used in the model heat conduction problems are as described below. Let $\Omega \subseteq \mathbb{R}^{nd}$ be an open bounded domain and $\partial\Omega$ be its boundary. 'nd' is the number of spatial dimensions. The boundary is divided into two complementary regions, $\partial\Omega_D$ where Dirichlet boundary conditions, i.e. temperature is prescribed; and $\partial\Omega_N$ where Neumann boundary conditions, i.e. heat flux is prescribed, such that $\partial\Omega_D \cup \partial\Omega_N = \partial\Omega$ and $\partial\Omega_D \cap \partial\Omega_N = \emptyset$. For uniqueness, we require $\text{meas}(\partial\Omega) > 0$. We let $t \in I$ denote the time, where I is an open interval and $\mathbf{x} \in \Omega$ denotes the spatial position vector. The temperature field is denoted by u.

The governing equations for transient heat conduction are then written as:

$$\rho c_p \dot{u} - \text{div}(k \, \text{grad}[u]) = f \qquad \text{in } \Omega \times I \tag{4.1}$$

$$-k \, \text{grad}[u] \cdot \mathbf{n} = q^p(\mathbf{x}, t) \qquad \text{on } \partial\Omega_N \times I \tag{4.2}$$

$$u(\mathbf{x}, t) = u^p(\mathbf{x}, t) \qquad \text{on } \partial\Omega_D \times I \tag{4.3}$$

$$u(\mathbf{x}, 0) = u_0(\mathbf{x}) \qquad \text{in } \Omega \tag{4.4}$$

where $k > 0$ represents the material conductivity, ρ denotes the material density, c_p denotes the specific heat of the material, the superimposed dot represents the time derivative, grad denotes the gradient operator, u_0 the prescribed initial temperature,

n the unit outward normal to $\partial\Omega$, f represents the volumetric heat source, u^p the prescribed temperature on the Dirichlet boundary, q^p denotes the prescribed heat flux on the Neumann boundary. In what follows, as a couple of model problems, we discuss the effects of subsystem domain sizes and material properties by dividing the domain of interest into two sub-domains, A and B and using the coupling algorithm to obtain the overall transient response of the system. It is to be noted that domain B is the *predicting domain*, i.e. provides the initial set of predictors on the first iteration.

A. Model problem 1

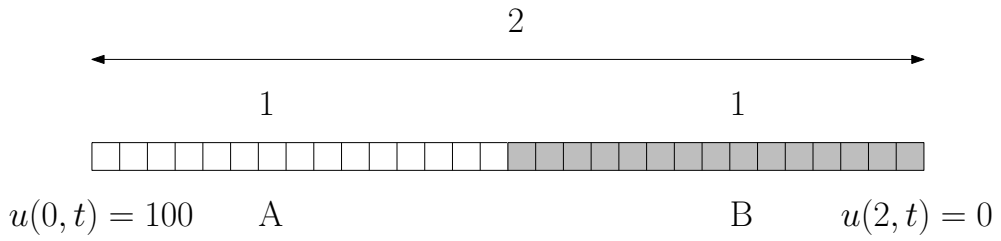

Fig. 17. Model problem 1 illustration. Domain divided into two equal sub-domains

We consider a one-dimensional linear heat conduction problem with piecewise uniform thermal conductivity, $k = 1$, uniform density $\rho = 100$, and uniform specific heat capacity $c_p = 1$. The domain $\Omega = \{x : x \in [0, 2]\}$ is divided into two sub-domains A and B. Dirichlet boundary conditions are imposed as shown in Fig. 17. Since we do not change any material properties of the sub-domains from those of the single undecomposed domain, the analytical solution for each of the cases remains the same, the following exercise essentially helps evaluate the effect of sub-domain sizes on the overall response of the system.

We consider the following cases by varying the domain sizes of A and B.

1. Sub-domain size ratio $A : B = 1 : 1$

   - $\Omega_A = \{x : x \in [0, 1]\}$ and $\Omega_B = \{x : x \in [1, 2]\}$
   - Time step size, $\Delta t = 10^{-2}$
   - Predicting domain $= B$

   Fig. 18 shows the response of the coupled domain against the analytical solution for the undecomposed domain.

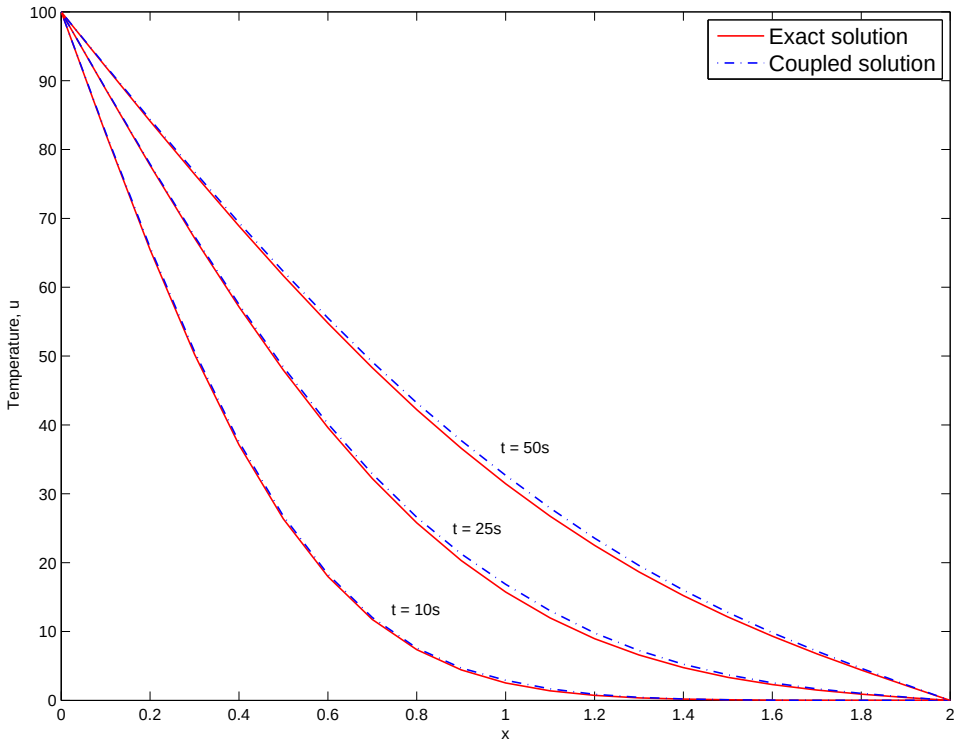

Fig. 18. The coupled response of the system plotted against the analytical solution when domain size ratio, $A : B = 1 : 1$

2. Sub-domain size ratio $A : B = 1 : 3$

   - $\Omega_A = \{x : x \in [0, 0.5]\}$ and $\Omega_B = \{x : x \in [0.5, 2]\}$
   - Time step size, $\Delta t = 10^{-2}$
   - Predicting domain $= B$

   Fig. 19 shows the response of the coupled domain against the analytical solution for the undecomposed domain.

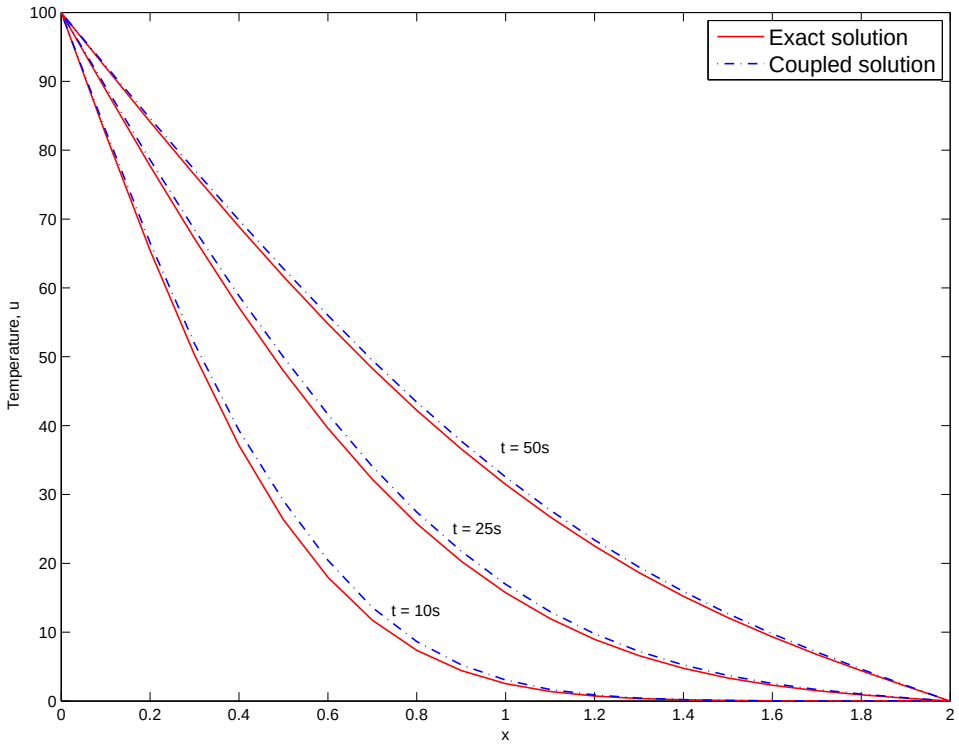

Fig. 19. The coupled response of the system plotted against the analytical solution when domain size ratio, $A : B = 1 : 3$

3. Sub-domain size ratio $A : B = 3 : 1$

   - $\Omega_A = \{x : x \in [0, 1.5]\}$ and $\Omega_B = \{x : x \in [1.5, 2]\}$
   - Time step size, $\Delta t = 10^{-2}$
   - Predicting domain $= B$

   Fig. 20 shows the response of the coupled domain against the analytical solution for the undecomposed domain.

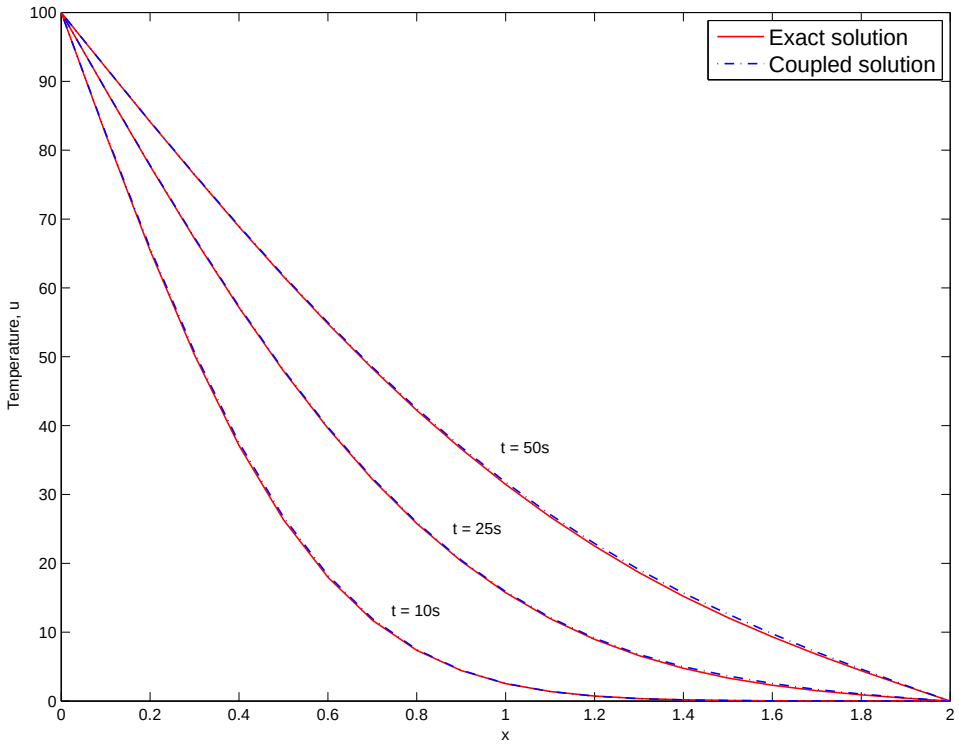

Fig. 20. The coupled response of the system plotted against the analytical solution when domain size ratio, $A : B = 3 : 1$

Convergence study for the problem shown in Fig (9) is carried out for the different cases described above. The rate of convergence with respect to the element size h is quantified via the following error norm:

$$\epsilon = \left(\int_0^L (u_{FEM} - u_{EXACT})^2 dx \right)^{1/2} \tag{4.5}$$

where the analytical response u_{EXACT} is given by [24] :

$$u_{EXACT}(x,t) = (-50x + 100) + \frac{200}{\pi^2} \sum_{n=0}^{\infty} \frac{sin(n\pi) - (n\pi)}{n^2} e^{-0.01n^2\pi^2 t/4} sin\left(\frac{n\pi x}{2}\right) \tag{4.6}$$

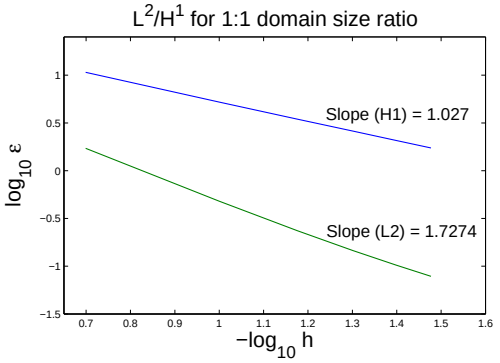

(a) $L^2 = 1.7274; H^1 = 1.0171$

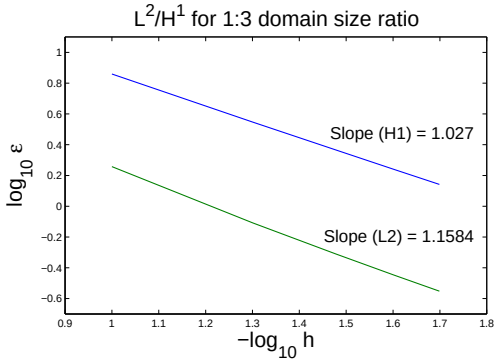

(b) $L^2 = 1.1584; H^1 = 1.027$

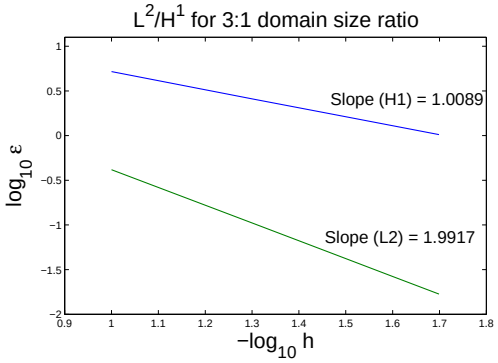

(c) $L^2 = 1.9917; H^1 = 1.0089$

Fig. 21. L^2-norm and H^1-seminorm convergence rates for the cases - $A : B = 1 : 1$ (a), $A : B = 1 : 3$ (b) and $A : B = 3 : 1$ (c)

From Figs. 18 - 20, for a given mesh size, h, and time step Δt, the absolute errors showed a dependence on the relative sizes of the two domains. Errors increase with the increase in the size of the predicting domain. The same condition held true for the convergence rates, as shown in Fig. 21. It was observed that smaller the size of the predicting domain, better the convergence rates and the accuracy of the algorithm. Another important observation here, was that the CSS coupling algorithm was stable for all choices of domain sizes made. The relative differences in the lengths of the sub-domains only affected the convergence rates, but the algorithm as such remained stable for all time step sizes tested.

B. Model problem 2

We consider the same problem of one-dimensional heat conduction as described in Fig. 17, and with the same Dirichlet boundary conditions imposed. However, the domain $\Omega = \{x : x \in [0, 2]\}$ is divided into two equal sub-domains A and B such that $\Omega_A = \{x : x \in [0, 1]\}$ and $\Omega_B = \{x : x \in [1, 2]\}$. Different cases are considered by changing the material properties. As in the previous case, sub-domain B is the predicting domain, i.e. provides the first set of predictors in the CSS algorithm.

We consider the following four cases by varying the material conductivities of the sub-domains, i.e. k_A and k_B.

1. $k_A = 2, k_B = 1$

   Keeping the other material properties constant, i.e. $\rho_A = \rho_B = 100, c_{p_A} = c_{p_B} = 1$; performance of the CSS algorithm was evaluated by varying the element size h, and the time step Δt. It was observed that the coupling algorithm remained unconditionally stable for all combinations of element sizes and time steps. Fig. 22 shows the temperature profile for this test case, and that the CSS is stable

for all time steps chosen.

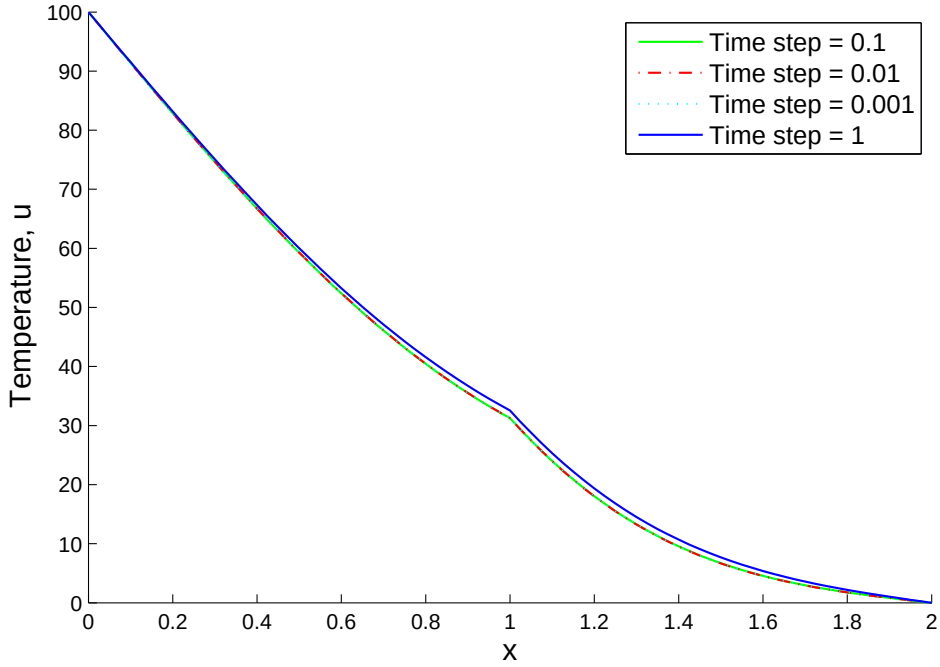

Fig. 22. Temperature profile for the coupled problem at $t = 20$ with element size, $h = 0.025$ plotted for varying time steps. The material properties are: $k_A = 2, k_B = 1, \rho_A = 100, \rho_B = 100$

2. $k_A = 1, k_B = 2$

   The other material properties being kept constant, i.e. $\rho_A = \rho_B = 100, c_{p_A} = c_{p_B} = 1$, and varying the times steps and element sizes, instability was observed for certain element sizes at different time steps. For a given choice of element size h, this test scenario showed that CSS was conditionally stable for different time steps. Table III shows the critical time steps for various element sizes, above which the CSS proved to be unstable. Fig. 23 shows a stable temperature profile, while Fig. 24 shows instability for a time step greater than $\Delta t = 0.1$.

Table III. Stability and critical time steps for $k_A = 1, k_B = 2$

No. of elements, 'Nele'	Element size, h	Critical time step, Δt
10	0.1	Stable
20	0.05	0.5 - 0.6
40	0.025	0.1 - 0.2
100	0.01	0.02 - 0.03
200	0.005	0.005 - 0.006

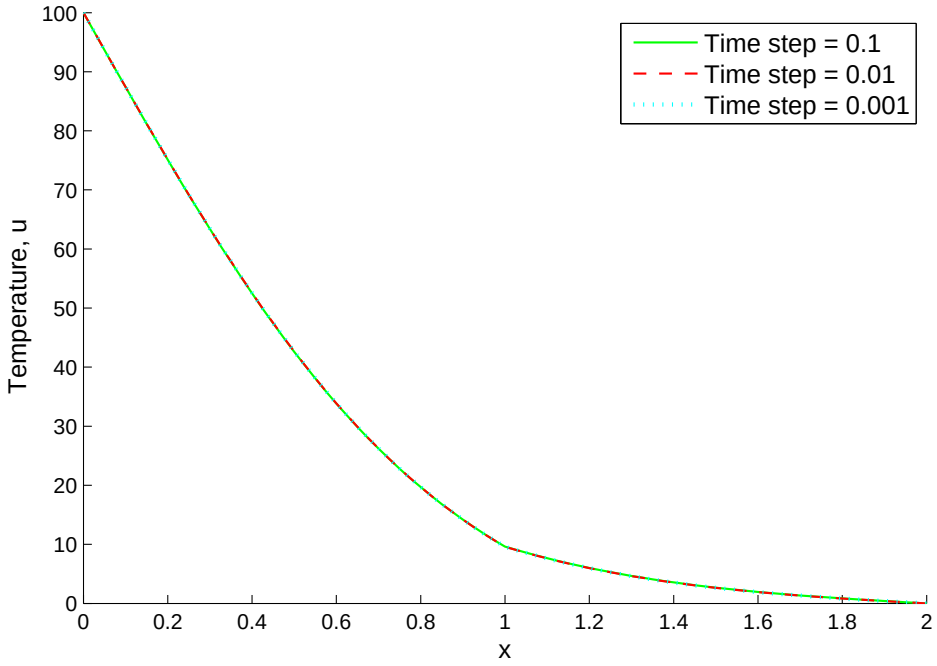

Fig. 23. Temperature profile for the coupled problem at $t = 20$ with element size, $h = 0.025$ plotted for varying time steps. The material properties are: $k_A = 1, k_B = 2, \rho_A = 100, \rho_B = 100$

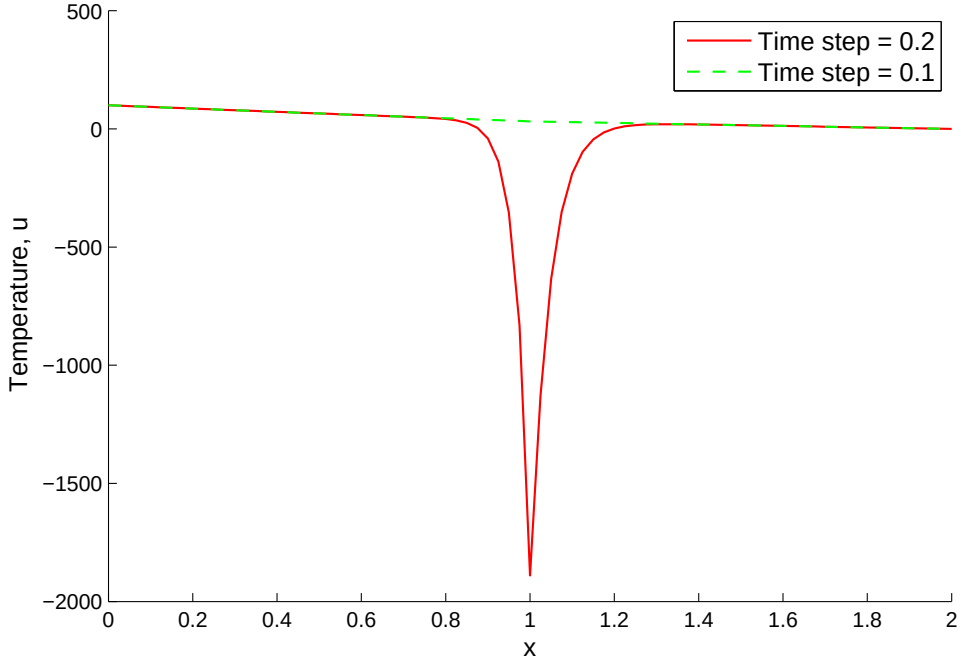

Fig. 24. Temperature profile for the coupled problem at $t = 20$ with element size, $h = 0.025$ plotted for varying time steps. The material properties are: $k_A = 1, k_B = 2, \rho_A = 100, \rho_B = 100$. Notice instability at $\Delta t = 0.2$

3. $k_A = 1, k_B = 10$

   This test case, similar to case 2, had similar results of conditional stability. It was observed though, that for the same element sizes considered as in case 2, the critical time steps were far smaller than those observed in case 2, indicating that instability is more apparent at larger differences in k_B and $k_A, (k_B > k_A)$. The table IV shows the element sizes and the respective critical time steps. Fig. 25 and Fig. 26 respectively, show the stable and unstable cases for the element size $h = 0.025$.

Table IV. Stability and critical time steps for $k_A = 1, k_B = 10$

No. of elements, 'Nele'	Element size, h	Critical time step, Δt
10	0.1	0.08 - 0.09
20	0.05	0.02 - 0.03
40	0.025	0.005 - 0.006
100	0.01	Unstable for 0.0001
200	0.005	Unstable for 0.0001

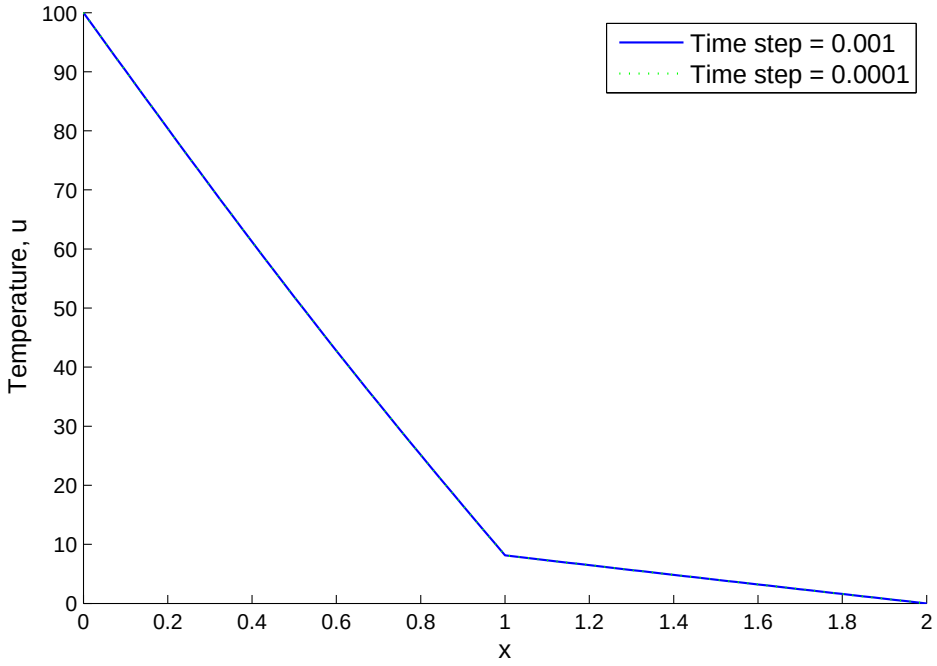

Fig. 25. Temperature profile for the coupled problem at $t = 20$ with element size, $h = 0.025$ plotted for varying time steps. The material properties are: $k_A = 1, k_B = 10, \rho_A = 100, \rho_B = 100$

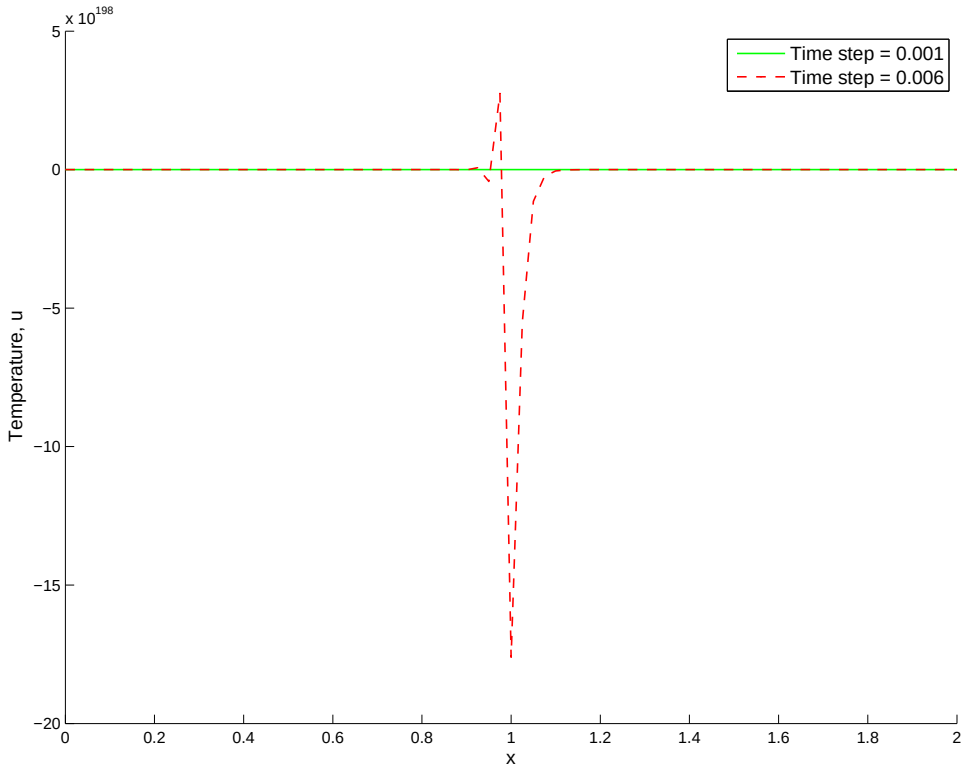

Fig. 26. Temperature profile for the coupled problem at $t = 20$ with element size, $h = 0.025$ plotted for varying time steps. The material properties are: $k_A = 1, k_B = 10, \rho_A = 100, \rho_B = 100$. Notice instability at $\Delta t = 0.006$

4. $k_A = 10, k_B = 1$

   Similar to the case 1 above, there was no observed instability for any choice of element size or time step. Fig. 27 shows the case with element size $h = 0.025$ plotted for various time steps. Unconditional stability is observed for any choice of element size or time step.

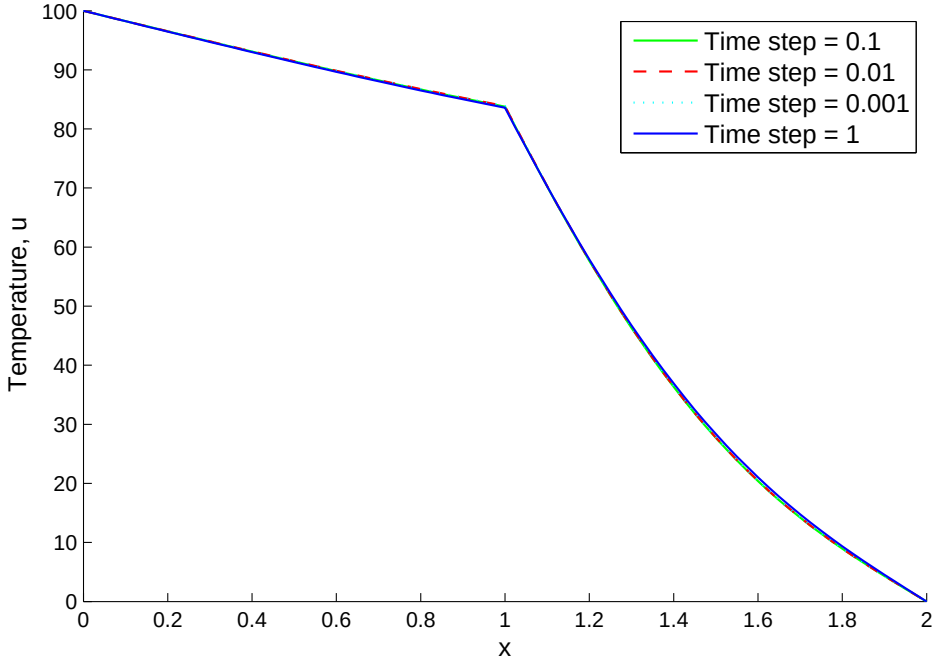

Fig. 27. Temperature profile for the coupled problem at $t = 20$ with element size, $h = 0.025$ plotted for varying time steps. The material properties are: $k_A = 10, k_B = 1, \rho_A = 100, \rho_B = 100$. Stability observed at all time steps

Figs. 22 - 27 show the temperature profiles for the four cases discussed. Numerous test cases were run by changing the relative sizes of the sub-domain conductivities, k_A and k_B. Cases considered, where $k_A > k_B$, or $k_A < k_B$, time steps were varied from $\Delta t = 1$ to $\Delta t = 10^{-4}$ and the mesh size from $h = 0.005$ to $h = 0.1$. In all cases where $k_A > k_B$, the temperature profile showed trends similar to that shown by Fig. 22 and Fig. 27. Results were absolutely stable for any mesh size chosen, and for any choice of the time step.

However, cases where $k_A < k_B$ (i.e., where the material conductivity of the predicting domain was larger than that of the other sub-domain,) mixed results were obtained. At any given mesh size, a critical time step was observed, when stability

broke. Use of any time step larger than this critical time step, shown in Table III and Table IV, resulted in instability, i.e. the solution grew unbounded with time (as shown in Fig. 24 and Fig. 26). The conditional stability of the algorithm is quite evident from this analysis. Similar results are seen by varying the density of the material of the sub-domains, i.e. conditional stability is observed in cases where $\rho_B > \rho_A$. This is shown in the following test cases, Fig.29 and Fig. 31. Fig. 28 and Fig. 30, however, show the stable region of the CSS, i.e., stability observed at smaller time steps. We consider the following four cases by varying the material densities of the sub-domains, i.e. ρ_A and ρ_B.

1. $\rho_A = 10, \rho_B = 20$

   Material properties kept constant, i.e. $k_A = k_B = 1, c_{pA} = c_{pB} = 1$; performance of CSS is evaluated by varying the element size h, and the time step Δt. Table V shows the critical time steps for the element sizes.

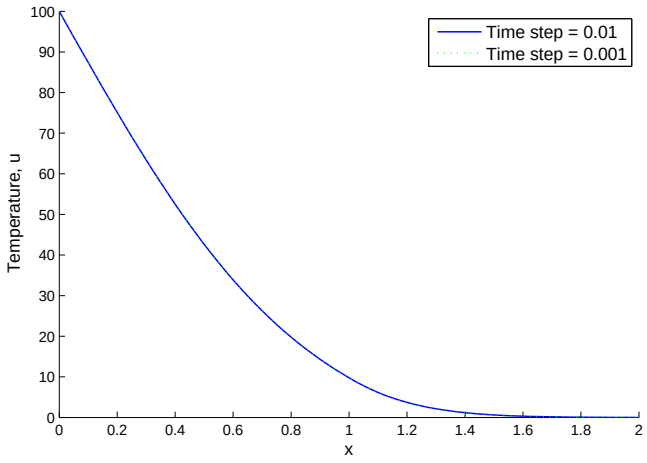

Fig. 28. Temperature profile for the coupled problem at $t = 5$ with element size, $h = 0.025$ plotted for varying time steps. The material properties are: $\rho_A = 10, \rho_B = 20, k_A = 1, k_B = 1$

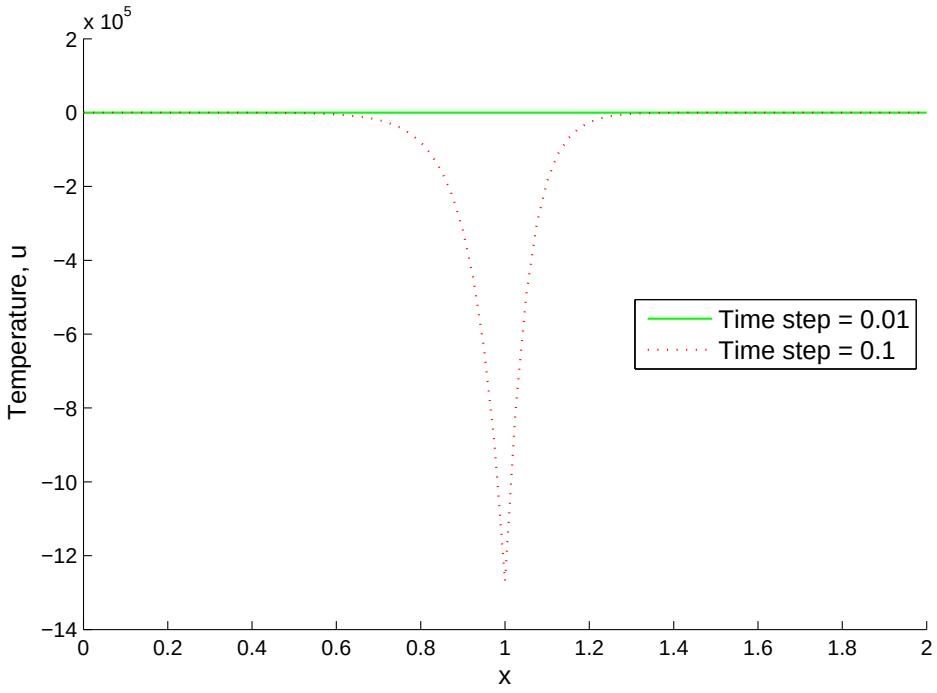

Fig. 29. Temperature profile for the coupled problem at $t = 20$ with element size, $h = 0.025$ plotted for varying time steps. The material properties are: $\rho_A = 10, \rho_B = 20, k_A = 1, k_B = 1$. Notice instability at $\Delta t = 0.1$

Table V. Stability and critical time steps for $\rho_A = 10, \rho_B = 20$

No. of elements, 'Nele'	Element size, h	Critical time step, Δt
10	0.1	0.7 - 0.8
20	0.05	0.1 - 0.2
40	0.025	0.04 - 0.05
100	0.01	0.007 - 0.008

2. $\rho_A = 10, \rho_B = 40$

The following table VI proves conditional stability of the above test case.

Table VI. Stability and critical time steps for $\rho_A = 10, \rho_B = 40$

No. of elements, 'Nele'	Element size, h	Critical time step, Δt
10	0.1	0.2 - 0.3
20	0.05	0.07 - 0.08
40	0.025	0.01 - 0.02
100	0.01	0.002 - 0.003

3. $\rho_A = 10, \rho_B = 100$

   The table VII shows the element sizes and the respective critical time steps indicating conditional stability for the test case.

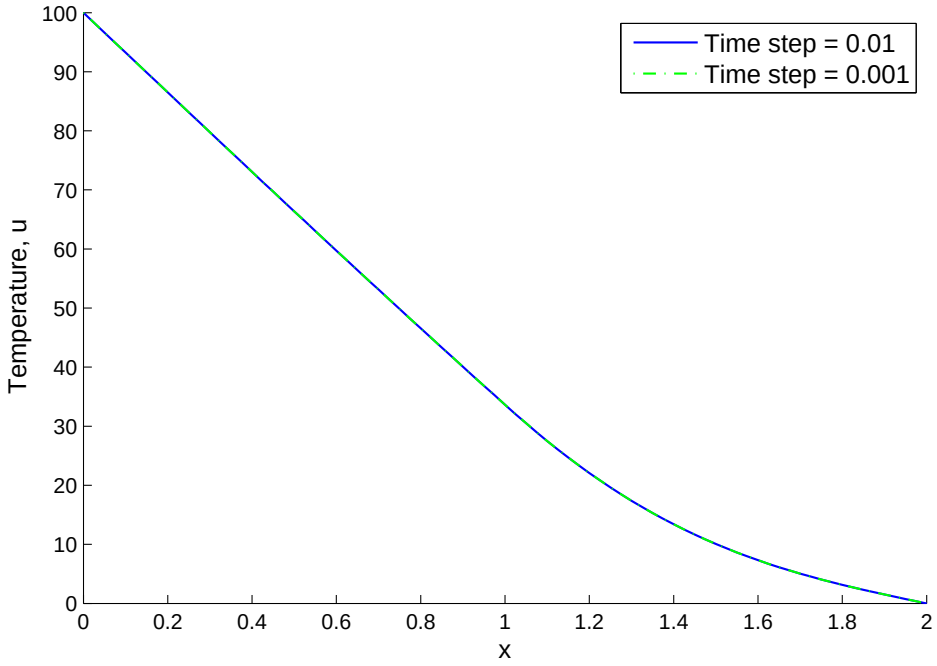

Fig. 30. Temperature profile for the coupled problem at $t = 5$ with element size, $h = 0.025$ plotted for varying time steps. The material properties are: $\rho_A = 10, \rho_B = 100, k_A = 1, k_B = 1$

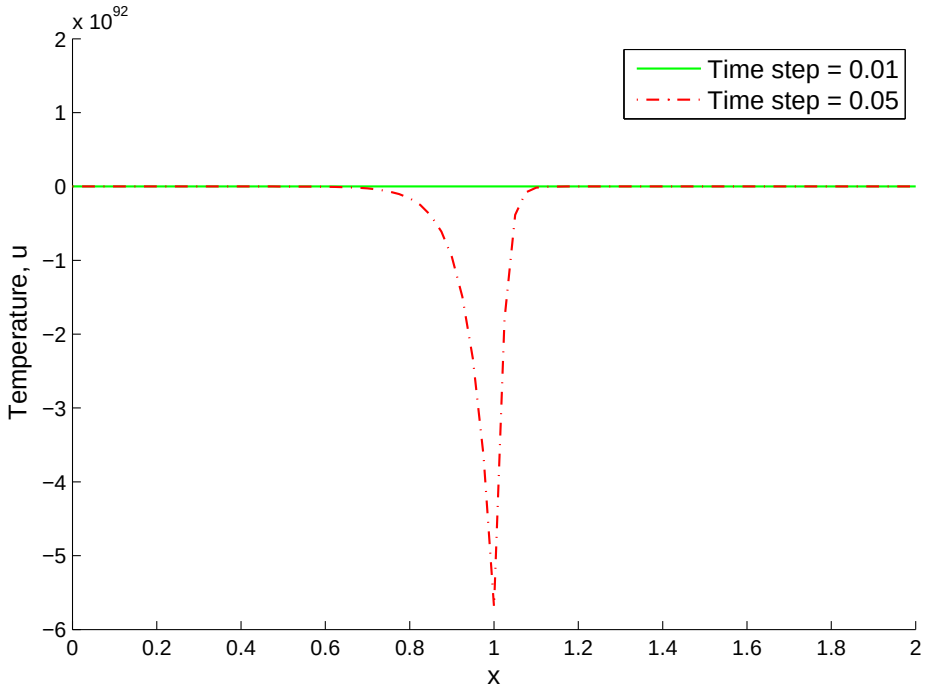

Fig. 31. Temperature profile for the coupled problem at $t = 20$ with element size, $h = 0.025$ plotted for varying time steps. The material properties are: $\rho_A = 10, \rho_B = 100, k_A = 1, k_B = 1$. Notice instability at $\Delta t = 0.1$

Table VII. Stability and critical time steps for $\rho_A = 10\rho_B = 100$

No. of elements, 'Nele'	Element size, h	Critical time step, Δt
10	0.1	0.1 - 0.2
20	0.05	0.04 - 0.05
40	0.025	0.01 - 0.02
100	0.01	0.001 - 0.002

4. $\rho_A > \rho_B$

Simulations with the magnitude of material density of the predicting domain

(ρ_B), lesser than that of the other domain, showed unconditional stability for any choice of element size, h and time step Δt. Fig. 32 shows the case where the density of the predicting domain is lesser than that of the iterating domain.

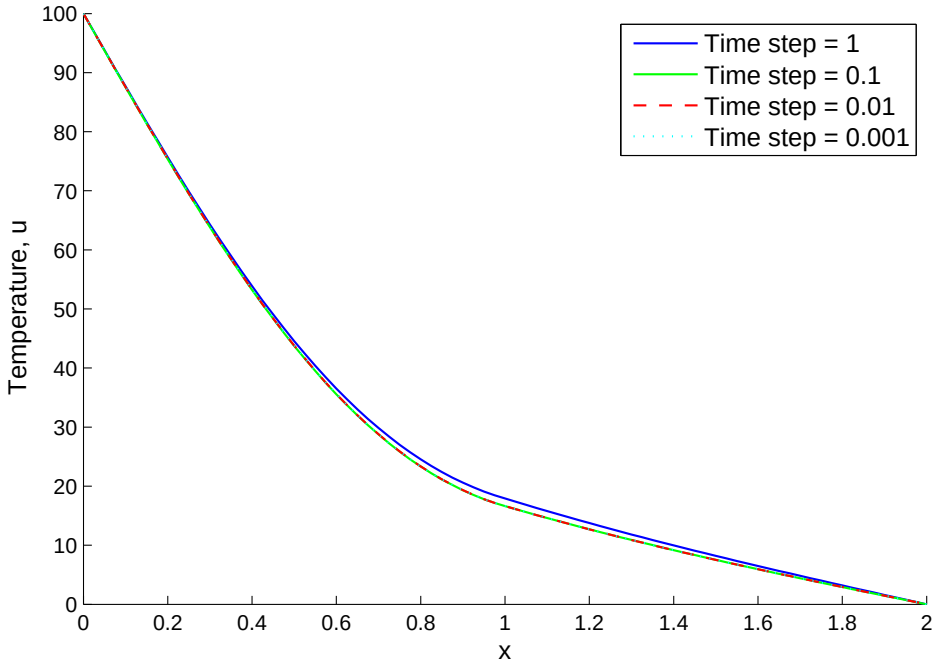

Fig. 32. Temperature profile for the coupled problem at $t = 20s$ with element size, $h = 0.025$ plotted for varying time steps. The material properties are: $\rho_A = 10, \rho_B = 100, k_A = 1, k_B = 1$. Unconditional stability observed for any time step chosen

C. Model problem 3

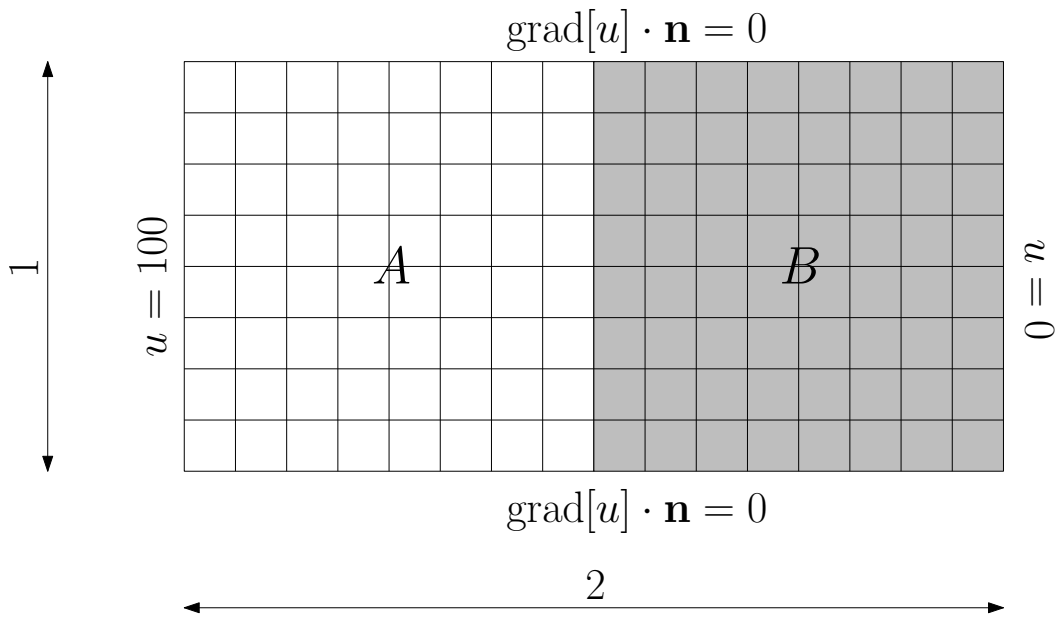

Fig. 33. Model problem 3 illustration. Domain divided into two equal sub-domains

We consider a two-dimensional linear heat conduction problem with piecewise uniform thermal conductivity, $k = 1$, uniform density $\rho = 100$, and uniform specific heat capacity $c_p = 1$. The domain $\Omega = \{(x, y) : x \in [0, 2], y \in [0, 1]\}$ is divided into two sub-domains A and B. Dirichlet boundary conditions are imposed as shown in Fig. 33. Since we do not change any material properties of the sub-domains from those of the single undecomposed domain, the analytical solution for each of the cases remains the same, the following exercise essentially helps evaluate the effect of sub-domain sizes on the overall response of the system.

We consider the following cases by varying the domain sizes of A and B.

1. Sub-domain size ratio $A : B = 1 : 3$

   - $\Omega_A = \{(x, y) : x \in [0, 1.5], y \in [0, 1]\}$ and $\Omega_B = \{(x, y) : x \in [1.5, 2], y \in [0, 1]\}$.
   - Predicting domain $= B$
   - Time step size, $\Delta t = 10^{-2}$.

2. Sub-domain size ratio $A : B = 3 : 1$

   - $\Omega_A = \{(x, y) : x \in [0, 0.5], y \in [0, 1]\}$ and $\Omega_B = \{(x, y) : x \in [0.5, 2], y \in [0, 1]\}$.
   - Predicting domain $= B$
   - Time step size, $\Delta t = 10^{-2}$.

3. Sub-domain size ratio $A : B = 1 : 1$

   - $\Omega_A = \{(x, y) : x \in [0, 1], y \in [0, 1]\}$ and $\Omega_B = \{(x, y) : x \in [1, 2], y \in [0, 1]\}$.
   - Predicting domain $= B$
   - Time step size, $\Delta t = 10^{-2}$.

Fig. 34 below shows the temperature contour plots for the cases discussed. The plots look similar and vary only in the terminal rates of convergence that are observed.

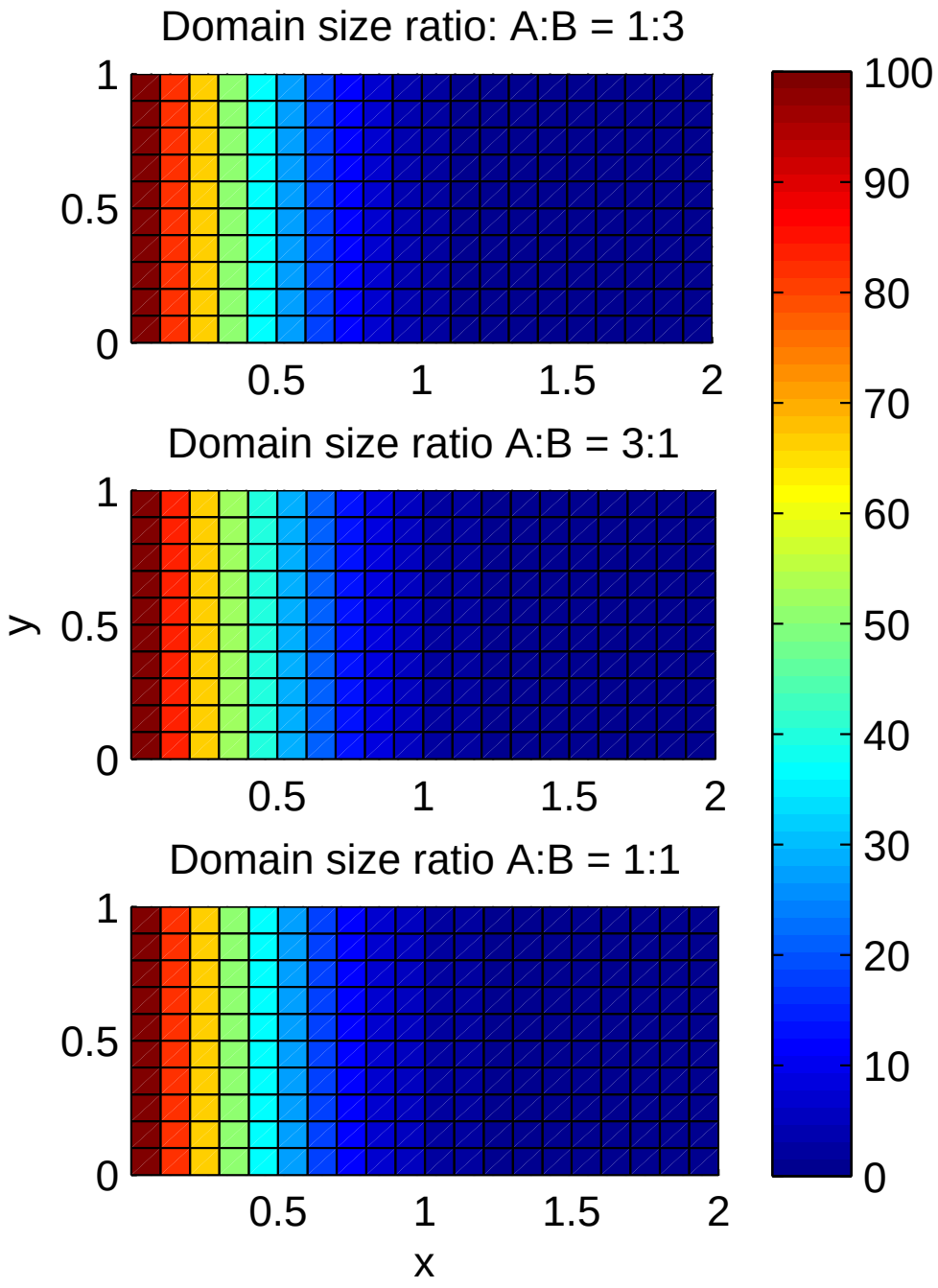

Fig. 34. The coupled response of the system for the various domain size ratios

Convergence study for the problem shown in Fig. 33 is carried out for the different cases described above.

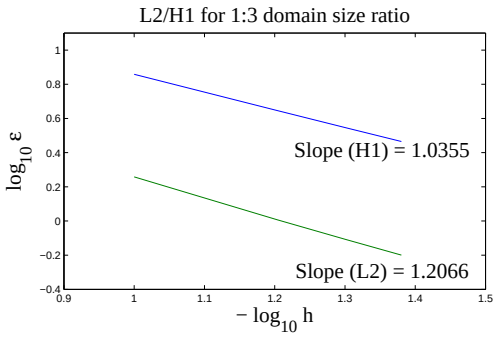

(a) $L^2 = 1.2066; H^1 = 1.0355$

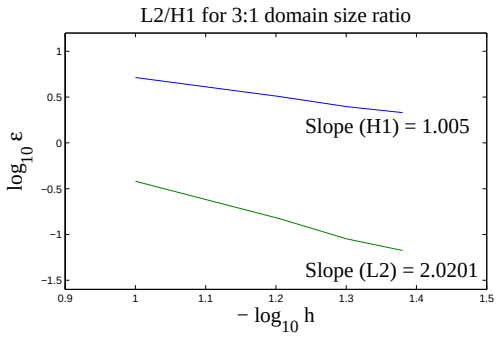

(b) $L^2 = 1.005; H^1 = 2.0201$

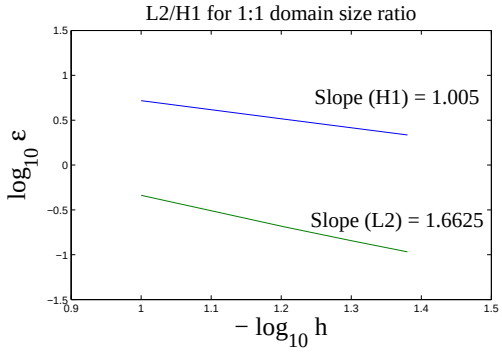

(c) $L^2 = 1.005; H^1 = 1.6625$

Fig. 35. L^2-norm and H^1-seminorm convergence rates for the cases - $A : B = 1 : 3$ (a), $A : B = 3 : 3$ (b) and $A : B = 1 : 1$ (c)

It is seen through the convergence studies, Fig. 35, the relative sizes of the sub-domains affect the absolute errors and the rates of convergence for the CSS algorithm for any given mesh size and time step. Smaller sizes of the predicting domain, showed better convergence rates which is similar to what was observed for Model problem 1. The relative sizes of the domain did not, however, affect the stability of the algorithm, as it was found to be stable under all test cases discussed.

CHAPTER V

CONCLUSIONS AND FUTURE DIRECTIONS

A. Conclusion

A systematic and fairly comprehensive investigation of the stability of the *conventional staggered scheme* coupling algorithm is made. It is seen that a complete study of the stability of coupling algorithms requires one to understand the complex interplay of not only the stability of the time integrators used, but also the effect of material properties on the overall response of the system. In this current investigation, through the analysis of split single-degree-of-freedom problems, we arrived at general response characteristics of the CSS algorithm when the two subsystems of a coupled system have different material properties. By implementing the algorithm to model heat conduction problems, a detailed study of the performance of the CSS algorithm was performed. Since analytical solutions are rarely available for coupled problems, numerical simulations seem to be the only way to understand the behavior of these systems, and hence stability of the coupling algorithms proves to be of utmost importance and this work provides those first steps towards understanding the behavior of the algorithm. Based on the model problem simulations, the following conclusions can be arrived at:

- The conventional staggered scheme is not a symmetric coupling algorithm, i.e., the overall response of the system depends on the domains which are iterated first, and the domains that predict first.

- The CSS coupling algorithm is conditionally stable, i.e., using an unconditionally stable time integrator does not guarantee an unconditionally stable response of the coupled system.

- The CSS coupling algorithm is also unstable with respect to an unconditionally stable predictor [5] used.

- The size of the predicting domain dictates the terminal convergence rates of the analysis procedure used, i.e., the smaller the size of the predicting domain, better the convergence rates.

- The material properties of the predicting domain play a very important role in the stability of the coupling algorithm; larger material properties (in case of similar fields for subsystems) tend to destabilize the coupling algorithm.

This assessment of the performance characteristics of the CSS algorithm based on simple canonical problems can be adaptively utilized in coupling real world problems. It is easy to observe that in the case of Fluid-Structure Interaction, having the fluid domain predict could make the CSS algorithm stable as opposed to having the structure domain predict, since the material property of the structure, namely rigidity, is greater than it is in fluids.

B. Scope for future work

Comprehensive studies of several staggered algorithms could be performed. Coupling algorithms with corrective steps within an iteration could be analyzed. There are numerous stable predictors, and the stability of these along with the effects due to material properties could be studied. A more detailed mathematical analysis addressing the effects due to material properties could provide a greater insight into the behavior of the coupling algorithms.

REFERENCES

[1] C.A. Felippa, K.C. Park, and C. Farhat, "Partitioned analysis of coupled mechanical systems," *Computer Methods in Applied Mechanics and Engineering*, vol. 190, pp. 3247–3270, 2001.

[2] C.A. Felippa and K.C. Park, "Staggered transient analysis procedures for coupled mechanical systems: formulation," *Computer Methods in Applied Mechanics and Engineering*, vol. 24, pp. 61–111, 1980.

[3] G.P. Guruswamy, "Interaction of fluids and structures for aircraft applications," *Computers & Structures*, vol. 30, pp. 1–13, 1988.

[4] S. Piperno, "Explicit/implicit fluid/structure staggered procedures with a structural predictor and fluid subcycling for 2D inviscid aeroelastic simulations," *International Journal for Numerical Methods in Fluids*, vol. 25, pp. 1207–1226, 1997.

[5] K.C. Park, "Partitioned transient analysis procedures for coupled-field problems: stability analysis," *Journal of Applied Mechanics - Transactions of the ASME*, vol. 47, pp. 370–376, 1980.

[6] T.J.R. Hughes, *The Finite Element Method: Linear Static and Dynamic Finite Element Analysis*, New York: Dover Publications, 2000.

[7] J.N. Reddy, *An Introduction to the Finite Element Method*, New York: McGraw-Hill, 1993.

[8] S.C. Brenner and L.R. Scott, *The Mathematical Theory of Finite Element Methods*, New York: Springer Verlag, 2008.

[9] D. Braess, *Finite Elements: Theory, Fast Solvers and Applications in Solid Mechanics*, Cambridge: Cambridge University Press, 2001.

[10] T.J.R. Hughes and W.K. Liu, "Implicit-explicit finite elements in transient analysis. I- Stability theory. II- Implementation and numerical examples," *Journal of Applied Mechanics - Transactions of the ASME*, vol. 45, pp. 371–378, 1978.

[11] T. Belytschko, H.J. Yen, and R. Mullen, "Mixed methods for time integration," *Computer Methods in Applied Mechanics and Engineering*, vol. 17, pp. 259–275, 1979.

[12] T. Belytschko and R. Mullen, "Explicit integration of structural problems," *in Proc. of the International Conference, Finite Elements in Nonlinear Mechanics, Geilo, Norway*, pp. 697–720, 1978.

[13] W.K. Liu and T. Belytschko, "Mixed-time implicit-explicit finite elements for transient analysis," *Computers & Structures*, vol. 15, pp. 445–450, 1982.

[14] W.L. Wood, *Practical Time-stepping Schemes*, Oxford: Clarendon Press, 1990.

[15] T. Belytschko and R. Mullen, "Mesh partitions of explicit-implicit time integration," *in Formulations and Computational Algorithms in Finite Element Analysis, Bathe, K.J., Oden J.T.and Wunderlich, W., (eds.), MIT Press, Cambridge, MA*, pp. 673–690, 1976.

[16] T. Belytschko and R. Mullen, "Stability of explicit-implicit mesh partitions in time integration," *International Journal for Numerical Methods in Engineering*, vol. 12, pp. 1575–1586, 1978.

[17] F.F. Felker, "Direct solution of two-dimensional Navier-Stokes equations for static aeroelasticity problems," *AIAA Journal*, vol. 31, pp. 148–153, 1993.

[18] O. Ghattas and X. Li, "A variational finite element method for stationary nonlinear fluid–solid interaction," *Journal of Computational Physics*, vol. 121, pp. 347–356, 1995.

[19] S. Piperno, "Staggered time integration methods for a one-dimensional Euler aeroelastic problem," *Rapport de Recherche CERMICS*, vol. 94-33, pp. 1–42, 1994.

[20] M.B. Giles, "Stability analysis of numerical interface conditions in fluid-structure thermal analysis," *International Journal for Numerical Methods in Fluids*, vol. 25, pp. 421–436, 1997.

[21] M.B. Giles, "Stability and accuracy of numerical boundary conditions in aeroelastic analysis," *International Journal for Numerical Methods in Fluids*, vol. 24, pp. 739–757, 1997.

[22] B.B. Prananta and M.H.L. Hounjet, "Aeroelastic simulation with advanced CFD methods in 2-D and 3-D transonic flow," *in Proc. of the Unsteady Aerodynamics Conference, London, United Kingdom*, pp. 7.1–7.16, 1996.

[23] R.M.M. Mattheij and J. Molenaar, *Ordinary Differential Equations in Theory and Practice*, Chichester: John Wiley & Sons, 1996.

[24] H.S. Carslaw and J.C. Jaeger, *Conduction of Heat in Solids*, Oxford: Clarendon Press, 1959.

APPENDIX A

SOME NUMERICAL EXAMPLES

Results - trends for conventional staggered scheme

First order system: Midpoint rule with *no* α dissipation

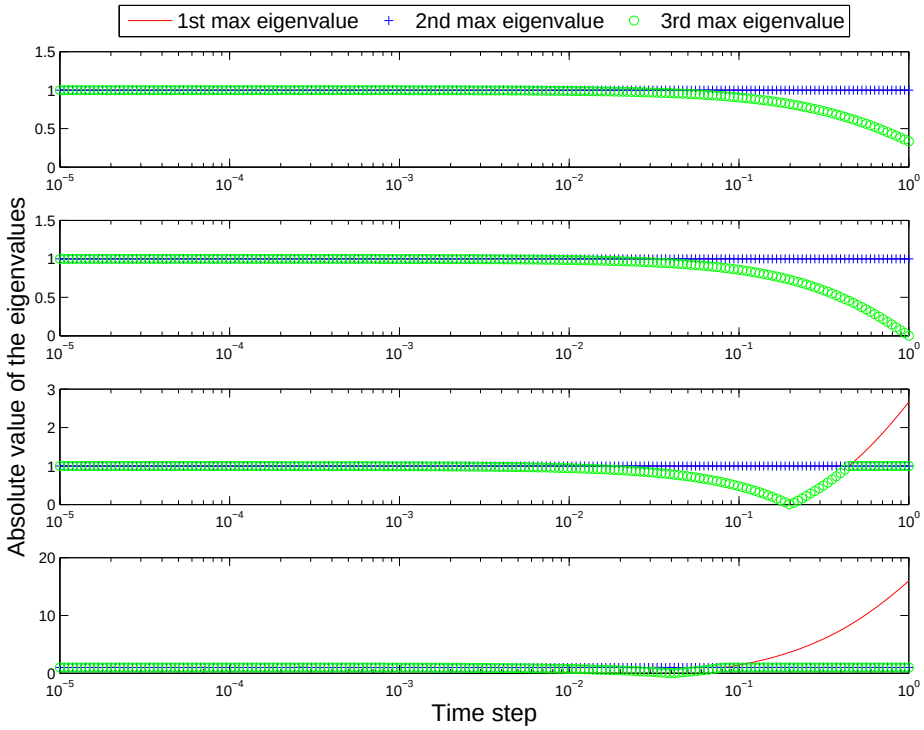

Fig. 36. $m_A = 1, m_B = 1, c_B = 1, c_A = 1, 2, 10, 50, \alpha = 1$

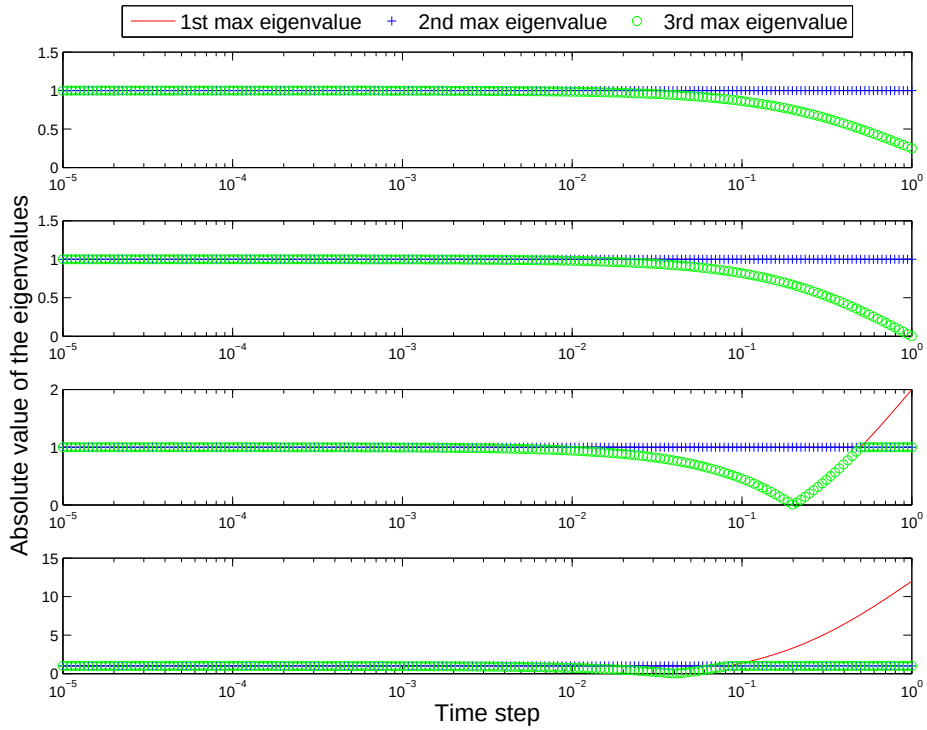

Fig. 37. $m_A = 1, m_B = 1, c_B = 2, c_A = 1, 2, 10, 50, \alpha = 1$

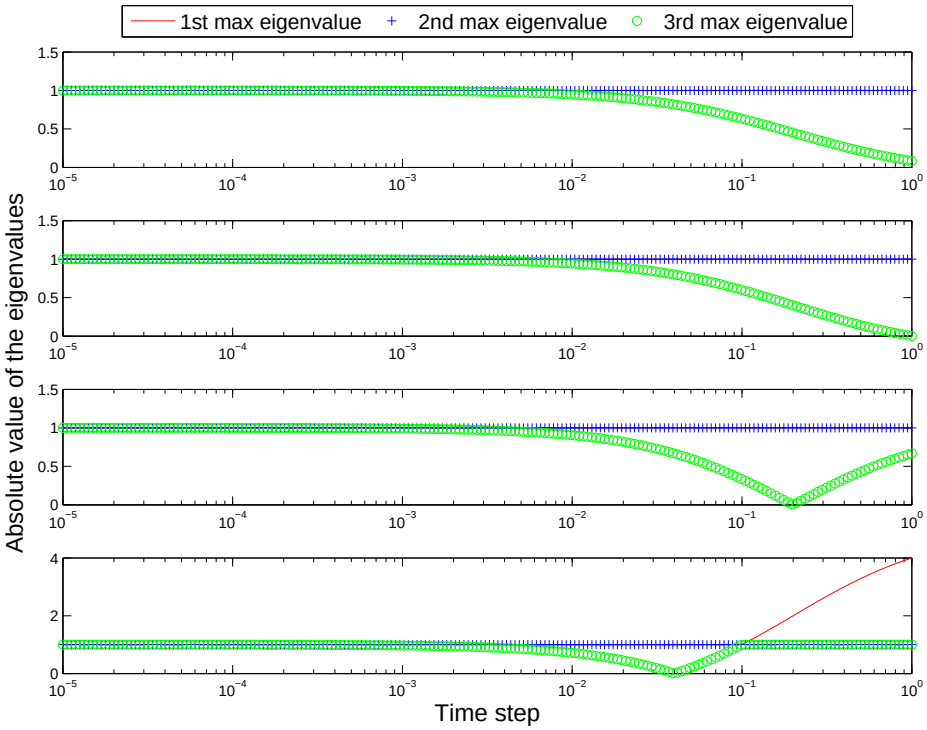

Fig. 38. $m_A = 1, m_B = 1, c_B = 10, c_A = 1, 2, 10, 50, \alpha = 1$

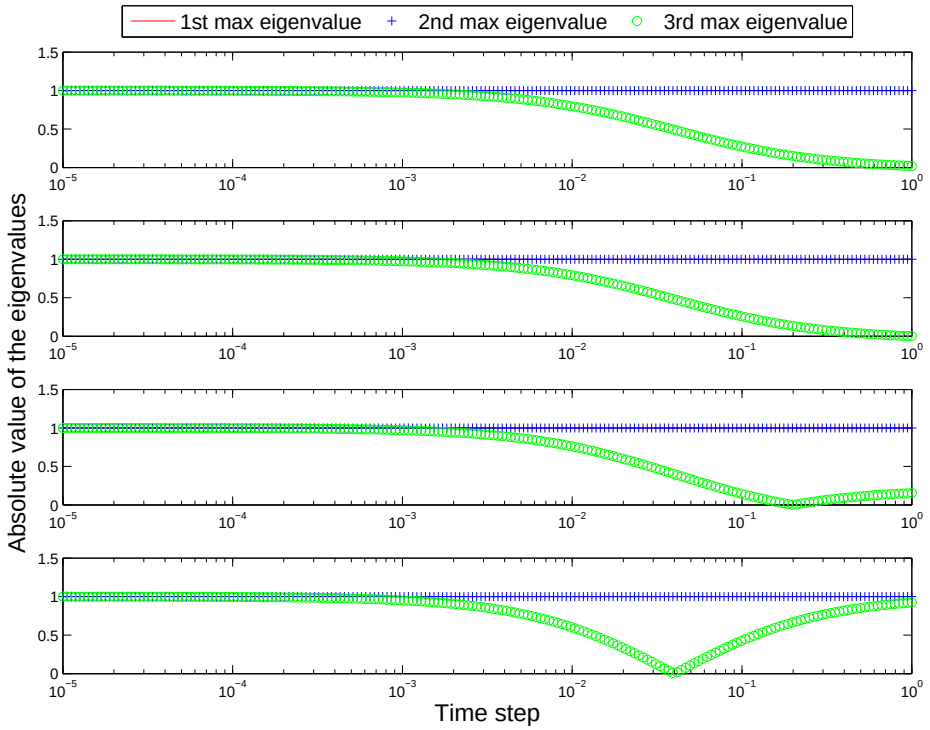

Fig. 39. $m_A = 1, m_B = 1, c_B = 50, c_A = 1, 2, 10, 50, \alpha = 1$

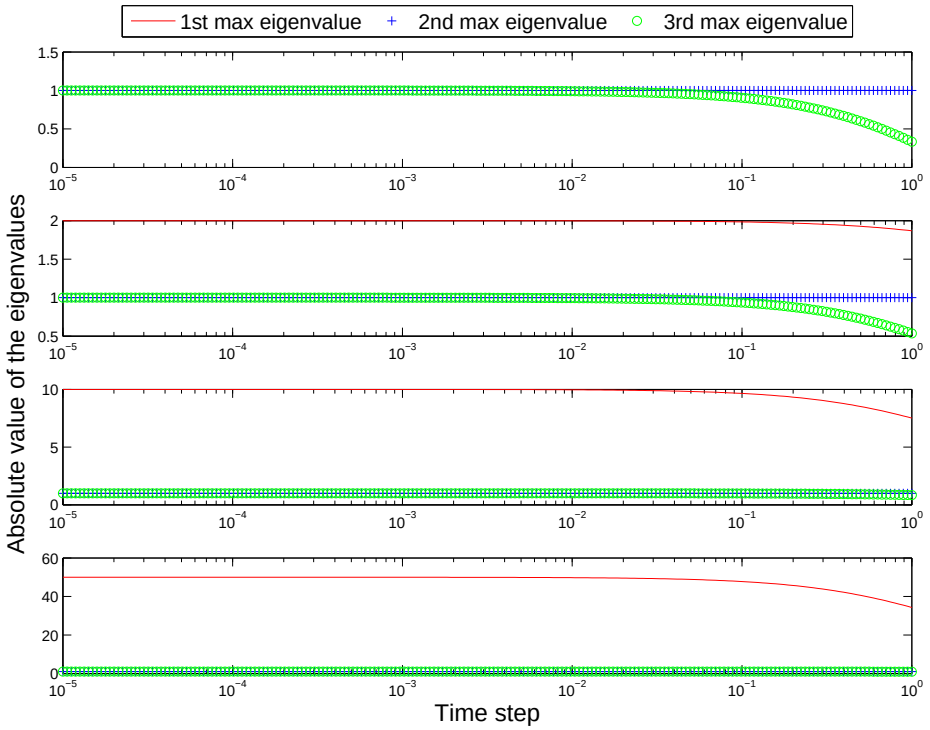

Fig. 40. $c_A = 1, c_B = 1, m_B = 1, m_A = 1, 2, 10, 50, \alpha = 1$

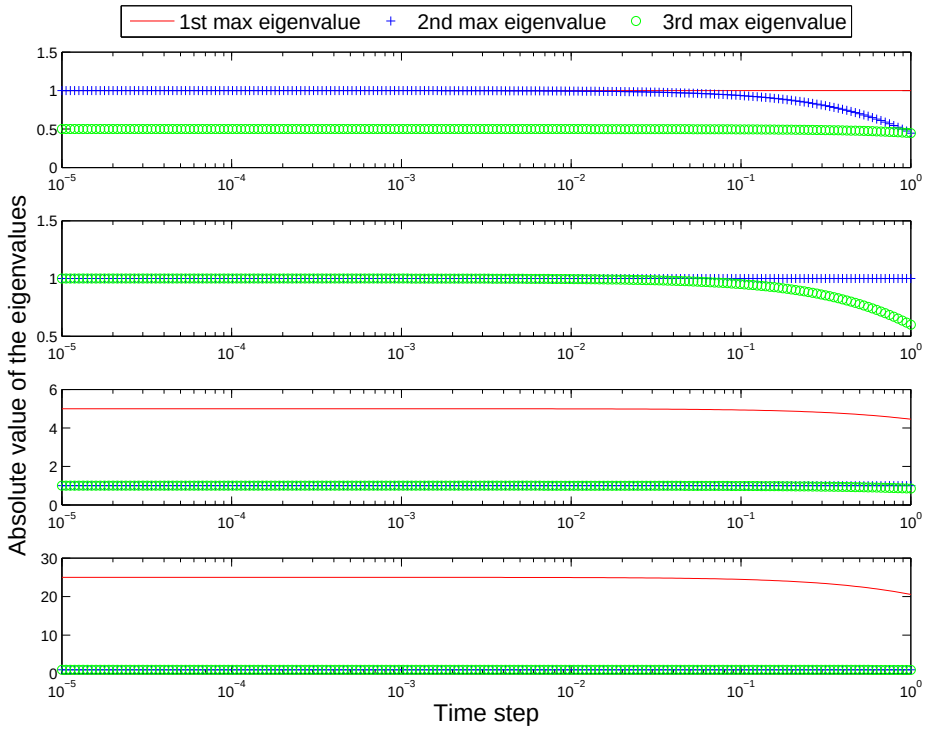

Fig. 41. $c_A = 1, c_B = 1, m_B = 2, m_A = 1, 2, 10, 50, \alpha = 1$

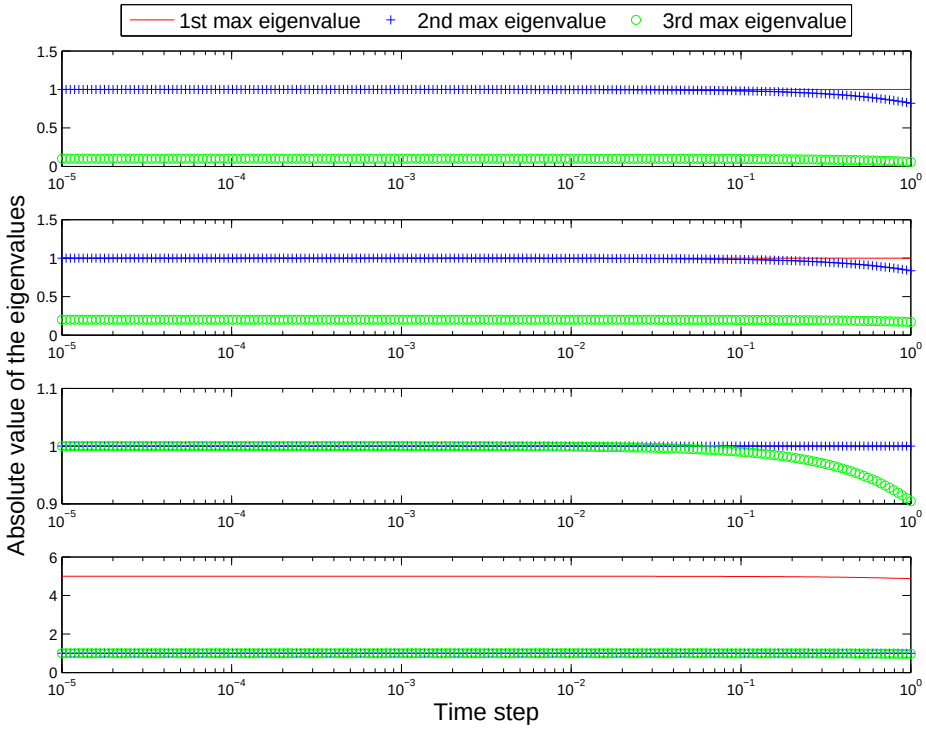

Fig. 42. $c_A = 1, c_B = 1, m_B = 10, m_A = 1, 2, 10, 50, \alpha = 1$

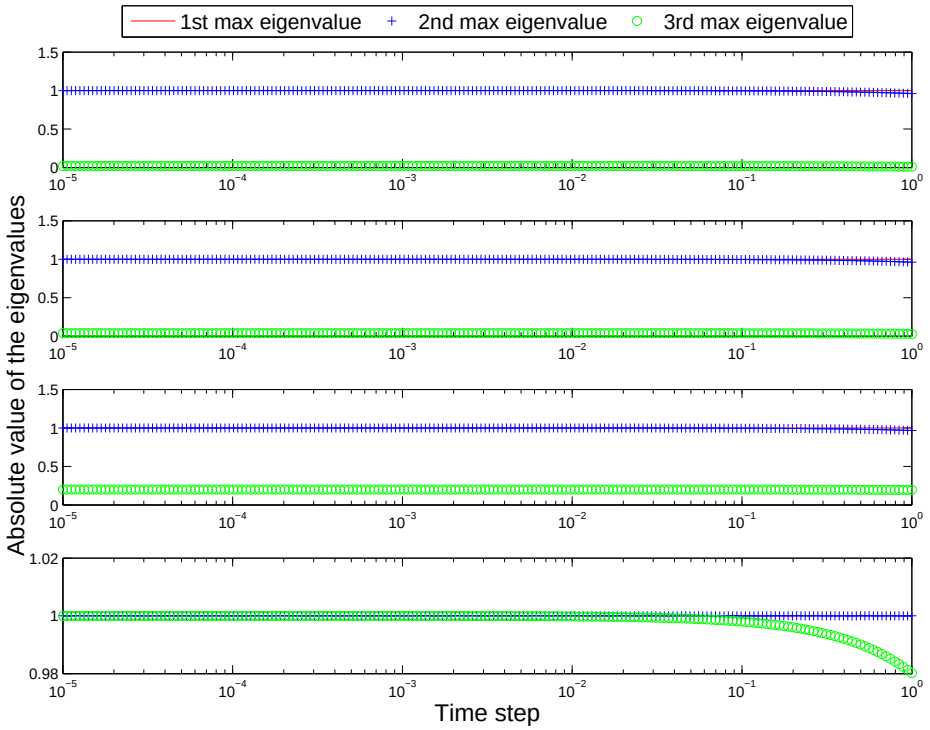

Fig. 43. $c_A = 1, c_B = 1, m_B = 50, m_A = 1, 2, 10, 50, \alpha = 1$

First order system: Midpoint rule *with* α dissipation

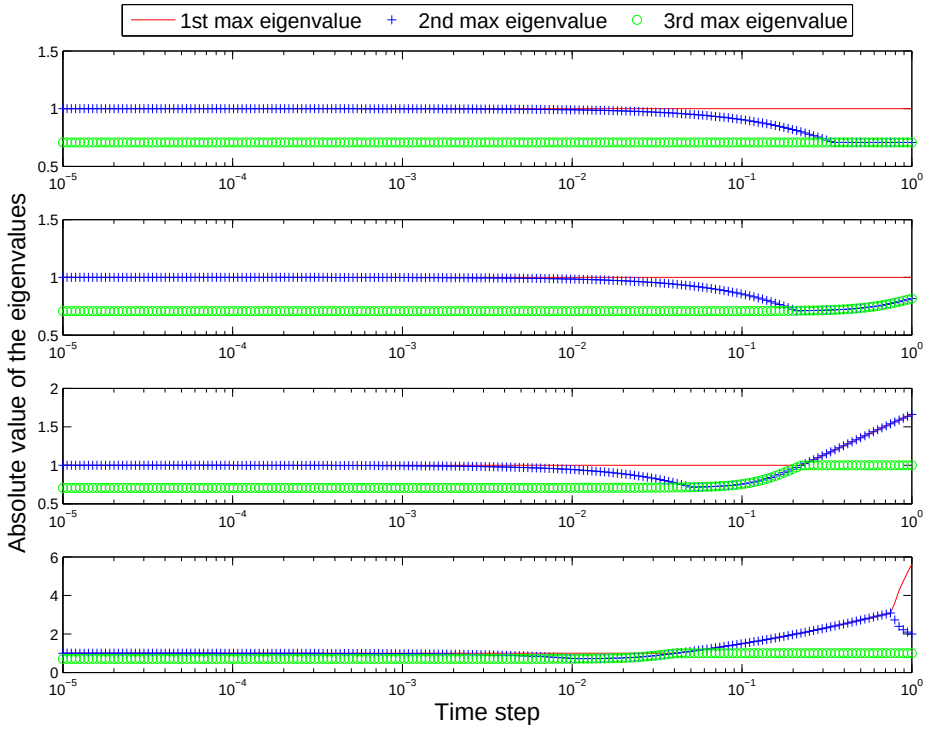

Fig. 44. $m_A = 1, m_B = 1, c_B = 1, c_A = 1, 2, 10, 50, \alpha = 0.5$

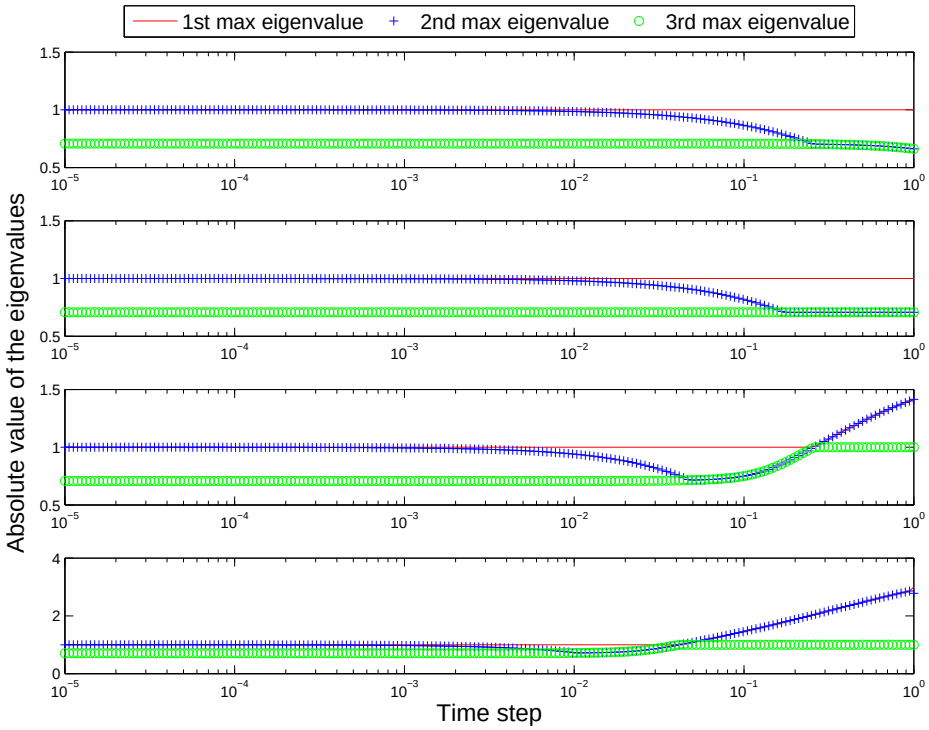

Fig. 45. $m_A = 1, m_B = 1, c_B = 2, c_A = 1, 2, 10, 50, \alpha = 0.5$

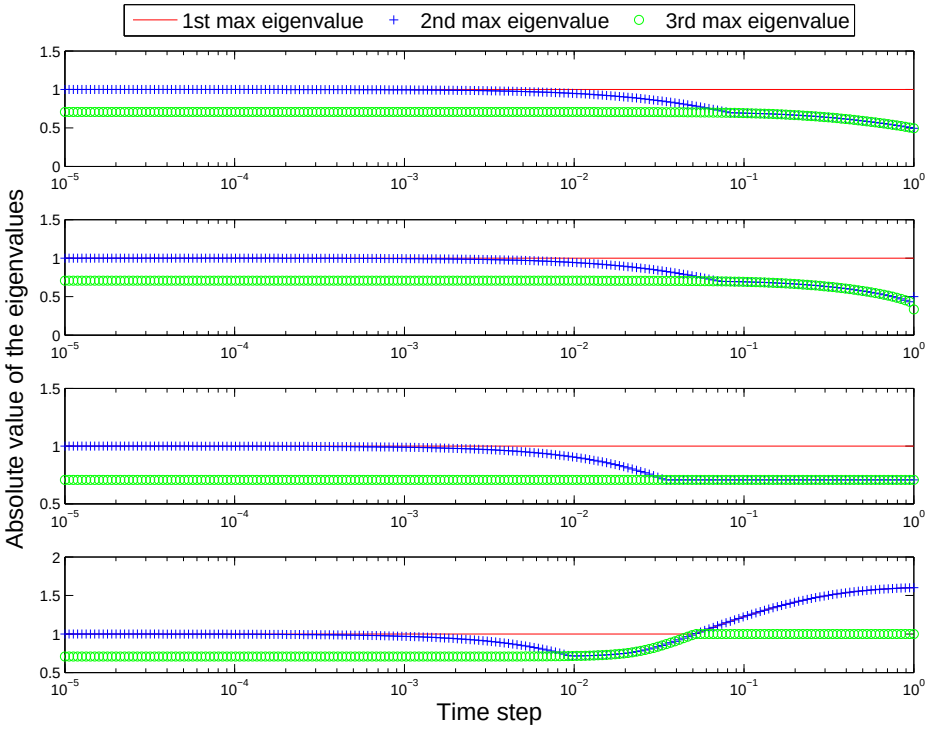

Fig. 46. $m_A = 1, m_B = 1, c_B = 10, c_A = 1, 2, 10, 50, \alpha = 0.5$

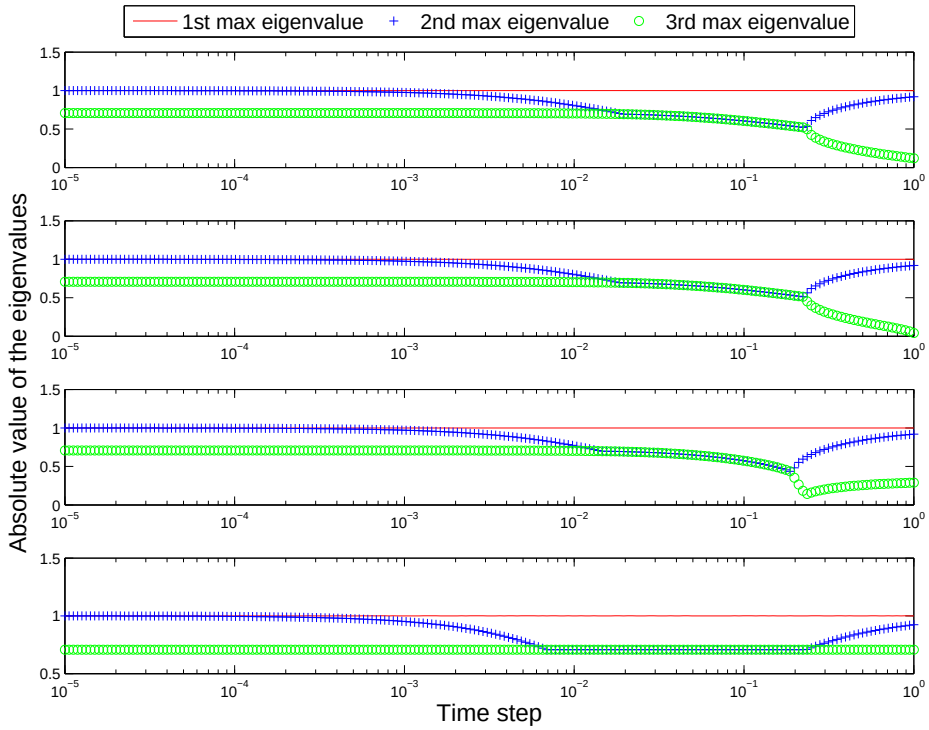

Fig. 47. $m_A = 1, m_B = 1, c_B = 50, c_A = 1, 2, 10, 50, \alpha = 0.5$

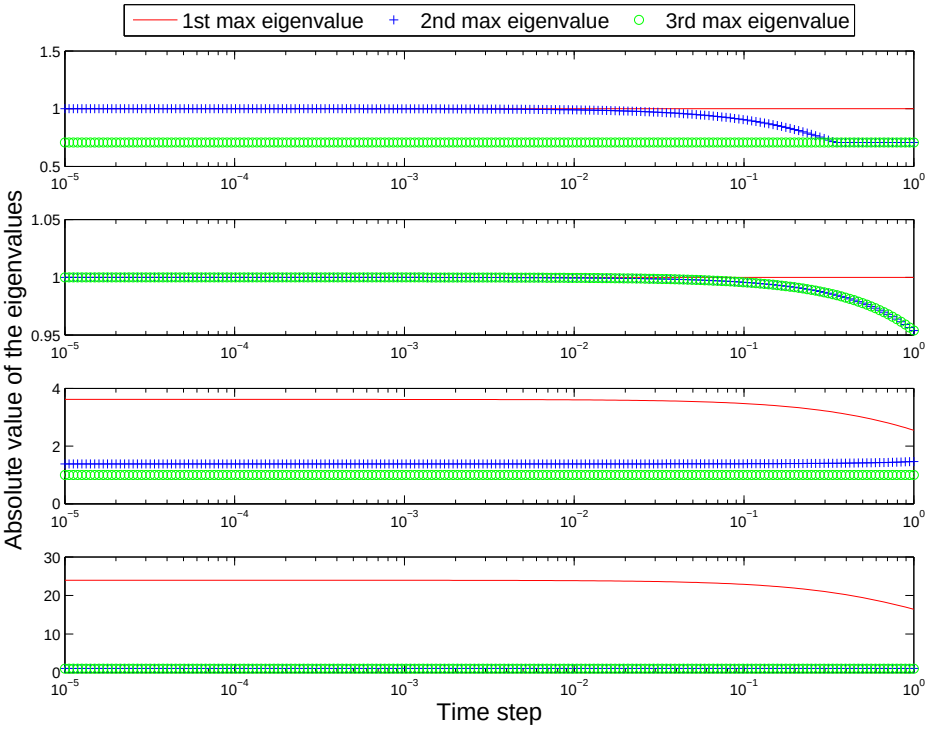

Fig. 48. $c_A = 1, c_B = 1, m_B = 1, m_A = 1, 2, 10, 50, \alpha = 0.5$

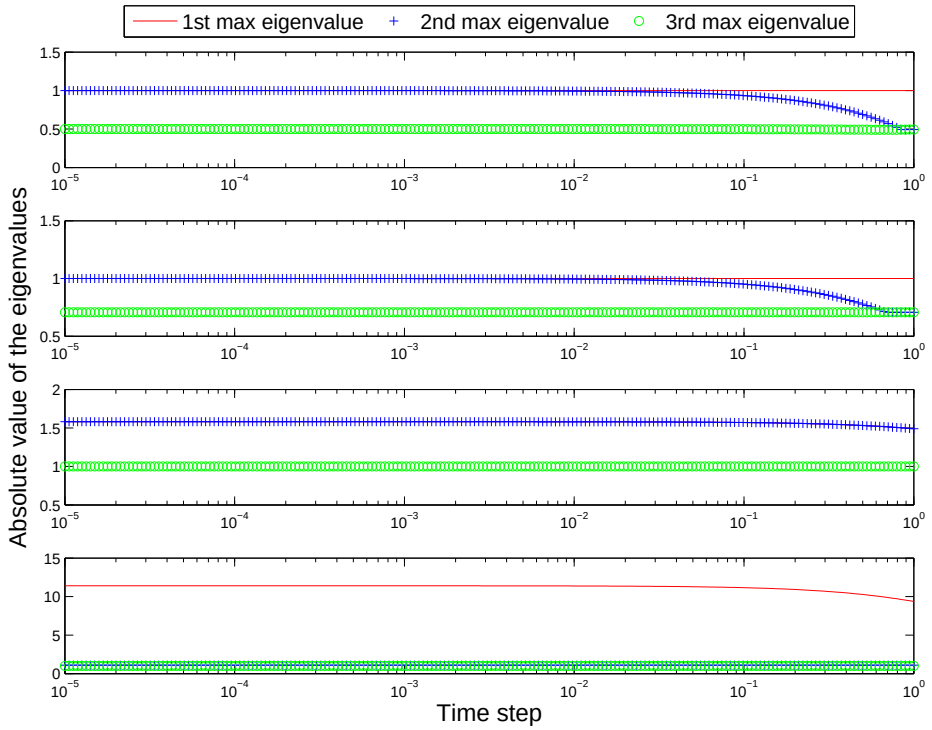

Fig. 49. $c_A = 1, c_B = 1, m_B = 2, m_A = 1, 2, 10, 50, \alpha = 0.5$

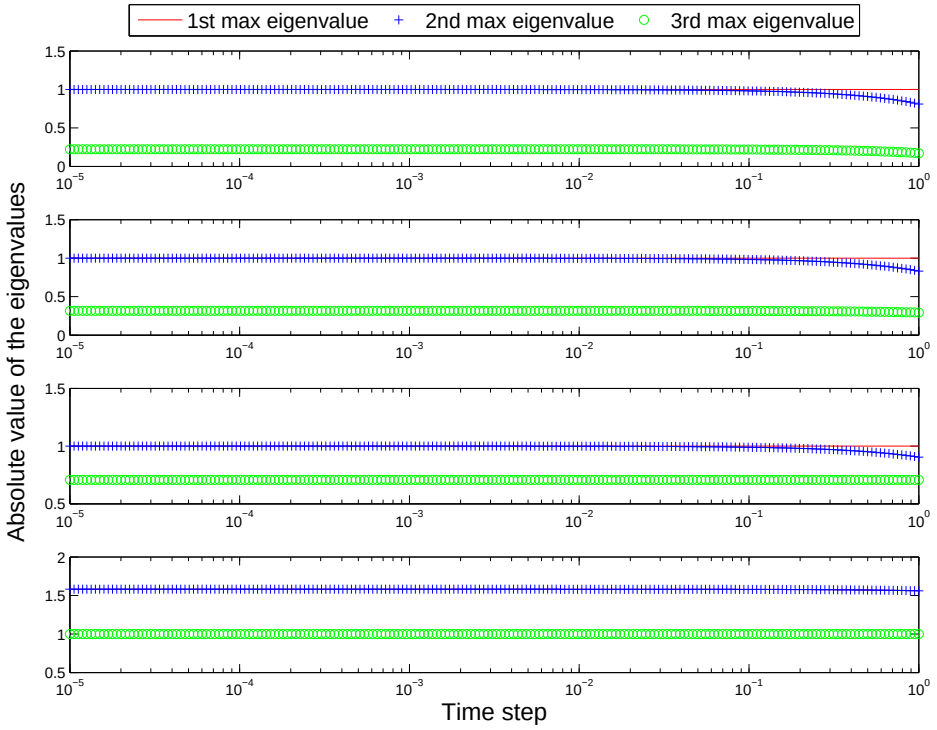

Fig. 50. $c_A = 1, c_B = 1, m_B = 10, m_A = 1, 2, 10, 50, \alpha = 0.5$

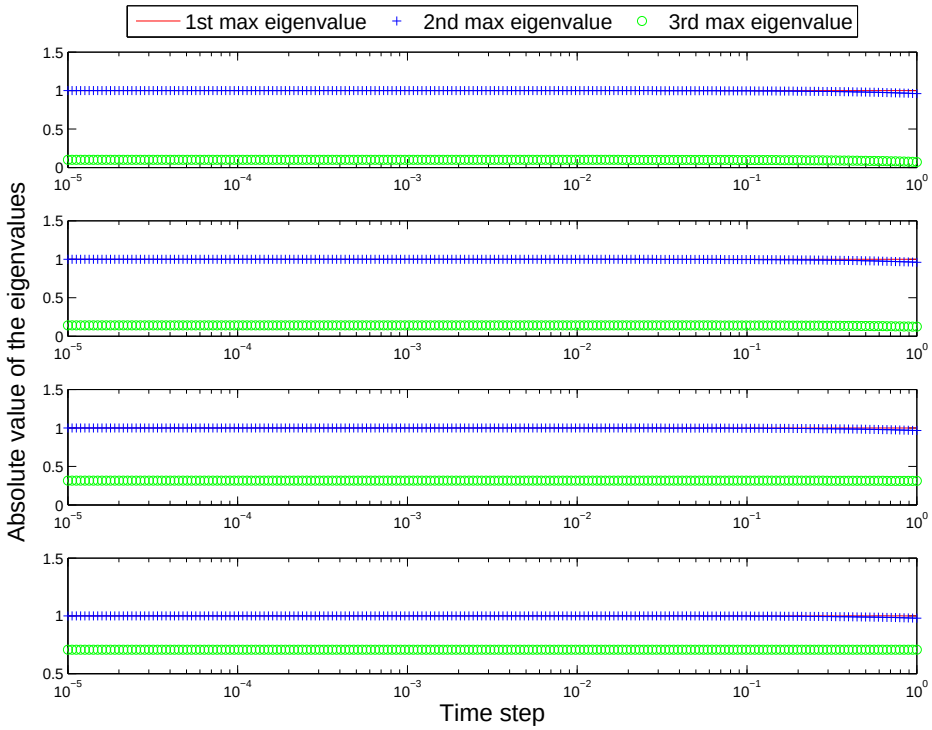

Fig. 51. $c_A = 1, c_B = 1, m_B = 50, m_A = 1, 2, 10, 50, \alpha = 0.5$

Second order system: Newmark average acceleration with *no* α dissipation

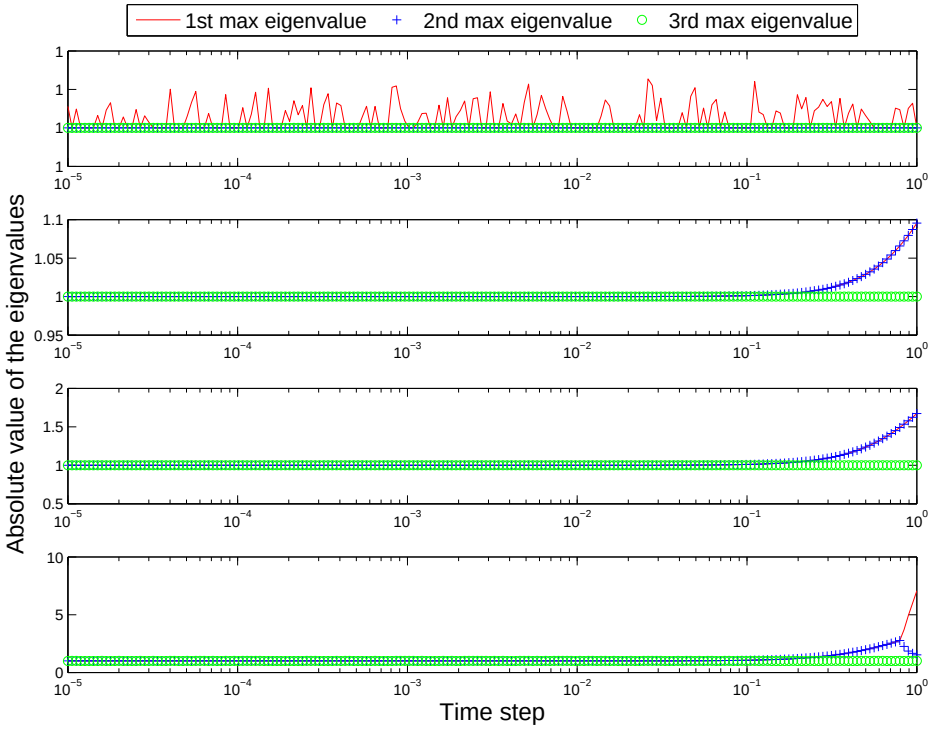

Fig. 52. $m_A = 1, m_B = 1, k_B = 1, k_A = 1, 2, 10, 50, \alpha = 1, \gamma = 0.5, \beta = 0.25$

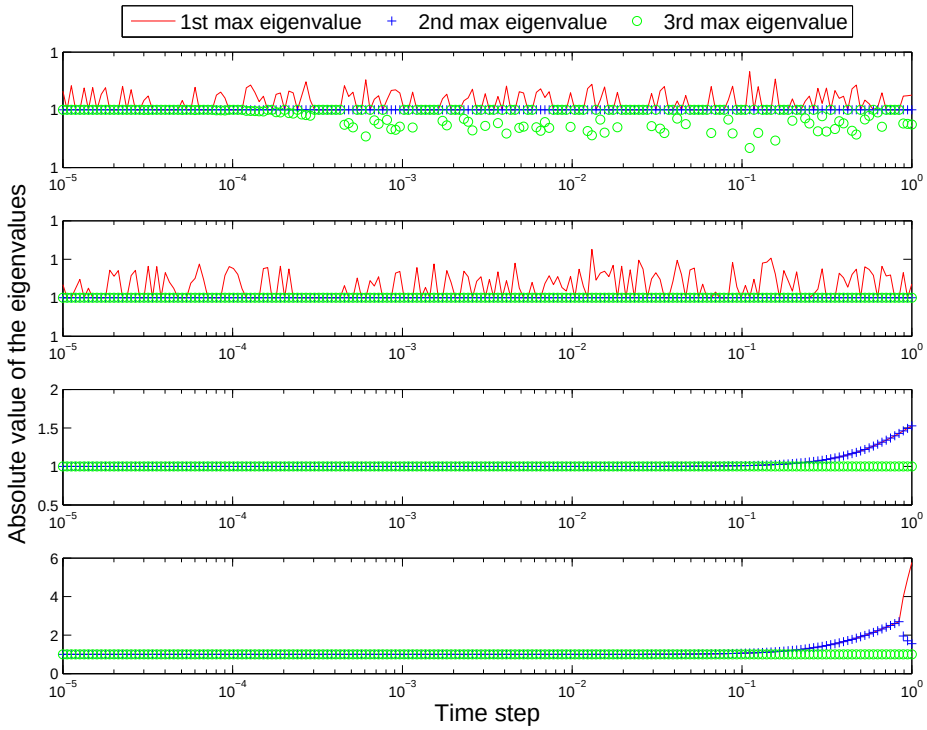

Fig. 53. $m_A = 1, m_B = 1, k_B = 2, k_A = 1, 2, 10, 50, \alpha = 1, \gamma = 0.5, \beta = 0.25$

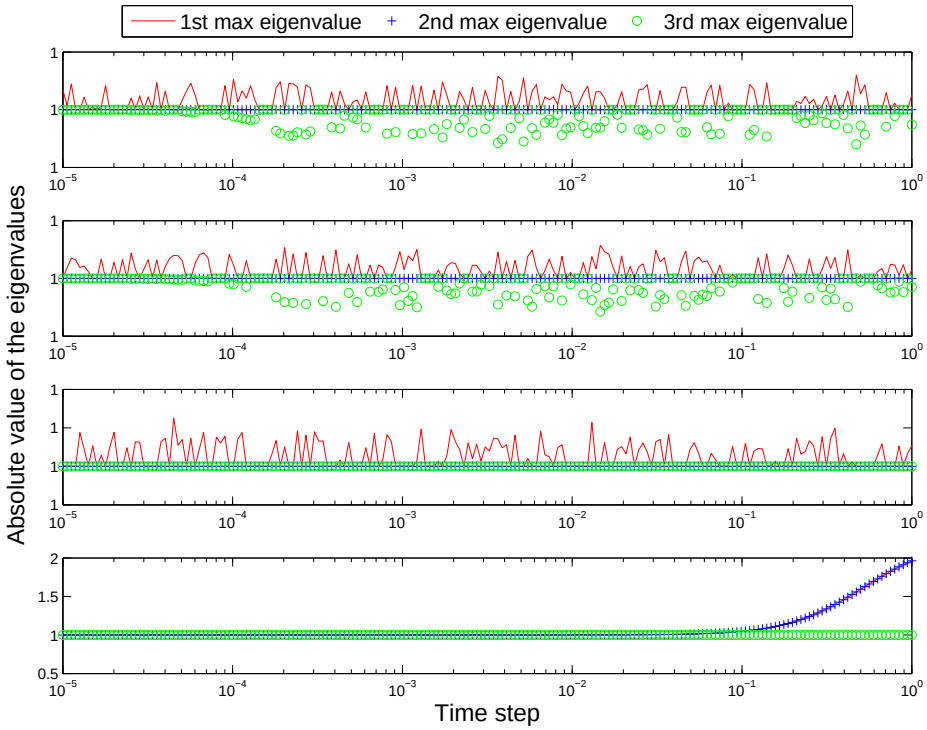

Fig. 54. $m_A = 1, m_B = 1, k_B = 10, k_A = 1, 2, 10, 50, \alpha = 1, \gamma = 0.5, \beta = 0.25$

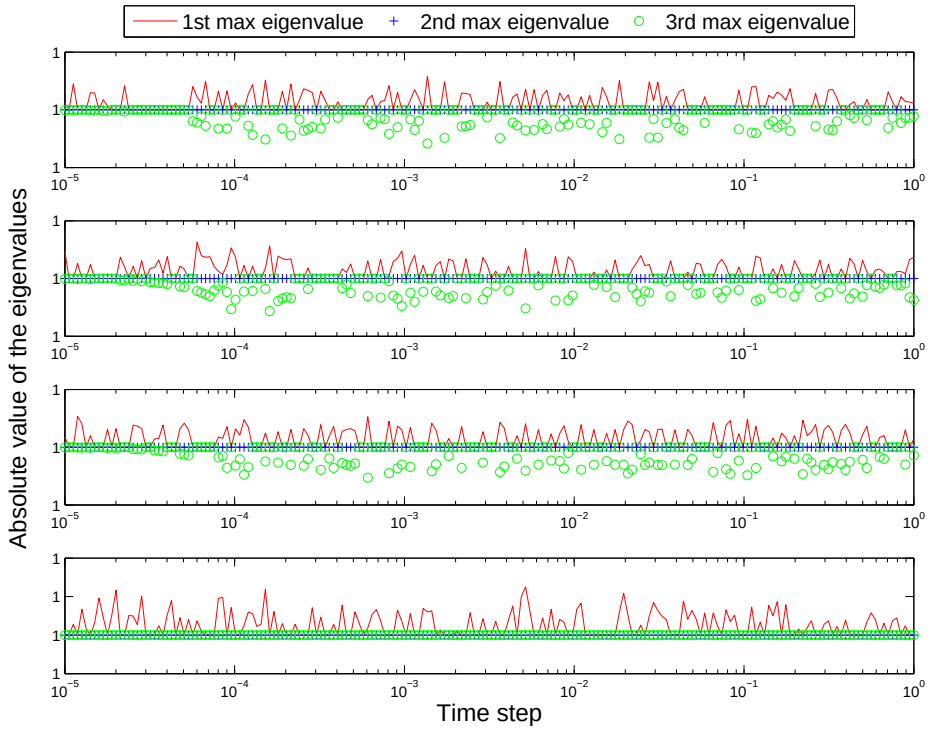

Fig. 55. $m_A = 1, m_B = 1, k_B = 50, k_A = 1, 2, 10, 50, \alpha = 1, \gamma = 0.5, \beta = 0.25$

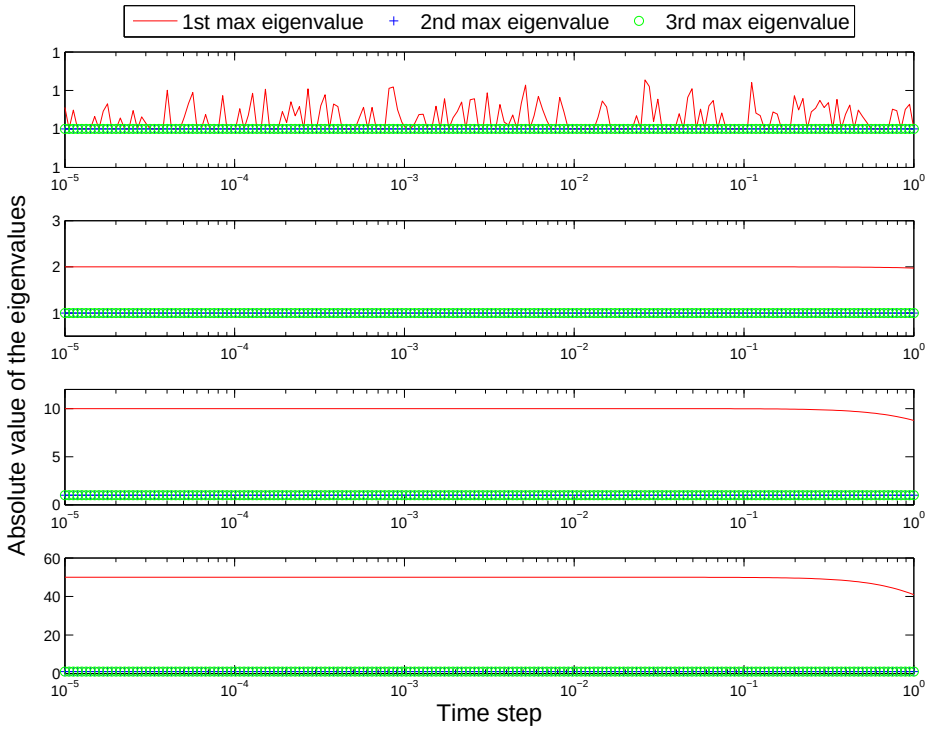

Fig. 56. $k_A = 1, k_B = 1, m_B = 1, m_A = 1, 2, 10, 50, \alpha = 1, \gamma = 0.5, \beta = 0.25$

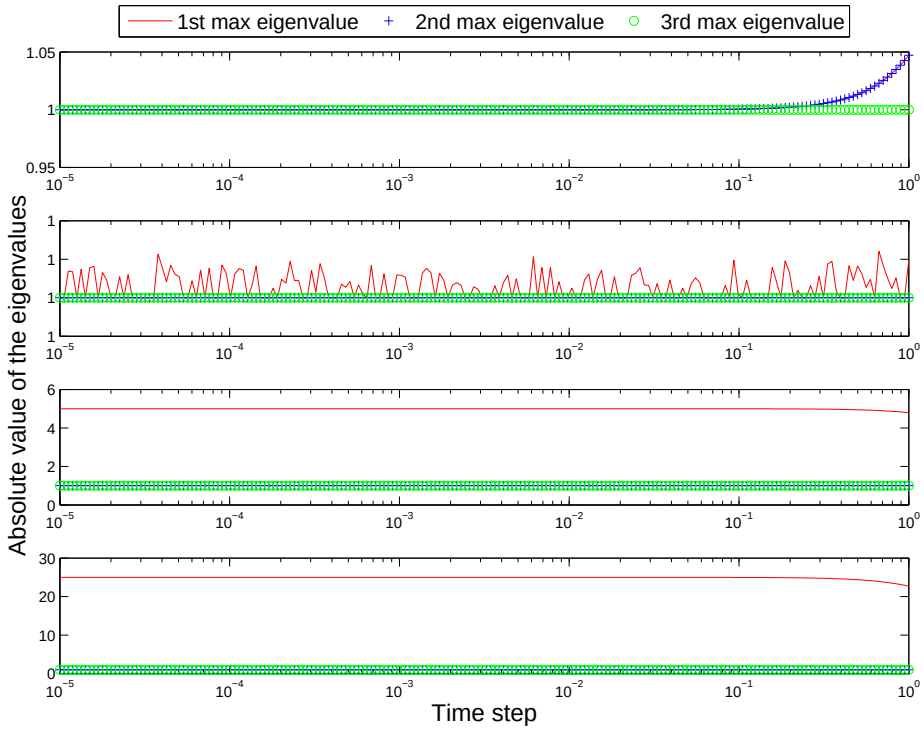

Fig. 57. $k_A = 1, k_B = 1, m_B = 2, m_A = 1, 2, 10, 50, \alpha = 1, \gamma = 0.5, \beta = 0.25$

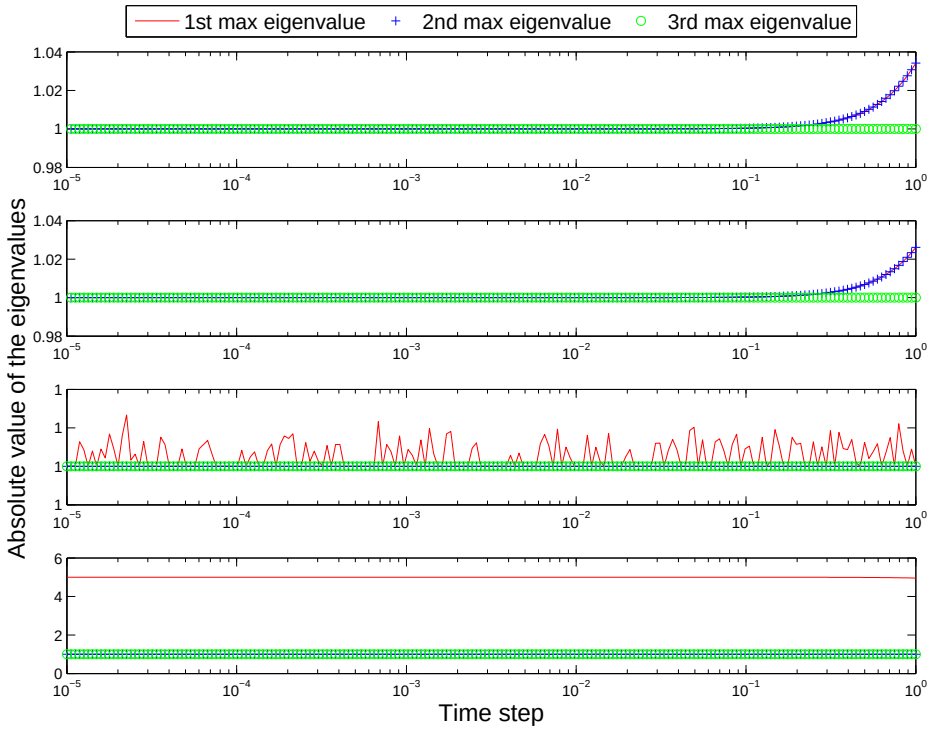

Fig. 58. $k_A = 1, k_B = 1, m_B = 10, m_A = 1, 2, 10, 50, \alpha = 1, \gamma = 0.5, \beta = 0.25$

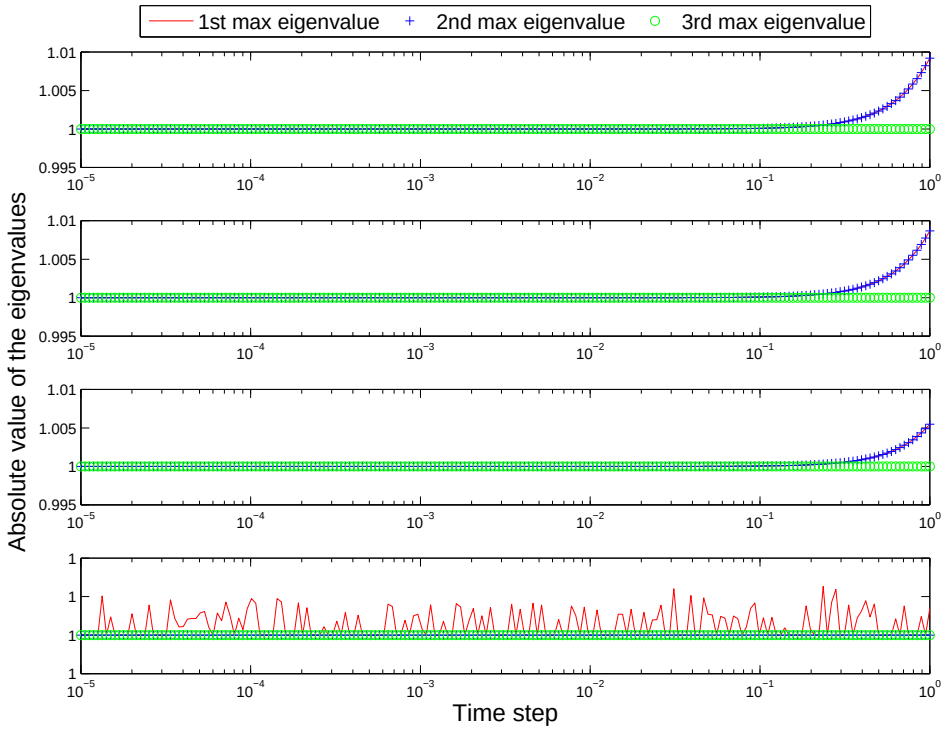

Fig. 59. $k_A = 1, k_B = 1, m_B = 50, m_A = 1, 2, 10, 50, \alpha = 1, \gamma = 0.5, \beta = 0.25$

Second order system: Newmark average acceleration *with* α dissipation

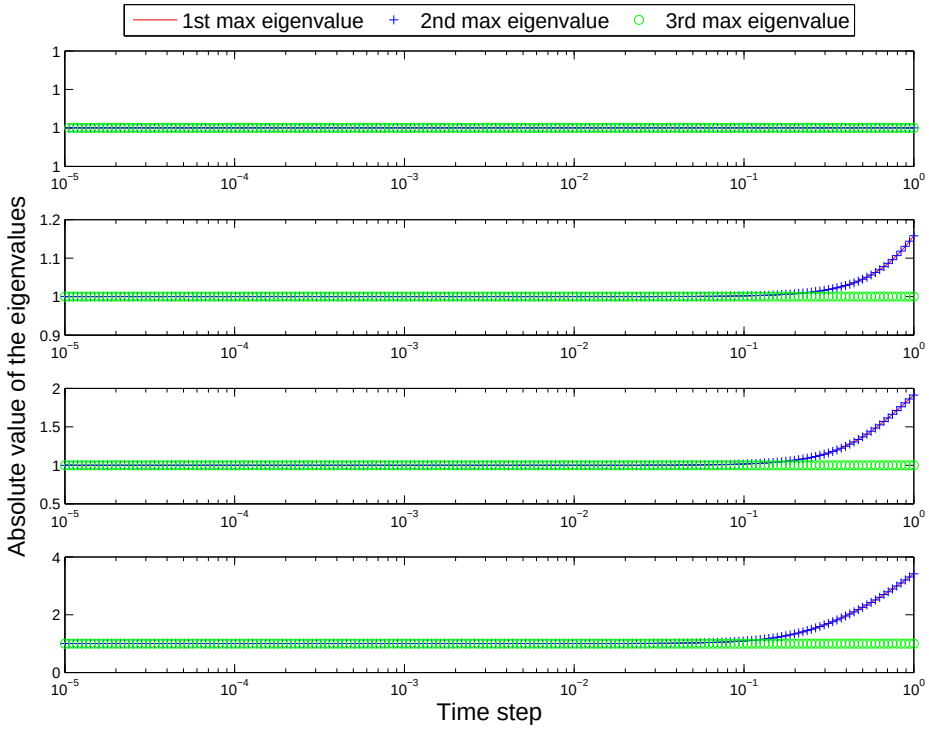

Fig. 60. $m_A = 1, m_B = 1, k_B = 1, k_A = 1, 2, 10, 50, \alpha = 0.5, \gamma = 0.5, \beta = 0.25$

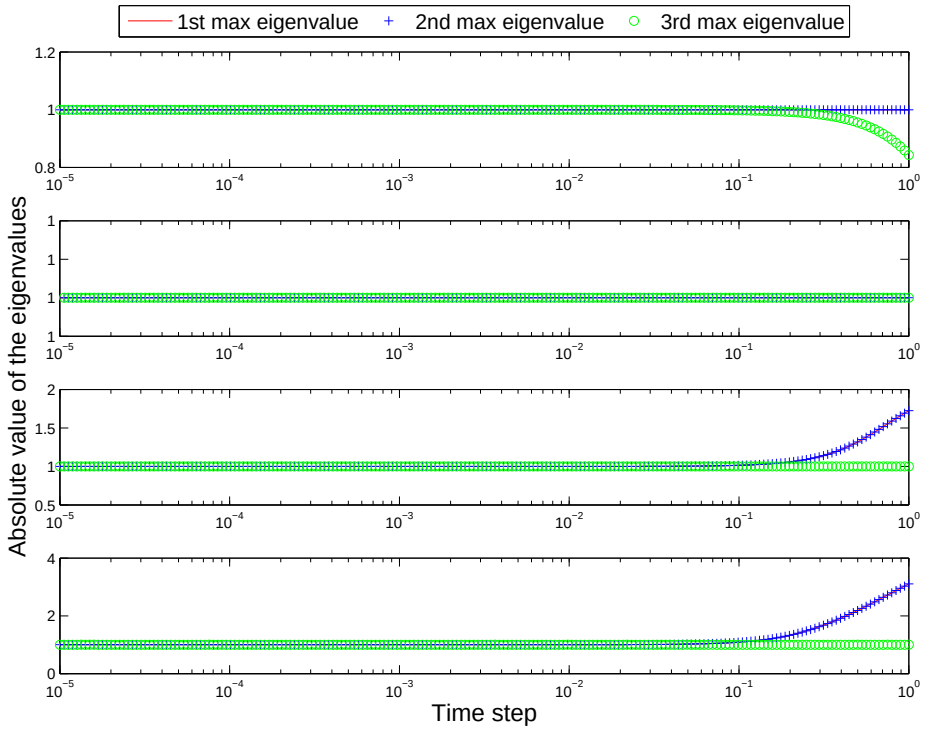

Fig. 61. $m_A = 1, m_B = 1, k_B = 2, k_A = 1, 2, 10, 50, \alpha = 0.5, \gamma = 0.5, \beta = 0.25$

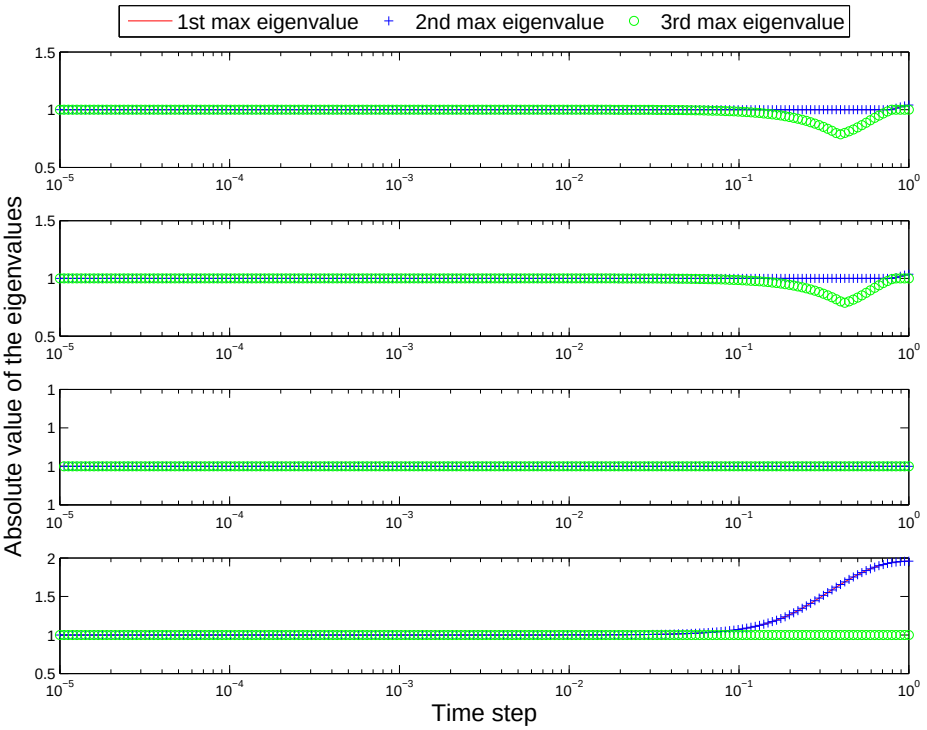

Fig. 62. $m_A = 1, m_B = 1, k_B = 10, k_A = 1, 2, 10, 50, \alpha = 0.5, \gamma = 0.5, \beta = 0.25$

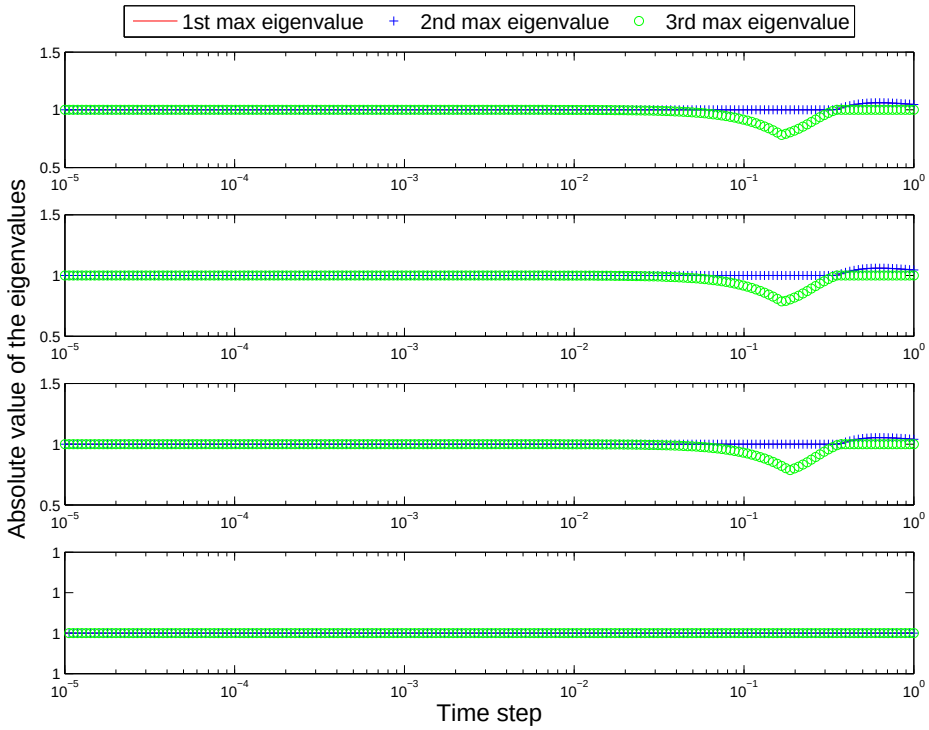

Fig. 63. $m_A = 1, m_B = 1, k_B = 50, k_A = 1, 2, 10, 50, \alpha = 0.5, \gamma = 0.5, \beta = 0.25$

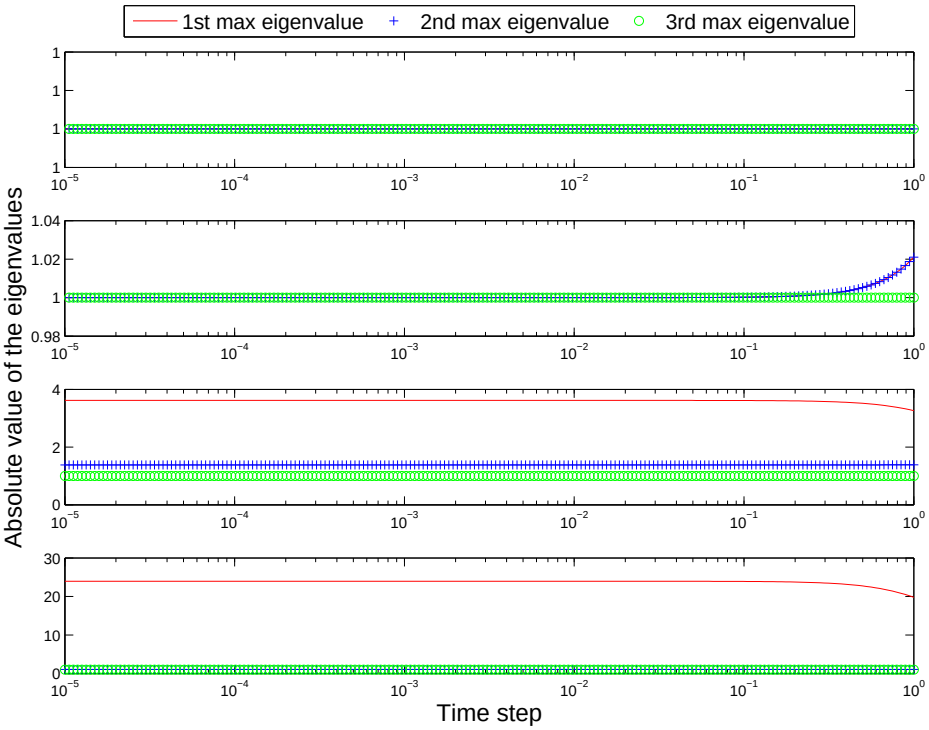

Fig. 64. $k_A = 1, k_B = 1, m_B = 1, m_A = 1, 2, 10, 50, \alpha = 0.5, \gamma = 0.5, \beta = 0.25$

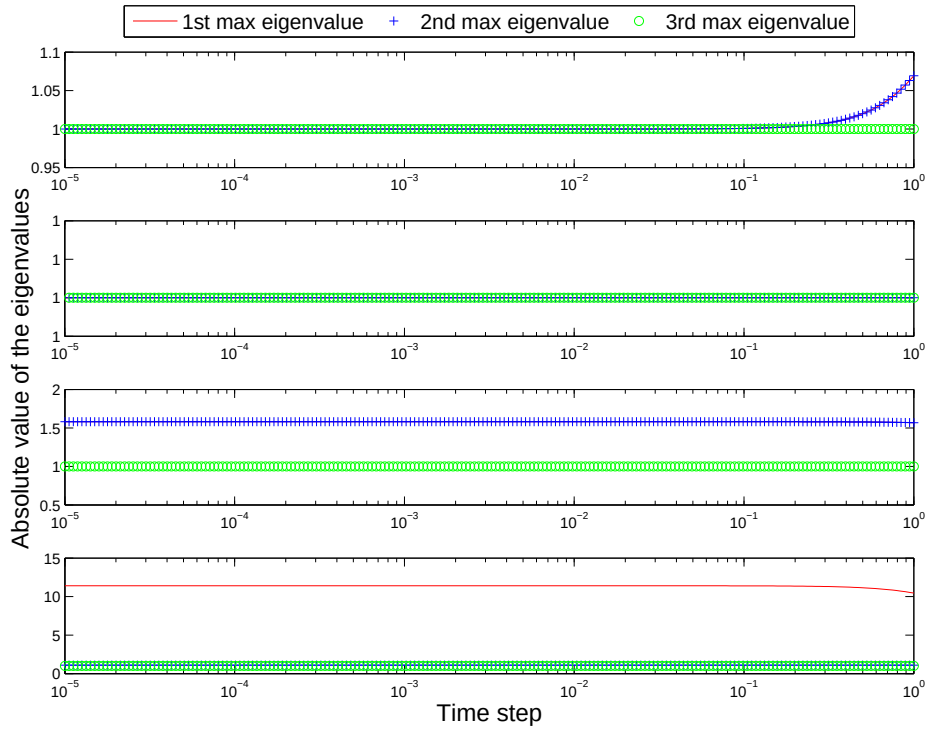

Fig. 65. $k_A = 1, k_B = 1, m_B = 2, m_A = 1, 2, 10, 50, \alpha = 0.5, \gamma = 0.5, \beta = 0.25$

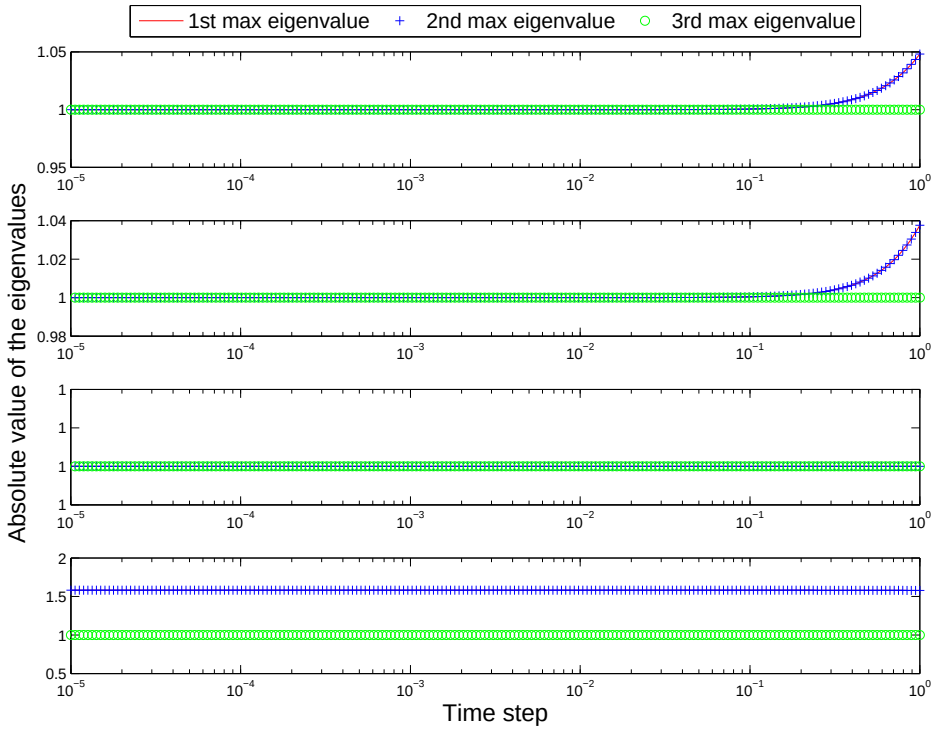

Fig. 66. $k_A = 1, k_B = 1, m_B = 10, m_A = 1, 2, 10, 50, \alpha = 0.5, \gamma = 0.5, \beta = 0.25$

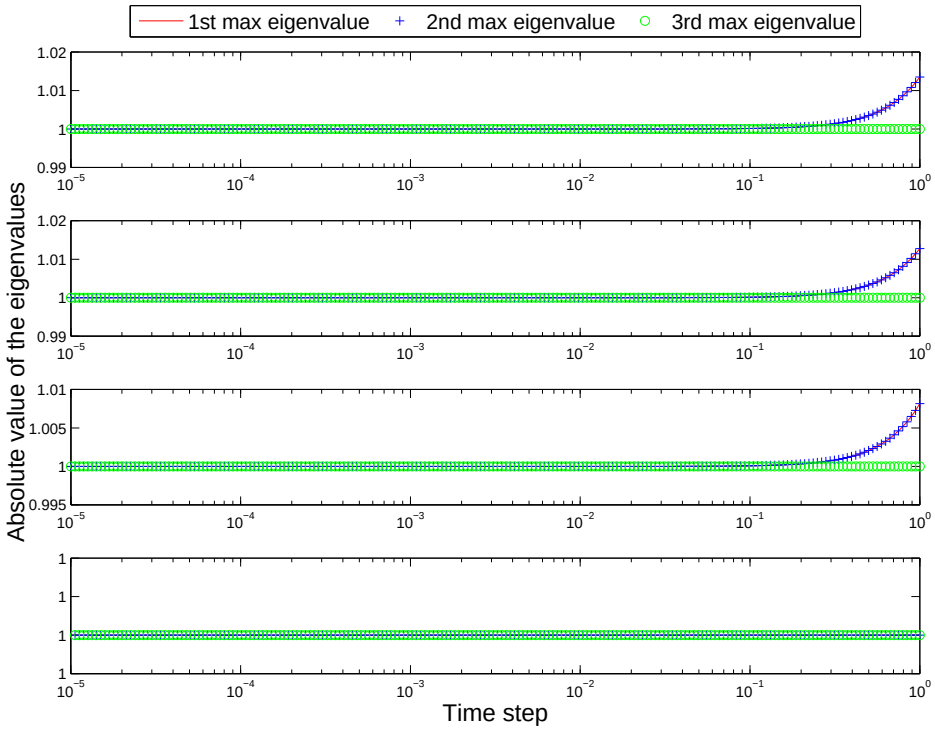

Fig. 67. $k_A = 1, k_B = 1, m_B = 50, m_A = 1, 2, 10, 50, \alpha = 0.5, \gamma = 0.5, \beta = 0.25$

Second order system: damped Newmark scheme *with* α dissipation

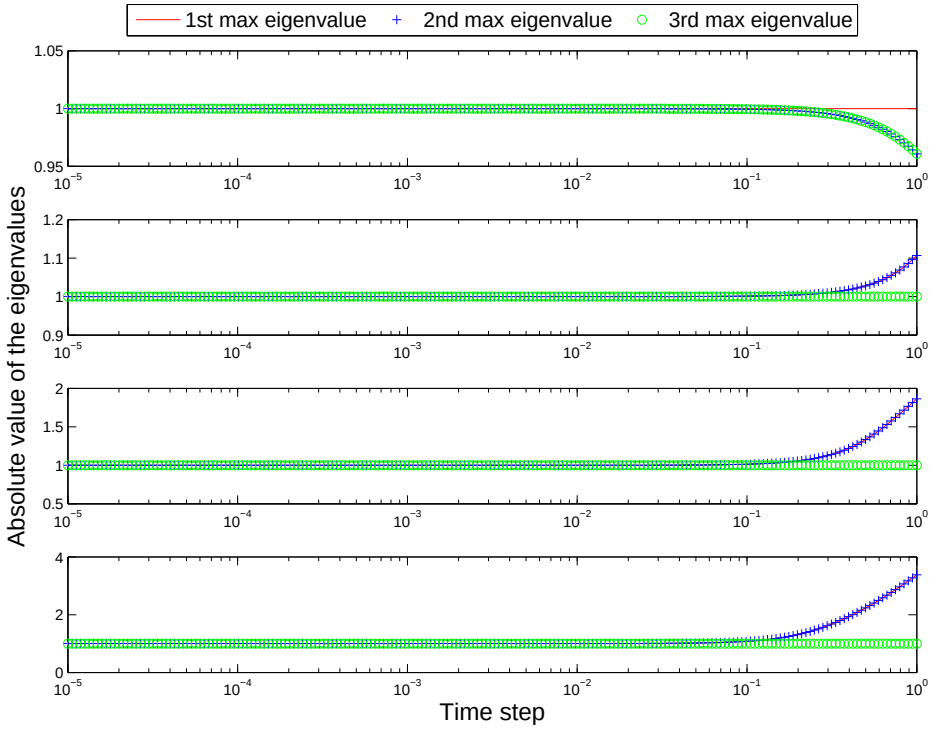

Fig. 68. $m_A = 1, m_B = 1, k_B = 1, k_A = 1, 2, 10, 50, \alpha = 0.5, \gamma = 0.6, \beta = 0.3025$

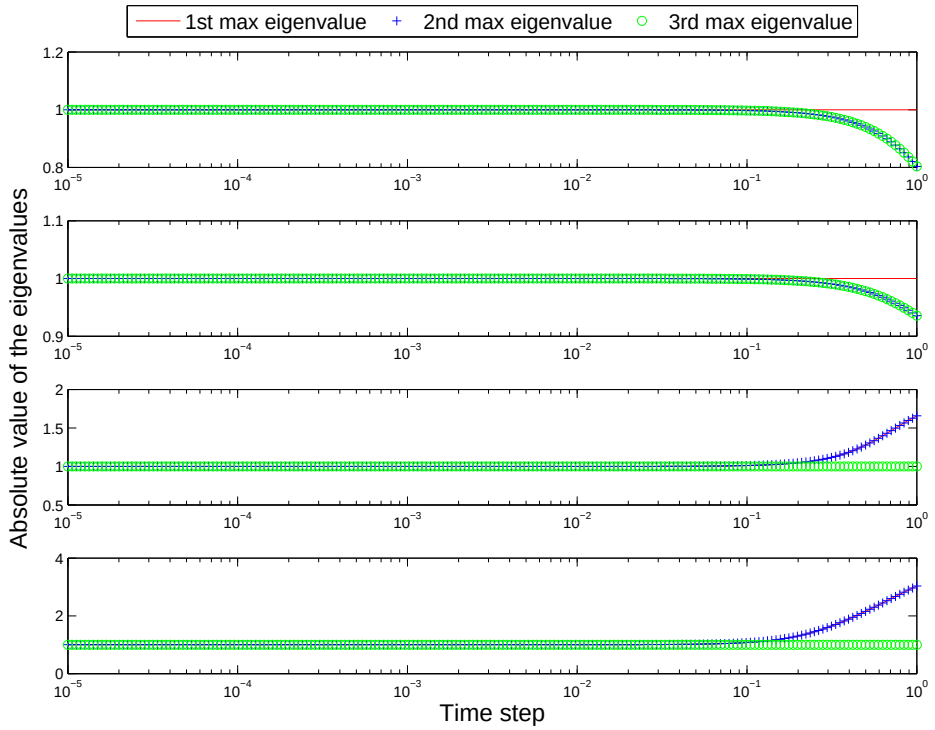

Fig. 69. $m_A = 1, m_B = 1, k_B = 2, k_A = 1, 2, 10, 50, \alpha = 0.5, \gamma = 0.6, \beta = 0.3025$

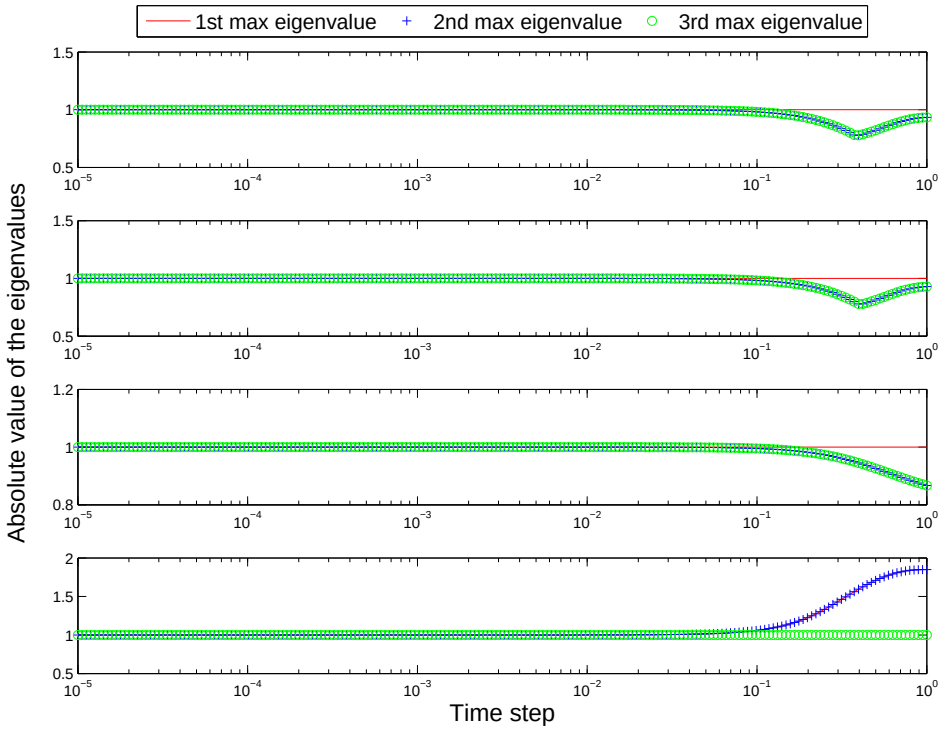

Fig. 70. $m_A = 1, m_B = 1, k_B = 10, k_A = 1, 2, 10, 50, \alpha = 0.5, \gamma = 0.6, \beta = 0.3025$

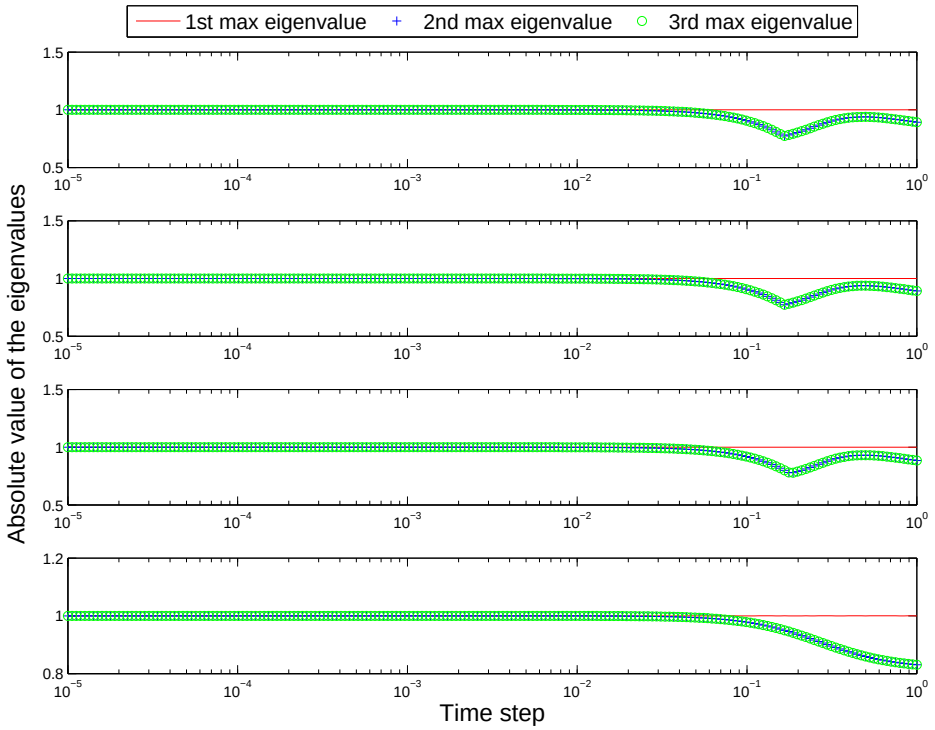

Fig. 71. $m_A = 1, m_B = 1, k_B = 50, k_A = 1, 2, 10, 50, \alpha = 0.5, \gamma = 0.6, \beta = 0.3025$

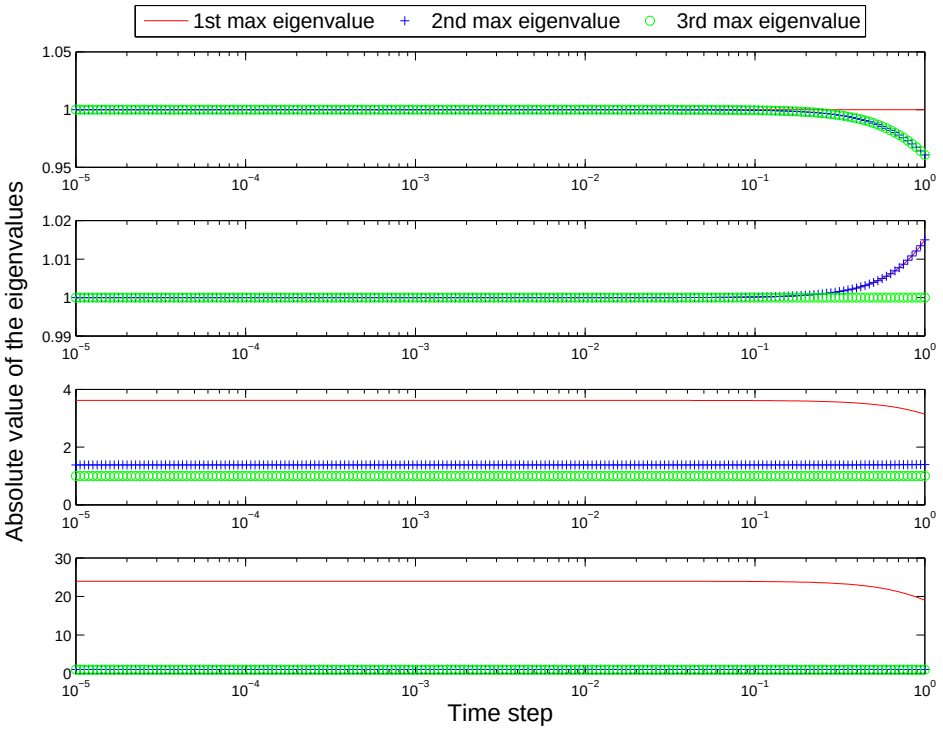

Fig. 72. $k_A = 1, k_B = 1, m_B = 1, m_A = 1, 2, 10, 50, \alpha = 0.5, \gamma = 0.6, \beta = 0.3025$

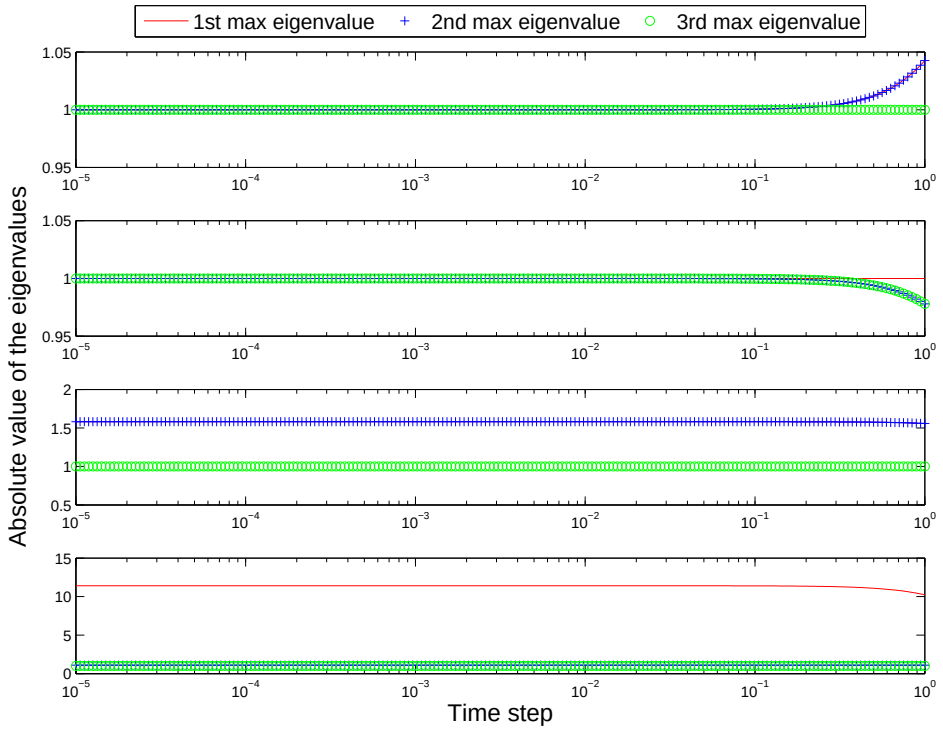

Fig. 73. $k_A = 1, k_B = 1, m_B = 2, m_A = 1, 2, 10, 50, \alpha = 0.5, \gamma = 0.6, \beta = 0.3025$

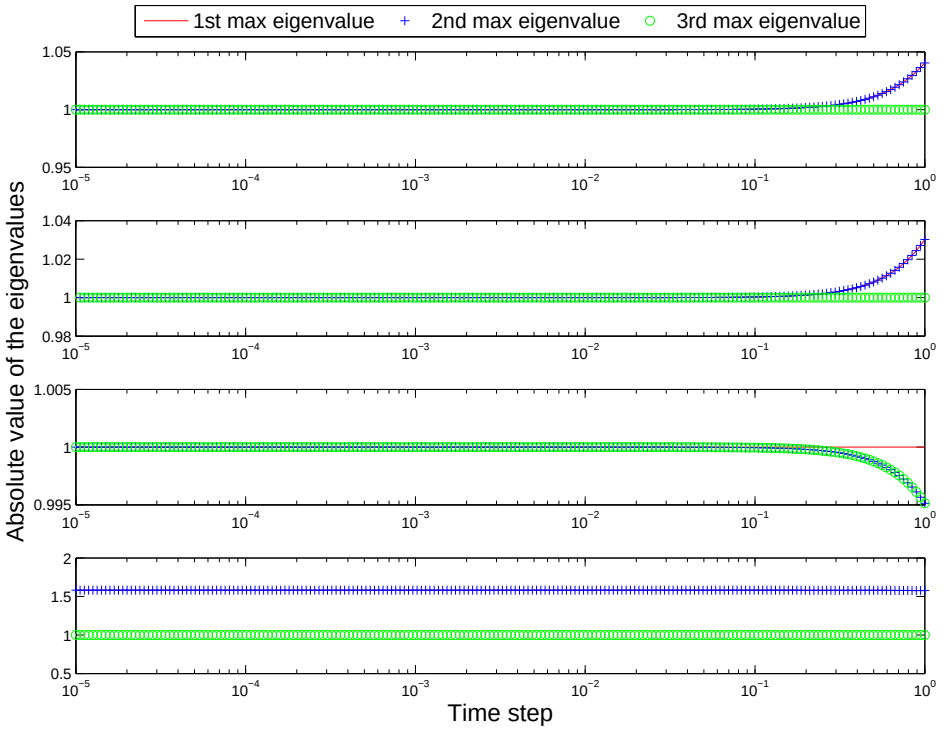

Fig. 74. $k_A = 1, k_B = 1, m_B = 10, m_A = 1, 2, 10, 50, \alpha = 0.5, \gamma = 0.6, \beta = 0.3025$

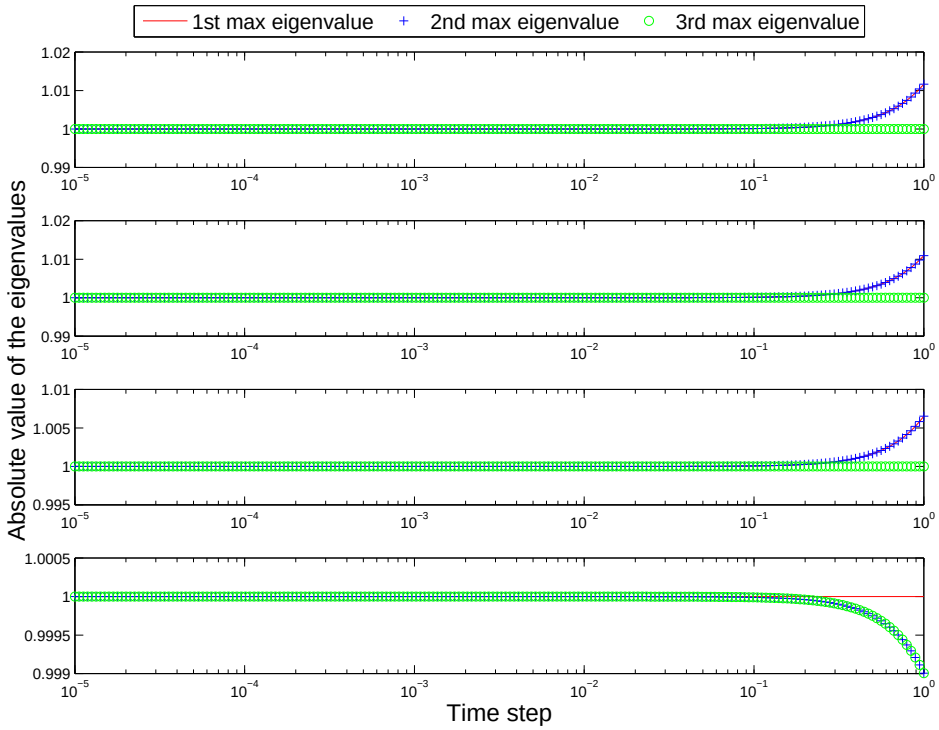

Fig. 75. $k_A = 1, k_B = 1, m_B = 50, m_A = 1, 2, 10, 50, \alpha = 0.5, \gamma = 0.6, \beta = 0.3025$

VITA

Abhineeth Akkasale lives in Bangalore and was educated at Vijaya High School. He received his Bachelor's degree in engineering, B.E., from Bangalore University in 2007. After a short stint as a graduate engineering trainee at Larsen & Toubro - Komatsu India Ltd., he joined the Department of Mechanical Engineering at Texas A&M University in Fall 2008. He received his Master's degree in mechanical engineering in May 2011. He can be reached at abhineeth.a@gmail.com.

Address: Department of Mechanical Engineering
c/o Dr. Kalyana B. Nakshatrala
Texas A&M University
College Station, Texas - 77843-3123, USA

The typist for this thesis was Abhineeth Akkasale.